Detrital zircon age and provenance constraints on late Paleozoic ice-sheet growth and dynamics in western and central Australia

Joe R. Martin[1]*§, Jonathan Redfern[1], Matthew S.A. Horstwood[2], Arthur J. Mory[3], Brian P.J. Williams[4]

[1] Basin Studies and Petroleum Geoscience, School of Earth, Atmospheric and Environmental Sciences, University of Manchester, M13 9PL, United Kingdom.

[2] NERC Isotope Geosciences Laboratory, British Geological Survey, Keyworth, NG12 5GG, United Kingdom.

[3] Department of Industry Regulation and Safety, Government of Western Australia, Mineral House, 100 Plain Street, East Perth, WA 6004, Australia.

[4] Department of Geology & Petroleum Geology, University of Aberdeen, AB24 3UE, United Kingdom.

* Corresponding author: joe.martin@shell.com

§ Current address: Shell Malaysia Ltd., Menara Shell, Jalan Tun Sambanthan 211, Kuala Lumpur, 50470, Malaysia.

ABSTRACT

U-Pb dating and Hf isotope provenance analysis of detrital zircons from the glaciogenic Lower Permian Grant Group of the Canning Basin indicates sources principally from basement terranes in central Australia, with subordinate components from terranes to the south and north. Integrating this data with field outcrop and subsurface evidence for ice-sheets, including glacial valleys and striated **pavements** along the southern and northern margins of the basin, suggests that continental ice sheets extended over several Precambrian upland areas of western and central Australia during the late Paleozoic ice age (LPIA). The youngest zircons constrain the maximum age for contemporaneous ice sheet development to the Late Carboniferous (Kasimovian), whereas palynology provides a minimum age of Early Permian (Asselian–Sakmarian). Considering the palynological age of the Grant Group within the context of regional and global climate proxies, the main phase of continental ice sheet growth was possibly in the Ghzelian–Asselian. The presence of ice sheets older than Kasimovian in western and central Australia remains difficult to prove given a regional gap in deposition possibly covering the mid-Bashkirian to early Ghzelian within the main depocentres and even larger along basin margins, and the poor evidence for older Carboniferous glacial facies. There is also no evidence for extensive glacial facies younger than mid-Sakmarian in this region as opposed to eastern Australia where the youngest regional glacial phase was Guadalupian.

Keywords: late Paleozoic ice age; Canning Basin; Grant Group; Permian; zircon provenance; U-Pb-Hf

INTRODUCTION

The record of the late Paleozoic ice age (LPIA) in Australia is extensive, with glaciogenic strata preserved in many basins across the continent (Crowell & Frakes, 1975; Hambrey and Harland, 1981; Eyles, 1993; Jones and Fielding, 2004; Birgenheier et al., 2007; Mory et al., 2008; **Isbell et al., 2012**; **Montanez & Poulsen, 2013**). The application of biostratigraphy, paleontology and SHRIMP U–Pb dating provide important constraints on the age and timing of events during the LPIA, thereby allowing significant advances in our understanding of this ice age (e.g. Foster and Waterhouse, 1998; Archbold, 1995, 1999; Archbold and Shi, 1995; Roberts et al., 1995, 1996; Fielding et al., 2008; Waterhouse & Shi, 2013). Sedimentological studies also demonstrate that parts of the continent experienced intermittent glacial conditions from the mid-Carboniferous through to the Late Permian. At c. 65 Myr, this is possibly the longest-lived record of the LPIA in Gondwana (Jones et al., 2006; Eyles et al., 2006; Birgenheier et al., 2007; Fielding et al., 2008). Stratigraphic data suggests the LPIA was most extensive during the Early Permian, with glaciogenic sediments of this age preserved in most Phanerozoic basins across the continent (e.g. Williams et al., 1987; Jones and Fielding, 2004; Fielding et al., 2008).

The majority of studies on the LPIA in Australia are on glacial successions that out-crop in eastern Australia whereas stratigraphic constraints on the evolution of the LPIA in western and central Australia are tenuous by comparison. This is despite, for example, the marine basins of Western Australia containing amongst the thickest glaciogenic successions in Gondwana (up to several km; Eyles et al., 2002, 2006; Mory et al., 2008). Within the context of these recent advances in the understanding of the LPIA in wider Australia, this paper presents new radiometric age constraints for the LPIA in western and central Australia based on uranium–lead (U–Pb) dating and lutetium–hafnium (Lu–Hf) isotope geochemistry of detrital zircons from the Grant Group of the Canning Basin (Western Australia). This analysis links the glaciation's depositional and erosional records **to** sedimentological and stratigraphic interpretations of field outcrops and equivalent subsurface successions (Redfern, 1990; Martin, 2008; Mory et al., 2008; Al-Hinaai & Redfern, 2015) to critically assess regional glaciation models for the LPIA in western and central Australia.

GEOLOGICAL SETTING AND CANNING BASIN LPIA STRATIGRAPHIC OVERVIEW

During the LPIA, Australia was situated at mid to high latitudes in eastern Gondwana, with subduction of the paleo-Pacific along its eastern margin and rifting predating the break-up with India and Himalayan terranes along its western margin (Veevers and Tewari, 1995; Metcalfe, 1996, 2013; Betts et al., 2002; Veevers, 2004; Glen, 2005). At this time the intracratonic Canning Basin was flanked by Precambrian upland areas. In central Australia elevation and exhumation of the Arunta Inlier and Musgrave Block followed the Devonian–Carboniferous Alice Springs Orogeny and, to the south and north, the Pilbara–Yilgarn cratons and Kimberley region were also long-lived areas of positive basement relief (Fig. 1; Hand et al., 1999; Veevers, 2004, 2009, Buick et al., 2008). Sedimentological and paleontological evidence indicates marine incursions into the northern Canning Basin from the northwest in the Early Permian (Archbold, 1995, 1999; Archbold and Shi, 1995; Martin et al., 2007). There is also widespread evidence for Early Permian glacial conditions across Australia and Gondwana (e.g. Blatchford, 1927; Crowell & Frakes, 1975; Crowe & Turner, 1976; Redfern, 1990; Redfern & Millward, 1994; Redfern & Williams, 2002; Isbell et al., 2003; Jones and Fielding, 2004; Osterloff et al., 2004; Fielding et al., 2008; Waterhouse & Shi, 2013).

The focus of this study is on the Lower Permian Grant Group of the Canning Basin (Fig. 1). Field and subsurface sedimentological and paleontological analyses of the group indicate it was deposited within glacial-influenced environments (Figs. 2A, B and C; Redfern, 1990; Redfern and Millward, 1994; Apak and Backhouse, 1998, 1999; Martin et al, 2007; Martin, 2008; Mory et al., 2008; Veevers, 2009). The age of the Grant Group is largely constrained by palynology (the *Pseudoreticulatispora confluens* and *Microbaculispora tentula* spore-pollen zones; Apak and Backhouse, 1998, 1999; Mory, 2010), and Asselian to early Sakmarian foraminifera-brachiopod-gastropod assemblages from exploration coreholes and wells on the Barbwire Terrace and outcrop in St. George Ranges (Foster and Waterhouse, 1988; Archbold, 1995, 1999; Taboada et al., 2015). SHRIMP U–Pb age control for equivalent ammonite and palynozones in eastern Australia (Roberts et al., 1995; 1996), corrected following Black et al. (2003), provide a lower absolute age limit of c. 296 Ma, indicating the Grant Group was deposited between the late Asselian and early Sakmarian (Fig. 3). However, preliminary TIMS U–Pb dating of eastern Australia successions suggests *P. confluens* could be slightly older with the *M. tentula* Zone extending into the latest Carboniferous, although Bodorokos et al. (2016) indicate this is based on relatively few sample analyses.

Although the underlying Reeves Formation has been considered to be glacial or preglacial (Redfern, 1990; Redfern and Millward, 1994; Kennard et al., 1994; Apak and Backhouse, 1998, 1999; Mory et al., 2008; Veevers, 2009), recent seismic interpretation suggests it is predominantly a syn-rift, pre-glacial succession (Al-Hinaai & Redfern, 2015). The age of the Reeves Formation in the Fitzroy Trough spans the late Visean to c. Moscovian based on relatively imprecise palynology (*Grandispora maculosa* to *Diatomozonotriletes birkheadensis* spore-pollen zones; Apak and Backhouse, 1998, 1999; Veevers, 2009; J. Backhouse, pers. comm., 2018). On the terraces flanking the Fitzroy Trough, palynomorphs in the Grant Group are now considered to be from the latest Pennsylvanian to Asselian or early Sakmarian *M.*

tentula and *P. confluens* spore-pollen zones. In those areas (Lennard Shelf to the north and Barbwire Terrace to the south) the group usually unconformably overlies Devonian and older rocks (Fig. 3). There is a probable depositional hiatus (and/or erosion) spanning at least the middle to late Pennsylvanian between the Reeves Formation and Grant Group in the Fitzroy Trough whereas on the flanking sub-basins that break is often larger.

RATIONALE AND METHODOLOGY

Detrital zircon provenance analysis on three sandstone core samples from the Grant Group of the Crossland Platform (sample DRO), Barbwire Terrace (sample CAP), and Fitzroy Trough (sample CYC) was undertaken to investigate the location of former glacial centres and associated ice-sheet dynamics, and to identify major sediment transport routes into Canning Basin during the LPIA (Fig. 1). Combined U–Pb dating and Lu–Hf isotope geochemistry was applied to detrital zircon samples using laser ablation multi-collector inductively coupled plasma mass spectrometry (LA-MC-ICPMS). U–Pb dating of detrital zircons is a well established method for determining provenance and improving paleogeographic reconstructions and tectonostratigraphic models (e.g. Cawood and Nemchin, 2000; Fedo et al., 2003; Veevers et al., 2005). It is particularly effective in regions with a good geochronological database of potential source areas, as is the case for Australia, where the complex evolution of many basement terranes have been resolved using SHRIMP technology (e.g. Camacho and Fanning, 1995; Bruguier et al., 1999; Buick et al., 2001). Increasingly, provenance studies combine Lu–Hf isotope geochemistry with U–Pb dating of detrital zircons to reveal further information on the composition of the source area. Lu–Hf isotope geochemistry provides information about the evolution of the crust in which the zircons crystallized, therefore is a useful supplement to the age information gained by U–Pb dating, particularly in differentiating sub-populations of zircons of the same age (e.g., Veevers et al., 2005; Flowerdew et al., 2007). A full explanation of the zircon geochronology methodology employed is provided in Appendix A. Correlation of detrital zircons with potential source areas using U–Pb age and Lu–Hf isotope data was constrained with field outcrop and subsurface interpretation (from Martin et al., 2007; Mory et al., 2008; Al-Hinaai & Redfern, 2015), and is summarized below.

FIELD AND SUBSURFACE OBSERVATIONS

The Grant Group outcrops along the northern, southern and eastern basin margins, and within a series of inversion-related anticlines along the Fitzroy Trough (Fig. 1 and 2H). Sedimentological evidence indicating the glacial origin of the Grant Group includes striated **pavements** overlain by **diamictite** (Fig. 2A; Playford, 2002), striated and faceted clasts within various glaciogenic facies, intraformational iceberg striae (O'Brien and Christie-Blick, 1992; Martin, 2008), cold-water marine fauna (e.g. the bivalve *Eurydesma*; Archbold and Shi, 1995), and ice-rafted debris (e.g. Figs. 2B and 2C). In the subsurface, the group is widely distributed and has been a target for numerous petroleum exploration wells with several modest discoveries made to-date, including the Sundown and Blina oil fields, both within the Lennard Shelf. About 30 fully cored boreholes in the Barbwire Terrace contain a typical suite of glaciogenic facies, including diamictite, varved mudrock with dropstones and rare facetted and striated clasts. These wells together with subsurface imaging provided by numerous seismic surveys provide important constraints on Grant Group stratigraphy and depositional settings across the wider Canning Basin. Field and subsurface observations pertinent to the regional glaciation model are outlined below.

Glacial erosional features

In the Pilbara and Yilgarn cratons south of the Canning Basin, striated **pavements** and tunnel valleys (Eyles and de Broekert, 2001; Playford, 2002; Williams, 2007; Mory et al., 2008), clearly indicate major ice sheets developed over cratonic uplands of Western Australia during the LPIA and advanced northwards and eastwards into the Canning Basin. Tillites overlying striated surfaces of the Paleoproterozoic Pinjian Chert Breccia in the Oakover River area of the Pilbara Craton (Williams, 2007) contain *P. confluens* palynomorphs, confirming an Early Permian age (Backhouse, 1992). In central Australia, east of the Canning Basin, glacial striated **pavements** near Dover Hills in the Amadeus Basin provide evidence of ice movement to the west (Haines et al., 2011). No striated **pavements** in basement terranes north of the Canning Basin have been reported to our knowledge, although Playford et al. (2009) described striated **pavements** on Devonian limestone in the eastern Lennard Shelf.

In the subsurface, the Grant Group rests unconformably on strata variably ranging from Ordovician to Carboniferous in age across the Canning Basin. Basal lithologies overlying the Base Grant Unconformity (BGU) are variably diamictite, conglomerate or coarse-grained sandstone facies that are typical of glacial successions. The BGU is marked in places by N to NE U-shaped valleys up to 400 m deep and 10 km wide that, in southern and central areas of the basin (e.g. Al-Hinaai & Redfern, 2015). On the Lennard Shelf, valleys directed to the S to SW and infilled by stacked channel successions have been mapped on both 2D (O'Brien et al., 1998) and 3D seismic (Al-Hinaai, 2013). Multiple intra-formational erosion surfaces are present throughout the basin. These are predominantly but not exclusively developed within lower Grant Group intervals (Al-Hinaai & Redfern, 2015).

Glacial depositional record

Seismic calibrated by wells indicate rifting in the northern Fitzroy Trough and along the Lennard Shelf during the Devonian–Carboniferous ('Pillara' extension) and subsequently, and to a greater magnitude, in the southern Fitzroy Trough along the Barbwire Terrace during the latest Carboniferous – earliest Permian ('Point Moody' extension; Kennard et al., 2004). The Carboniferous succession within the Fitzroy Trough thickens southwards, with seismic showing significant expansion of the Reeves Formation towards the southern major basin bounding faults, such as the Fenton Fault (Al-Hinaai & Redfern, 2015). The majority of these faults terminate at the BGU, indicating the Grant Group was deposited during a phase of post-rift thermal subsidence in the northern Canning Basin, contrary to some sedimentological models, which interpret it as a syn-rift succession (e.g. Eyles & Eyles, 2000).

Based on sedimentological and stratigraphical evaluations of the Fitzroy Valley outcrops and subsurface cored sections from the Barbwire Terrace and Crossland Platform, the Grant Group in the northern Canning Basin was deposited within glaciated shallow marine and proglacial fluvial-deltaic environments (Redfern & Williams, 2002; Martin, 2008). Lower facies associations comprise a complex succession of basin marginal facies, deposited from gravity flows (Fig. 2C), turbidity currents (Fig. 2D), and sediment remobilisation and suspension processes. Basin axial facies record deposition in storm-influenced glaciomarine environments with proglacial channel complexes (Fig. 2G). Lower facies evidently were deposited whilst ice-margins were in direct contact with the Fitzroy Trough seaway (as shown by diamictites with striated clasts, ice-rafted debris; Fig. 2B). Upper facies associations record gradual retreat of ice from the northern Canning Basin with 'direct' evidence for glaciation generally diminishing up-sections. Extensive fossiliferous glaciomarine mudstone facies record maximum flooding in the Canning Basin, and were followed by progressive shoreline regression marked by fluvial-dominated delta systems (Figs. 2E, 2F and 2H). Paleocurrents and sedimentary structures from various intervals within the glaciomarine and deltaic successions, including intraformational striae and cross-bedding of stacked channel sandstones, record predominantly offshore directed (towards NW) axial sediment paleo-flow in the Fitzroy Trough (Fig. 4).

Implications for the regional glaciation model

Seismic and well interpretation provides important constraints on the Grant Group depositional and regional LPIA glaciation models. They indicate the Grant Group is dominantly a post-rift succession with deposition strongly influenced by pre-existing rift topography and glacial processes. Seismic mapping of glacially-eroded valleys and their sedimentary fill provide important constraints on paleo-ice flow directions and can facilitate correlation of detrital zircons with their source areas. There is good evidence for valley systems emanating from the basement areas flanking all margins of the Canning Basin, implying there is potential for a complex provenance model (Al-Hinaai & Redfern, 2015). Outcrop measurements further constrain provenance of the Grant Group, notably: 1) basin marginal striated **pavements** indicate ice advanced basinwards from the south and east, and 2) paleocurrent measurements from proglacial successions in the Fitzroy Trough indicate offshore-directed axial sediment transport from source areas in the east, possibly influenced by lateral sediment input from the south and north.

DETRITAL ZIRCON SAMPLE ANALYSES

Detrital zircons analysed for this study were from cored Grant Group intervals in the northern Canning Basin (Fig. 1). A total of 181 U–Pb ages were determined from three samples, with Hf isotope geochemistry performed on a sub-population of 117 zircons. Samples for zircon extraction were selected from a larger set following detrital heavy mineral petrography. Heavy minerals in all samples are dominated by garnet, tourmaline and zircon, and a wide variety of minor constituent minerals including anatase, apatite, and rutile (Table 1).

Sample DRO

Sample DRO is from a thick turbidite/density flow sandstone succession in petroleum well Drosera-1 (192.9 m) on the northern margin of the Crossland Platform (Fig. 1), interpreted as glacial gravity flow deposits released directly from an ice margin (Martin, 2008; Fig. 6). A total of 61 U–Pb zircon age determinations were obtained from this sample, ranging from 2828 to 306 Ma (Table 2; Fig. 8). Lu–Hf isotope geochemical analysis was applied to a sub-population of 41 zircons, yielding a wide variety of $^{176}Hf/^{177}Hf$ ratios corresponding with εHf values ranging from -22.1 – +14.4, and T_{DM} model ages of 3.04 – 0.72 Ga (Table 5; Fig. 9). Significant $^{207}Pb^{*}/^{206}Pb^{*}$ age populations include: 1) Paleoproterozoic to Early Mesoproterozoic (1796–1449 Ma), with εHf values of -3.8 – +8.3, and T_{DM} model ages of 2.22–1.72 Ga, and 2) Mesoproterozoic (1289–1164 Ma), with εHf values of -5.6 – +7.6, and T_{DM} model ages of 1.87–1.43 Ga. Late Neoproterozoic to Cambrian $^{206}Pb^{*}/^{238}U$ ages of 602–508 Ma also form a relatively significant population with εHf values of –22.2 – +0.9, and T_{DM} model ages of 1.93–1.11 Ga. Remaining zircon ages include a single Archean age, several Paleoproterozoic and Neoproterozoic ages, and four Devonian to Pennsylvanian ages. The youngest zircon from sample DRO (dro66c) has a $^{206}Pb^{*}/^{238}U$ age of 306±8 Ma (2σ, 96% concordant), εHf of -0.8, and T_{DM} model age of 0.94 Ga (Tables 2 and 5).

Sample CAP

Sample CAP is from a massive sandstone associated with matrix-supported diamictites in petroleum well Capparis-1 (106.9 m) on the Barbwire Terrace (Fig. 1), interpreted as glacial density flow deposits released directly from an ice margin (Martin, 2008; Fig. 6). A total of 60 U–Pb age determinations were obtained from CAP zircons, ranging from 2908 to 298 Ma (Table 2; Fig. 8). Lu–Hf isotope geochemical analysis applied to a sub-population of 39 zircons, yielded a wide variety of $^{176}Hf/^{177}Hf$ ratios corresponding with εHf values ranging from -21.3 – +10.4, and T_{DM} model ages from 3.25–1.05 Ga (Table 5; Fig. 9). Significant $^{207}Pb^{*}/^{206}Pb^{*}$ populations include, 1) Paleoproterozoic to Early Mesoproterozoic ages of 1802–1492 Ma with εHf values of -4.3 – +4.0, and T_{DM} model ages of 2.25–1.93 Ga, and 2) Mesoproterozoic ages of 1329–1086 Ma with εHf values of -10.2 – +5.7, and T_{DM} model ages of 2.03–1.38 Ga. Late Neoproterozoic to Devonian $^{206}Pb^{*}/^{238}U$ ages of 604–408 Ma, with εHf values of –21.3 – -1.1 and T_{DM} model ages of 1.93–1.16 Ga, also form a relatively significant population (Tables 2 and 5). Remaining zircon ages include a single Archean age, several Paleoproterozoic and Neoproterozoic ages, and several Mississippian to Early Permian ages. The youngest zircons from sample CAP (cap44b and cap103a) have $^{206}Pb^{*}/^{238}U$ ages of 298±6 Ma (82% concordant) and 304±8 Ma (94% concordant), with εHf values of -11.4 and -11.5, respectively and T_{DM} model ages of 1.35 Ga for both suggesting a common origin (Tables 3 and 4). Additional ablations for samples cap44b and cap103a yielded $^{206}Pb^{*}/^{238}U$ ages of 305±5 and 306±5 Ma, respectively. The weighted average U–Pb age for these four CAP ages is 303.8±2.8 Ma (Fig. 10).

Sample CYC

Sample CYC is from a cross-bedded sandstone succession in petroleum well Cycas-1 (999.6 m) in the Fitzroy Trough (Fig. 1), interpreted as a proglacial fluvial channel sandstone analogous to cross-bedded channel sandstones identified in the Grant Group outcrops at Grant Range (Martin, 2008; Figs. 2G & 6). A total of 60 U–Pb age determinations were obtained from CYC zircons, ranging from 3359 to 297 Ma (Table 2; Fig. 8). Lu–Hf isotope geochemical analysis was applied to a sub-population of 37 zircons, yielding a wide variety of $^{176}Hf/^{177}Hf$ ratios corresponding with εHf values ranging from -27.7 – +11.1, and T_{DM} model ages from 3.05–0.75 Ga (Table 5; Fig. 9). Significant $^{207}Pb^{*}/^{206}Pb^{*}$ populations include, 1) Paleoproterozoic to Early Mesoproterozoic ages of 1866–1472 Ma with εHf values of -3.6 – +7.6 and T_{DM} model ages of 2.38–1.77 Ga, and 2) Mesoproterozoic ages of 1374–1037 Ma with εHf values of -6.8 – +5.1 and T_{DM} model ages of 2.55–1.44 Ga. Remaining ages include several Archean to Early Paleoproterozoic, Neoproterozoic, and Cambrian to Early Permian ages. The youngest zircon from sample CYC (cyc78b) has a $^{206}Pb^{*}/^{238}U$ age of 297±7 Ma (2σ, 91% concordant; Table 2).

Detrital zircon age distribution summary

The U–Pb age probability distribution and U–Pb age versus εHf plots (Figs. 8 and 9) show two major populations: 1) zircons with Paleo- to Early Mesoproterozoic $^{207}Pb^{*}/^{206}Pb^{*}$ ages (1850–1450 Ma), εHf values from -4 to +8, and T_{DM} model ages of 2.4–1.7 Ga, and 2) zircons with Mesoproterozoic $^{207}Pb^{*}/^{206}Pb^{*}$ ages (1350–1050 Ma), εHf values from -11 to +6, and T_{DM} model ages of 2.6–1.4 Ga. Zircon $^{206}Pb^{*}/^{238}U$ ages < 1000 Ma are also relatively abundant in all samples (total N = 58; Table 2; Figs. 7 and 8). Hf isotope data for these grains is defined by an array of highly negative to low positive εHf values (Table 5). Zircons with Archean to Paleoproterozoic $^{207}Pb^{*}/^{206}Pb^{*}$ ages of c. 3350–1900 are very scarce in all samples.

DETRITAL ZIRCON CORRELATION WITH POTENTIAL SOURCE AREAS

Archean detritus

DESCRIPTION

Archean zircons are generally rounded and their textures reveal a relatively complex history with igneous growth zoning, convoluted by late-to-post magmatic recrystallization (Fig. 5A). They all have thin, variably homogeneous and zoned rim phases presumably formed by a later metamorphic or magmatic event, and some have xenocrystic cores. Rims and cores are too small to ablate without overlapping with other phases.

ARCHEAN PB-PB CRYSTALLISATION AGES

Only five detrital zircons from this dataset have Archean crystallization ages, with $^{207}Pb^{*}/^{206}Pb^{*}$ ages of 3359–2858 Ma (Table 2; Figs. 7 and 8). These are broadly similar to ages from the Pilbara and Yilgarn cratons that record several tectonic episodes spanning ~3.5 – 2.8 Ga with inherited zircons up to ~3.72 Ga (e.g. Hickman, 2004; Van Kronendonk et al., 2007). Archean detrital and inherited zircons are also reported from meta-sedimentary and –igneous units of the Capricorn Orogen, Hamersley Basin and Rudall Complex, which also lie south of the Canning Basin (Fig. 1; Neumann and Fraser, 2007). To the north of the Canning Basin, primary Archean basement exposures are limited, although geophysical surveys indicate the North Australian Craton is widespread in the subsurface of the region. Archean outcrops are present within the Neoarchean Pine Creek Orogen, although their age (2.67–2.5 Ga) is younger than the Canning Basin detrital zircons (Worden et al., 2008; Hollis et al., 2009).

In addition, detrital zircons with ages of ≤ 2.55 Ga are reported from the Hooper Complex in the Kimberley region (Tyler et al., 1999), and several detrital ages of 3.12 – 3.68 Ga from the Paleoproterozoic Crater Formation in the Pine Creek Orogen (Hollis et al., 2010). An imprecise Re–Os isochron age of ~ 3.4 Ga has also been recorded from xenoliths and chromites of the Kimberley region (Graham et al., 1999). Neoarchean crystallization ages equivalent to those from the Pine Creek Orogen are also reported from areas east of the Canning Basin in the Tanami Billabong Complex (Joly et al., 2013 and references therein).

ARCHEAN T_{DM} MODEL AGES AND εHF VALUES

Hf isotope data for several detrital zircon samples analysed have εHf values from -3.4 to +5.5 and T_{DM} model ages of 3.25–3.04 Ga (Table 5). Sample cyc1a has similar $^{207}Pb^*/^{206}Pb^*$ and T_{DM} model ages and positive εHf values suggesting it formed from primitive melts closely approximating the crystallization age (Fig. 9). Low negative εHf values indicate remelting and/or mixing of older Archean crust during crystallization (Kinny and Maas, 2003). Potential source areas with similar Nd isotope characteristics, albeit with only positive εNd values, are reported from various units of the Western and Eastern Pilbara terranes (Van Kronendonk et al., 2007). Hf isotope data from the Yilgarn Craton also has similar εHf values and T_{DM} model ages as the Canning Basin detrital zircons, including low negative εHf values (Griffin et al., 2004; Ivanic et al., 2013). In the Pine Creek Orogen, magmatic zircons with 2.67–2.5 Ga crystallization ages from the granitic Nimbuwah Domain have εHf values from -8.9 to 3.4 and T_{DM} model ages of 3.65 – 3 Ga. By comparison, detrital zircons with 3.68–3.12 Ga U-Pb crystallization ages have εHf values between -5.7 and -0.3 and T_{DM} model ages of ~ 4–3 Ga (Hollis et al., 2010).

IMPLICATIONS FOR SOURCE AREA CORRELATION

Archean detrital zircons constitute only a minor component of the total dataset hence it is apparent that Archean cratons were not significant sediment source areas for the northern Canning Basin. This is despite striated **pavements** and tunnel valleys clearly indicating the Early Permian ice sheet advanced northwards from the Pilbara region into the Canning Basin (e.g. Fig. 2A). It is not possible with available isotopic data to distinguish whether Grant detrital zircons came from Archean basement to the south, north or east of the Canning Basin, and/or from recycling of detrital grains.

Paleoproterozoic to Lower Mesoproterozoic detritus

DESCRIPTION

Zircons with Paleo- to Early Mesoproterozoic $^{207}Pb^{*}/^{206}Pb^{*}$ ages have a diverse range of textures of both igneous and metamorphic origin, with many recording a complex crystallization history. Igneous zircons vary considerably with homogeneous centres passing into zoned margins, fine oscillatory zoning sometimes with truncation surfaces formed during resorption, acicular grains with a relatively muted CL response (Fig. 5B), and convoluted zoning related with post-to-late magmatic recrystallization (Corfu et al., 2003). Xenocrysts in many grains commonly are surrounded by new magmatic zircon growth (Fig. 5C). Homogeneous rim overgrowths are also present. Grain morphology is relatively varied with preservation of terminations on some whereas others appear more rounded. It is difficult to deduce if older rounded grains came from primary sources or were reworked, as rounded zircons can also develop from in-situ growth of metamorphic rims around euhedral magmatic grains (Corfu et al., 2003).

PALEOPROTEROZOIC TO LOWER MESOPROTEROZOIC PB-PB CRYSTALLISATION AGES

Paleo- to Early Mesoproterozoic $^{207}Pb^{*}/^{206}Pb^{*}$ ages of ~1800–1450 Ma constitute a major component of the total dataset within all three samples analysed (Table 2). Although relative abundances of such ages varies slightly between samples, all are characterized by age spikes of ~1765–1715, 1660–1600 and 1555–1550 Ma (Figs. 8 and 9). Paleoproterozoic $^{207}Pb^{*}/^{206}Pb^{*}$ ages > 1900 Ma are scarce in all three samples, with only several scattered ages between ~2385 Ma and ~1919 Ma recorded in the three samples. Sample CYC has three $^{207}Pb^{*}/^{206}Pb^{*}$ ages between ~1890 Ma and ~1865 Ma that are not present in samples CAP and DRO (Table 2).

Paleoproterozoic zircon-forming events of c. 1.8–1.7 Ga are widely reported from basement terranes adjacent to the Canning Basin. To the north, these include a ~1.79 Ga intrusive event from the Halls Creek Orogen, Tanami granite intrusion at ~ 1.82–1.79 Ga (Sener et al., 2005), the ~1.71 Ga Devils Suite granites and dykes from the Tennant region and the ~1.8–1.75 Ga Shoobridge Event in the Pine Creek Orogen. East of the basin, these include the 1.81–1.80 Ga Stafford and 1.74–1.69 Ga Strangeways events from the Arunta Inlier (Giles et al. 2004; Maidment et al., 2005; Hoatson et al., 2005) and, to the south, the ~1.83–1.79 Ga Capricorn Orogeny (Cawood and Tyler, 2004) and the ~1.80–1.76 Ga Yapungku Orogeny from the Rudall Complex (Bagas, 2004). Grant Group detrital zircons with 1.8–1.7 Ga Pb–Pb ages could be sourced from any of these basement terranes, which make direct correlation with Pb–Pb ages alone difficult.

Ages of 1.69 – 1.52 Ga that correspond with age spikes at c. 1550 Ma in all three samples, and age spikes at c. 1660 in samples CAP and CYC (Table 2), are widely reported from basement terranes to the east and south of the Canning Basin. To the east, they are equivalent with the c. 1.69–1.63 Ga Liepig Event, the c. 1.59–1.57 Ga Chewings Event and several other igneous events of the Arunta Inlier (Collins et al., 1995; Rubatto et al., 2001; Hoatson et al., 2005), volcanics in the Limbunyah Group of the Tanami Region dated at c. 1.64 Ga, and c. 1.60–1.54 Ga protoliths of the Musgrave Block (White et al., 1999; Neumann and Fraser, 2007; Wade et al., 2005, 2006). To the south of the Canning Basin, these ages are equivalent with the c. 1.68–1.62 Ga Mangaroon Orogeny of the Capricorn Orogen, and c. 1.59–1.55 Ga Tabletop Intrusives of the Rudall Complex (Neumann and Fraser, 2007). Ages of 1690–1520 Ma ages are not widely recorded from basement terranes to the north of the Canning Basin; the exceptions are recorded from several igneous intrusive bodies in the Pine Creek Orogen dated at ~1.72–1.60 Ga (Neumann and Fraser, 2007). Early Mesoproterozoic magmatic events are also widely reported from terranes of central and eastern Australia, including the Gawler Craton, Curnamona Province, and Georgetown and Mount Isa Inliers (Betts et al., 2002, 2006; Giles et al., 2004).

In basement terranes surrounding the Canning Basin, zircons > 1800 Ma are less widespread than those of < 1800 Ma. A cluster of three ages between ~ 1890 Ma and 1865 Ma in sample CYC possibly corresponds to the Hooper Orogeny, recorded in the Halls Creek and King Leopold orogens, and the Nimbuwah Event, in the Pine Creek Orogen (Bodorokos et al., 1999; Griffin et al., 2000). Basement terranes in Western Australia with Paleoproterozoic zircon-forming events > 1900 Ma include the Capricorn Orogen, which records a wide range of igneous and metamorphic events at ~ 2.55–1.62 Ga (Cawood and Tyler, 2004; Griffin et al., 2004), and, to lesser extents, the Halls Creek Orogen, with igneous intrusions dated at ~ 1.91 Ga (Bodorokos et al., 1999), and the Pine Creek Orogen, with igneous intrusions of ~ 2.47 and 2.02 Ga (Hollis et al., 2010).

PALEOPROTEROZOIC TO LOWER MESOPROTEROZOIC T_{DM} MODEL AGES AND εHF VALUES

Paleoproterozoic detrital zircons with 1.79–1.61 Ga Pb–Pb ages have low negative and positive εHf values and Paleoproterozoic Hf T_{DM} model ages > 1.9 Ga (Fig. 9) indicating they were derived from partially juvenile melts which assimilated variable amounts of evolved, continental crust. Many of these are equivalent to available Hf and Nd isotope data from subduction, back-arc and intracontinental intrusions of the Arunta Inlier (Zhao and McCulloch, 1993, 1995; Sun et al., 1995; Hoatson et al., 2005; Hollis et al., 2013), with some of the older grains (~1800–1760 Ma Pb–Pb) slightly overlapping with Lu–Hf data from the Capricorn Orogen, Rudall Complex and Hall's Creek Orogen (Fig. 11; Griffin et al., 2004; Kirkland et al., 2013). Other Paleoproterozoic detrital zircons have crystallization ages > 1800 Ma but constitute only isolated samples hence have limited correlative potential. These include a cluster of several grains with 1830–1810 Ma Pb–Pb ages with εHf values from -3.5 to +1.0 and ~ 2.21 – 2.17 Ga Hf T_{DM} model ages that overlap with Lu–Hf data from potential source regions to the east (Arunta; Hollis et al., 2013), south (Rudall; Kirkland et al., 2013) and north (Kimberley and Hall's Creek Orogen; Griffin et al., 2000; Sheppard et al., 2001; Downes et al., 2007) of the Canning Basin. A couple of older Paleoproterozoic grains have moderately negative εHf values and Neoarchean Hf T_{DM} model ages (Fig. 9).

Early Mesoproterozoic detrital zircons with ~1600–1500 Ma Pb–Pb ages have low positive and negative εHf values and Paleoproterozoic model ages that are correlative with several potential source terranes flanking the basin, including Hf and Nd isotope data from the

Musgrave Block (Wade et al., 2006; Kirkland et al., 2012), Rudall Complex (Kirkland et al., 2013) and Yilgarn (Griffin et al., 2004; Fig. 11). Farther afield in Queensland, Hf isotope data from Mt Isa Inlier for zircons with U–Pb ages of 1590–1540 Ma yield a variety of positive and negative εHf values, with a major peak of +3 (Griffin et al., 2006).

IMPLICATIONS FOR SOURCE AREA CORRELATION

Overlapping Pb–Pb and Lu–Hf values between Grant Group detrital zircons and data from various basement terranes flanking the Canning Basin suggest candidate source terranes to the east, south and north of the basin. This can be further constrained using three key observations: 1) the overall paucity of Pb–Pb ages > 1900 Ma suggests terranes to the south and to the north of the Canning Basin were not principal source areas, 2) Grant Group detrital zircons with ~1700–1600 Ma Pb–Pb ages have Hf isotopic data very similar to Hf and Nd isotopic data reported from the Arunta Inlier (Zhao and McCulloch, 1993, 1995; Sun et al., 1995; Hoatson et al., 2005; Hollis et al., 2013) and 3), Pb–Pb ages of ~ 1890–1865 Ma in Fitzroy Trough sample CYC may be correlated with terranes to the north of the Canning Basin, although reworking of detrital zircons of similar ages reported from other areas cannot be ruled out (Claoué-Long et al., 2008).

Mesoproterozoic detritus

DESCRIPTION

Zircons with c. 1350–1050 Ma Mesoproterozoic $^{207}Pb^{*}/^{206}Pb^{*}$ ages have both igneous and metamorphic textures, with some recording a complex crystallization history. Textures observed include growth zoning, sometimes as a relatively homogeneous core conformably succeeded by oscillatory zoned margins (Fig. 5D), occasionally with evidence for resorption and late-to-post magmatic (possibly metamorphic) recrystallization. Xenocrystic cores are present in several grains, encased by new magmatic zircon with distinct growth zoning (Fig. 5E). In such cases, the younger phase was ablated when possible. Several grains have rims that may represent a younger metamorphic or magmatic event, although they are too thin to analyse. Rims are often homogeneous, although zoned igneous rims were also observed (Fig. 5F).

MESOPROTEROZOIC PB-PB CRYSTALLISATION AGES

Detrital zircons with Mesoproterozoic Pb–Pb ages of 1350–1050 Ma are abundant in all Canning Basin samples and correspond with an age spike at c. 1150 Ma in all three samples, and an age spike at c. 1090 Ma in samples CAP and CYC (Table 2; Fig. 9).

1350–1050 Ma ages are equivalent with major Grenvillian events in the Musgrave Block, including widespread granitoid intrusion dated at c. 1.18–1.15 Ga during the Musgrave Orogeny, a younger phase of felsic magmatism, mafic dyke intrusion and metamorphism of c. 1.09–1.07 Ga and the magmatic Giles Event at 1.08–1.04 Ga (Camacho and Fanning, 1995; White et al., 1999; Schmidt et al., 2006). Other Grenvillian-aged events include dyke intrusion in the Arunta Inlier (Zhao and McCulloch, 1993) and, to the south of the Canning Basin, 1.29 Ga pegmatites and a 1.22 Ga microgneiss in the Connaughton Terrane of the Rudall Complex (Neumann and Fraser, 2007). To the north, 1.32 Ga mafic magmatism is reported from the Arnhem Shelf (Neumann and Fraser, 2007).

MESOPROTEROZOIC T_{DM} MODEL AGES AND εHF VALUES

Lu–Hf isotope data indicates Grant Group detrital zircons with Mesoproterozoic crystallization ages broadly cluster into two groups: an older Early Mesoproterozoic group described above, and a younger group with 1350–1050 Ma Pb–Pb ages, predominantly low positive and negative εHf values and Mesoproterozoic model ages (Fig. 9). This latter group strongly correlates with Hf and Nd isotope data from various units with equivalent Pb–Pb ages in the Musgrave Block, with some of the older grains having mild overlap with Hf data from the Yilgarn (Fig. 11; Zhao et al., 1992; Zhao and McCulloch, 1993; Nelson et al., 1995; Griffin et al., 2004; Wade et al., 2005, 2006; Kirkland et al., 2012).

IMPLICATIONS FOR SOURCE AREA CORRELATION

Pb–Pb and Lu–Hf isotopic data suggests Early to Middle Mesoproterozoic detrital zircons were sourced predominantly from the Musgrave Block to the SE of the Canning Basin. A couple of older zircons show overlap with Hf data from more evolved source terranes in the Yilgarn.

Neoproterozoic to Cambrian detritus

DESCRIPTION

Zircons with c. 600–500 Ma Neoproterozoic and Cambrian $^{206}Pb^{*}/^{238}U$ ages have zoned textures indicative of an igneous origin whereas others appear homogeneous suggesting a possible metamorphic origin. Zoning varies in both CL intensity and width, with both thicker bands and fine oscillatory zoning sometimes present within the same grain (Fig. 5C). Truncations within zoned grains are also relatively common, indicating resorption during recrystallization (Corfu et al., 2003). Thin metamorphic rims are present on several grains.

NEOPROTEROZOIC TO CAMBRIAN PB-PB CRYSTALLISATION AGES

Detrital zircons with Neoproterozoic and Cambrian $^{206}Pb^{*}/^{238}U$ ages are a significant population in all samples (Table 2; Figs. 7 and 8). Many of the ages are > 10% discordant, as is typical for relatively young grains containing limited amounts of radiogenic Pb. Samples DRO and CAP are characterized by two broad populations with U–Pb ages between c. 965–745 Ma and c. 600–510 Ma that are less abundant in sample CYC (Table 2).

Potential source areas for Neoproterozoic detrital zircons > 745 Ma lie to the east and south of the Canning Basin. These include the c. 825 Ma Gairdner and Amata dolerite dykes intruded throughout the Musgrave Block and Gawler Craton during inception of the Centralian Superbasin (Aitken and Betts, 2009; de Vries et al., 2008; Evins et al., 2010), the c. 1000 Ma Kullal Dolerite (Aitken and Betts, 2009; Evins et al., 2010) and a 980 Ma spike in the population of detrital zircons from an Irindina Gneiss metapelite in the Arunta (Buick et al., 2005). In the Capricorn Orogen, the intracratonic 1070–750 Ma Edmundian Orogeny deformed the Edmund and Collier Basins with pre- and post-deformation mafic intrusions of this age constraining the age (Cawood and Tyler, 2004). Ar–Ar mica ages of 960–820 Ma from several terranes of the Capricorn Orogen indicate regional early greenschist metamorphic conditions (Occhipinti and Reddy, 2009), but it is uncertain if this was a primary zircon-forming event. The Mundine Well dyke swarm is dated at c. 755 Ma along the NW margin of the Yilgarn Craton, and the west margin of the Pilbara Craton (reference in de Vries et al., 2008).

Potential source areas for Neoproterozoic–Cambrian detrital zircons < 600 Ma near the Canning Basin include the Paterson and Peterman Orogens to the south and east, and the King Leopold Orogen to the north, all of which record crustal shortening in the Late Neoproterozoic and Early Cambrian (c. 600–530 Ma; Maboko et al., 1992; Scrimgeour et al., 1999; Betts et al., 2002; Bagas, 2004; Veevers, 2004; Wade et al., 2005; de Vries et al., 2008; Evins et al., 2010). Other igneous events reported from Western Australia include Cambrian volcanic rocks of the c. 520–500 Ma Kalkarinji Large Igneous Province (Buick et al., 2005), the Boyagin dyke swarm along the western Yilgarn Craton (578–548 Ma), granites in the Paterson Orogen (631–622 Ma), granitoid and dyke intrusions at 540–520 Ma within the Leeuwin Complex (Wilde, 1999; Collins, 2003; Fitzsimons, 2003), and several doleritic intrustions (513–500 Ma; Veevers, 2004). Elsewhere in Australia, 600–500 Ma U–Pb ages are widely distributed in central (Hart's Range, Arunta Inlier; Veevers, 2004), and southern and eastern areas (Delamarian Orogeny; Glen, 2005) during an extensive late Neoproterozic to Cambrian orogenic phase in East Gondwana, with equivalent terranes in Antarctica (Veevers, 2004). Furthermore, detrital zircon studies of Permian and modern sediments confirm their abundance in Western Australia (Sircombe and Freeman, 1999; Cawood and Nemchin, 2000; Veevers et al., 2005).

NEOPROTEROZOIC TO CAMBRIAN T_{DM} MODEL AGES AND εHF VALUES

Lu–Hf isotope data indicates Neoproterozoic to Cambrian detrital zircons have predominantly low positive and negative εHf values with Mesoproterozoic model ages (Fig. 9). Several grains with more complex textures have highly negative εHf values with model ages > 2.0 Ga. Overall when compared with the relatively limited published Lu–Hf dataset from potential source terranes, the Grant Group detrital zircons show overlap with a range of samples from the Musgrave, Yilgarn and Officer Basin (Fig. 11; Zhao & McCulloch, 1993; Griffin et al., 2004; Wade et al., 2005; Kirkland et al., 2012). However, given the paucity of Hf–Nd data from other potential basement terranes, it is difficult to make confident interpretation of source area correlation.

IMPLICATIONS FOR SOURCE AREA CORRELATION

Although Neoproterozoic–Cambrian U–Pb ages form a relatively significant population of the total Grant Group detrital zircon dataset, scattered ages imply they were not sourced from a single principal source area. Given their ubiquity in basement terranes in Western Australia and beyond, together with the limited availability of equivalent Hf–Nd data, no significant conclusions can be made with respect to source area correlation. The only general observation that can be made is that Grant Grout detrital zircons of this age are more abundant in the Crossland Platform and Barbwire Terrace samples DRO and CAP relative to the Fitzroy Trough sample CYC (Fig. 9).

Ordovician to Lower Permian detritus

DESCRIPTION

Younger Phanerozoic zircons ranging from Ordovician to Early Permian are exclusively of igneous origin, with predominantly euhedral, prismatic forms, occasionally sub-rounded, and growth zoning which sometimes grade from thicker bands in the centre to fine oscillatory zoning at the margins (Fig. 5B).

ORDOVICIAN TO LOWER PERMIAN U-PB CRYSTALLISATION AGES

Detrital zircons with Ordovician to earliest Permian $^{206}Pb^{*}/^{238}U$ ages between c. 490 Ma and 297 Ma are present in all three samples, particularly samples CYC and CAP (Table 2). Dates from the youngest grains measured are within 2σ error of the biostratigraphic age of the host sediments, implying they approximate 'first-cycle' detritus. Zircon-forming events of this age are widely reported from central Australia where the Arunta Inlier underwent granulite facies metamorphism during the Early Ordovician prior to being exhumed during the Devonian–Carboniferous Alice Springs Orogeny. The Harts Range Metamorphic Complex experienced peak metamorphism at c. 470 Ma (the Larapinta Event of Hand et al. 1999) in the Irindina Gneiss and Harts Range Meta-Igneous Complex (Hand et al. 1999; Mawby et al. 1999; Buick et al. 2001, 2008). Overgrowths from several units have yielded U–Pb ages of c. 452 and 484 Ma (Buick et al., 2005). This was followed by intrusion of basaltic dykes during extension that terminated with onset of the Alice Springs Orogeny at c. 450 Ma (Buick et al., 2005). Inherited zircons with c. 387 Ma U–Pb ages are dated from granite intrusives in the Harts Range (Buick et al., 2005). Younger (c. 330 Ma) zircon overgrowths are interpreted as the maximum age of amphibolite-grade metamorphism in Hart's Range (Hand et al., 1999). However, Canning Basin detrital zircons with these ages are relatively euhedral and of magmatic rather than metamorphic origin (e.g. Fig. 5A), suggesting another source. SHRIMP U–Pb monazite and zircon ages of c. 450–300 Ma from numerous pegmatites that cross-cut the Harts Range Metamorphic Complex and Entia Gneiss Complex record episodic emplacement throughout the duration of the Alice Springs Orogeny in central Australia (Buick et al., 2008). Similarly aged zircon-forming events have not, to our knowledge, been reported elsewhere in the immediate vicinity of the Canning Basin or Western Australia.

Potential source areas elsewhere in Australia include the Big Lake Granites of the Cooper Basin, dated at c. 330–300 Ma (Ito, 2010), and terranes of the Delamerian Orogen (515–490 Ma), Lachlan Fold Belt (485–340 Ma), and New England Orogen (305–230 Ma), collectively referred to as the "Tasmanides", which record a protracted period of arc-related magmatic activity throughout the Paleozoic to Early Mesozoic (Fig. 1; Betts et al., 2002; Glen, 2005; Kemp et al., 2007). Terranes equivalent with the Tasmanides of eastern Australia are present in Marie Byrd Land of Antarctica but not from present-day East Antarctica that adjoined SW Australia during the LPIA (Veevers, 2004). Carboniferous plutons and volcanics are associated with incipient rifting between Australia and India/Himalaya in northern India (Veevers and Tewari, 1995). Phanerozoic detrital zircons from the Permian (Artinskian to Roadian) of the Perth Basin were inferred by Cawood and Nemchin (2000) as having a probable western or southern source, although specific terranes were not named.

ORDOVICIAN TO LOWER PERMIAN T_{DM} MODEL AGES AND εHF VALUES

Hf isotope data for Ordovician to Early Permian detrital zircons suggests their sources formed from both relatively juvenile, mantle-derived crust and older, more evolved Proterozoic crust (Table 5; Fig. 9). To our knowledge, there is no published Hf or Nd data from potential Paleozoic source terranes near the Canning Basin. Hf isotope data from various Tasmanide units have yielded a variety of εHf values ranging from highly positive to negative similar to those recorded from Canning Basin detrital zircons (Belousova et al., 2006; Hawkesworth and Kemp, 2006; Offler and Shaw, 2006; Kemp et al., 2007). However, very low εHf values have not been reported from the Tasmanides (e.g. Betts et al., 2002). Furthermore, Kemp et al. (2007) reported increasingly juvenile isotopic compositions from the Delemarian Orogeny adjacent to cratons towards the outboard and younger New England Orogeny that contains minimal cratonic material. This suggests the youngest Grant Group detrital zircons with ages equivalent to the earliest stages of the New England Orogeny were most likely derived from more isotopically-evolved source terranes, such as late intrusions associated with the Alice Springs Orogeny in central Australia (e.g. Buick et al., 2008).

IMPLICATIONS FOR SOURCE AREA CORRELATION

Detrital zircon U–Pb ages are broadly equivalent with Ordovician to Late Carboniferous metamorphic and igneous events of central Australia, particularly in the Arunta Inlier, as well as Tasmanide events in eastern Australia. Grant Group Hf isotope data overlap with both these potential source areas but the presence of young zircons that originated from evolved crust suggests an Arunta Inlier source area is more likely.

DISCUSSION

Correlation of detrital zircons with potential source areas

EASTERN SOURCE AREAS

Paleo- and Mesoproterozoic detrital zircons with Pb–Pb crystallization ages between c.1870–1450 and 1375–1035 Ma dominate the three samples. These Pb–Pb ages, together with associated εHf and Hf model ages, are widely comparable to published data from the Arunta Inlier and Musgrave Block suggesting eastern basement terranes were the principal source areas for the Grant Group in the northern Canning Basin. Remaining uncertainties include whether Paleoproterozoic zircons from the Rudall Complex have a similar or different

Hf-isotopic signature to those from the Arunta Inlier, and the source of a minor population of Mesoproterozoic detrital zircons with a Lu–Hf composition more evolved than that reported from the Musgrave Block. Alternative source areas with similar Mesoproterozoic crystallization ages include the Kimberley, Arunta and Rudall basement terranes. Further Lu–Hf or Sm–Nd dating of these terranes is required to adequately address these provenance uncertainties.

Further evidence for eastern basement terranes being principal source areas is the population of late Paleozoic detrital zircons in all samples, which is consistent with measurements from striated **pavements** measurements showing paleo-ice flow to the west in central Australia (Haines et al., 2011). Sediment eroded and entrained within ice eroding the central Australian uplands were subsequently deposited within proglacial environments with an axial component of sediment routing along the NW–SE Fitzroy Trough (as shown by paleocurrents recorded from Grant Group outcrops along the Fitzroy River; Fig. 4). Detrital zircon U–Pb ages are broadly equivalent with the timing of Ordovician to latest Carboniferous metamorphic and igneous events of central Australia, particularly those of the Alice Springs Orogeny recorded within the Arunta Inlier. Comparable Paleozoic zircon-forming events are unknown elsewhere in Western Australia. The closest alternative source areas lie farther east and associated with the orogenic events related with subduction along Australia's paleo-Pacific margin recorded within the Delamarian, Lachlan and New England orogens (e.g. Betts et al., 2002; Glen, 2005). Whereas Hf isotope data for these young detrital zircons are partly comparable with eastern basement terranes (Belousova et al., 2006; Hawkesworth and Kemp, 2006; Offler and Shaw, 2006; Kemp et al., 2007), the εHf and Hf model ages for the Grant Group samples reveal a more evolved crustal signature unlike that in eastern Australia but consistent with the Arunta Inlier.

SOUTHERN SOURCE AREAS

Despite striated **pavements** clearly indicating that an Early Permian ice sheet advanced northwards from the Pilbara–Yilgarn cratons into the Canning Basin (e.g. Fig. 2A), detrital zircons with Archean ages constitute only a minor component of the total dataset. It is not possible to differentiate between Archean source areas to the south and reworked detrital grains from the north (Kimberley) based on U–Pb ages alone. Hf data from several Grant zircons are similar to published data from the Pilbara–Yilgarn cratons, raising the possibility they were ultimately sourced from that region (Fig. 11). However, it is apparent that Archean cratons were not significant source areas for the Grant Group in the northern Canning Basin. There is also a similar paucity in Archean detrital zircons from younger, post-glacial Permian successions of the Perth Basin (Artinskian Irwin River Coal Measures; Cawood and Nemchin, 2000; and Artinskian to Wuchiapingian Collie Coal Measures; Veevers et al., 2005), despite their proximity to the Yilgarn Craton. **Nevertheless, Dillinger et al. (2018) found significant Archean zircons in samples from the Irwin River Coal Measures but only in those close to the Yilgarn Craton.** Apatite fission track studies demonstrate a regional cooling episode over the northern Yilgarn Craton that commenced in the Late Carboniferous to Early Permian and continued until the Late Jurassic to Early Cretaceous times, which suggests several kilometres of denudation of sedimentary cover overlying the craton (Kohn et al., 2002; Weber et al., 2005). The paucity of Archean detrital zircons in the northern Canning Basin samples may therefore be due to the **Pilbara Craton** not being exposed during deposition of the Grant Group. Possible alternative explanations are: Archean zircons from south of the Canning Basin were transported into areas now situated offshore NW Australia (consistent with directions measured from striae in the Pilbara), or not transported farther north than the Kidson

Sub-basin, or their relative abundance in the northern Canning Basin was diluted by the volume of detritus eroded from central Australian cratonic areas during Carboniferous uplift.

NORTHERN SOURCE AREAS

Generally, there are few detrital zircons in this dataset that can be correlated confidently with basement terranes north of the Canning Basin. The notable exception is the small population of c. 1890–1865 Ma detrital zircons in sample CYC that are equivalent to the Hooper Orogeny ages in the Halls Creek and King Leopold orogens, and the Nimbuwah Event in the Pine Creek Orogen. Their absence in samples DRO and CAP, from the Crossland Platform and Barbwire Terrace, implies sediment routing from the north did not extend farther south than the Fitzroy Trough, which is consistent with the structural configuration of the basin. However, this apparent paucity of northern source area detritus contradicts seismic evidence for major glacially incised valleys and associated channel systems along the northern margins of the Canning Basin (e.g. O'Brien et al., 1998; Al-Hinaai & Redfern, 2015) and in the southern Bonaparte Basin (Gorter et al., 2008). Further sampling from locations within the Lennard Shelf and Fitzroy Trough is required to identify and understand lateral sediment input routes into the basin.

Implications for scale and timing of Early Permian glaciation in Australia

There is abundant stratigraphic, sedimentological and seismic evidence for Early Permian glaciation in western and central Australian basins (Redfern, 1990; Martin et al., 2007; Gorter et al., 2008; Mory et al., 2008; Al-Hinaai & Redfern, 2015). From these and the current study, it is clear that Early Permian ice sheets over different cratonic uplands of Western and central

Australia advanced basinwards during glacial phases (Fig. 12B). This is contrary to earlier models that invoked a single continental-scale ice sheet that advanced northward across the region (e.g. Playford, 2002). It is not possible to determine if individual ice sheets coalesced during maxima phases but, for the Early Permian at least, these combined datasets suggest multiple rather than unidirectional paleo-ice transport directions across the Canning Basin towards the episodically marine Fitzroy Trough and presumably eventually into basinal areas now lying along the North West Shelf.

This interpretation is supported by data from eastern Australia that suggests limited or no glaciation in the late Pennsylvanian followed by protracted glaciation in the Early Permian spanning 299–290 Ma, interpreted by Fielding et al. (2008) as peak glaciation in eastern Australia. This is broadly consistent with two very low diversity brachiopod and bivalve faunal assemblages from the Asselian in eastern Australia (Waterhouse and Shi, 2013) Additionally, stable isotope data for the Early Permian indicate significant global cooling during the Asselian followed by deglaciation in the early Sakmarian. This data includes the $^{87}Sr/^{86}Sr$ seawater curve for the Permian which declines from a maximum in the Asselian through the Sakmarian (Korte et al., 2006), a trend similarly reflected by the $\delta^{18}O$ curve (Gradstein et al., 2012), and estimations of pCO_2, which indicate maximum expansion of Gondwanan ice sheets in the Asselian (Montañez et al., 2007). Detrital zircon evidence for a continental-scale ice sheet in Australia outlined in this paper is consistent with these independent datasets and provides further evidence for significant climate cooling at the onset of, or just prior to, the Permian.

The youngest detrital zircons from this dataset provide a maximum depositional age for the glaciogenic Grant Group, thereby constraining the maximum age of continental ice sheet development. The youngest zircon from this dataset (cyc78b) has a $^{206}Pb^{*}/^{238}U$ age of 297±7 Ma (2σ, 91% concordant; Table 2), giving an imprecise maximum range of late Kasimovian to Asselian. The youngest zircons from sample CAP (cap44b and cap103a) have a weighted average $^{206}Pb^{*}/^{238}U$ age of 303.8±2.8 Ma, giving a maximum age range of Kasimovian to Gzhelian (Fig. 10). These Grant Group samples therefore constrain the onset of contemporaneous glaciation to a maximum age of Kasimovian, but possibly ranging into the Asselian. In the future, more and increasingly accurate zircon dating methodologies should be able to constrain this better (e.g. Griffis et al., 2018).

Timing of deglaciation is constrained by the biostratigraphic age of the ?Gzhelian to lower Sakmarian Grant Group (*P. confluens* and possibly *M. tentula* palynozones; Apak and Backhouse, 1998, 1999; Mory, 2010), with an upper limit provided by the overlying post-glacial upper Sakmarian to Artinskian Poole Sandstone (*P. pseudoreticulata* and *S. fucus* palynozones; Archbold, 1999; Haig et al., 2014). The boundary between *P. confluens* and *P. pseudoreticulata* corresponds with an absolute age of c. 290 Ma, making the Grant Group broadly equivalent with Fielding et al.'s (2008) P1 glacial phase in eastern Australia (Fig. 3). Deglaciation was marked by extensive proglacial sedimentation as glacial detritus previously stored in the ice sheets was carried by meltwaters into basinal areas. Up to several kilometres of Lower Permian glacial successions, including the Grant Group, are preserved in Western Australian basins and attest to significant influx of glacial meltwater and sediment (Mory et al., 2008). There is only limited evidence for glacial conditions persisting beyond the Sakmarian in Western Australia. Eyles et al. (2006) reported ice-rafted debris and cold-water fauna within mudstones of the Carynginia Formation (Kungurian) of the Perth Basin, **and Haig et al. (2017) noted dropstones in equivalent strata from the Southern Carnarvon Basin**, implying a seasonally cold climate. This contrasts with eastern Australia, where three discrete glacial epochs following peak glaciation in the Early Permian are identified across several basins in New South Wales and Queensland (e.g. Sydney, Bowen and Gunnedah basins) with glaciomarine deposits containing ice-rafted debris and glendonites in strata as young as Capitanian (Jones et al., 2006; Birgenheier et al., 2007; Fielding et al., 2008). Furthermore, Waterhouse and Shi (2013) were able to define six cold Permian climatic periods up to the Changhsingian from low diversity faunal assemblages in eastern Australia and New Zealand.

Implications for scale and timing of Carboniferous glaciation in Australia

Current regional models for the LPIA in eastern Australian basins show four discrete glacial phases between the c. Serpukhovian and Moscovian followed by a Kasimovian–Gzhelian inter-glacial phase, based on sedimentological and biostratigraphic data with absolute ages partially constrained by U–Pb dating of tuffs (Roberts et al., 1995; Jones and Fielding, 2004; Fielding et al., 2008). In central and Western Australian basins, onset of mid-Carboniferous (c. Visean) ice sheet growth is inferred from the timing of central Australian uplift associated with the Alice Springs Orogeny, palynological ages based dating of possible glaciogenic successions and associated lacunas, and far-field cyclothemic sedimentations patterns (Eyles et al., 2006; Veevers, 2009). However, although these are valid circumstantial reasons to explain the onset of glaciation in the mid-Carboniferous, there is very limited direct evidence for glaciation reported, such as classic glacial sedimentary facies, nor are there any absolute age constraints such as those applied in eastern Australia and elsewhere in Gondwana (e.g. Griffis et al., 2018). This issue is compounded by an apparent absence of tuffs or other intraformational volcanics within mid-Carboniferous successions of western and central Australian basins. Some Western Australian post-glacial successions do have dateable volcanics, but these are stratigraphically younger and do not yet provide age constraints on the LPIA (Mory et al., 2017).

Currently, there is very limited evidence for Carboniferous glaciation in the Canning Basin. Seismic interpretation suggests the Reeves Formation is a fluvial-dominated, syn-rift rather than a *sensu stricto* glacial succession (Al Hinaai & Redfern, 2015). The Reeves Formation is restricted to a limited number of sub-surface sections in petroleum wells with minimal core available. Lithological and wireline log data from these wells indicate the Reeves Formation is composed predominantly of homogeneous sandstone with minor intervening silt- and mudstone. 'Direct' evidence for glaciation (e.g. diamictites or varved units with dropstones or striated clasts) has not been identified. The partly coeval Visean to Sakmarian Nangetty Formation of the Perth Basin contains speculated Carboniferous glacial deposits in Western Australia (Eyles et al., 2006), thus it is possible the Reeves Formation represents a well-sorted, distal proglacial succession. However, not only has the glacial affinity of the Carboniferous succession in the Perth Basin been questioned by Playford & Mory (2017), but it is unclear if that basin contains any lower to mid-Pennsylvanian strata. In the southeastern Bonaparte Basin strata coeval with the Reeves Formation (Wadeye Group) are considered possibly glaciogenic but there is little definitive evidence for this (Gorter et al., 2005). Consequently, until further sedimentological and biostratigraphic data becomes available, models for middle to Late Carboniferous glaciation in the Canning Basin and the wider region remain speculative (Fig. 12A).

Alternative regional glaciation models

The present detrital zircon dataset provides new stratigraphic constraints on the LPIA in the Canning Basin and surrounding region but, as discussed above, there remains significant uncertainty in the absolute ages of glaciogenic successions in western and central Australia. Until these are better resolved with more accurate dating techniques (e.g. Bodorokos et al., 2016), there remains scope for different regional glaciation models to be considered. There are essentially two end-member models; firstly, one where the main phase of continental ice sheet growth was in the Pennsylvanian prior to Early Permian deglaciation, and secondly, one where both the main phase of continental ice sheet growth and deglaciation was during the latest Carboniferous to Early Permian. The challenge for the former is the highly fragmented and poorly exposed Carboniferous stratigraphic record in this region seriously limits the availability of direct evidence for glaciation during this period. Consequently, it is only via circumstantial evidence such as widespread lacunas (e.g. Veevers, 2009) and climatic indicators from relatively far-field outcrops (e.g. Davydov et al., 2013) that models for Pennsylvanian ice sheet growth in this region can be explained. **The challenge for the latter is that preservation bias associated with better evidence of younger glaciations likely causes any evidence for former glaciations to be overlooked.** There are also challenges related with what is preserved in ancient glaciogenic successions, which in many cases are marine-influenced and/or deglaciation-related (e.g. Eyles, 1993; Pedersen, 2012), thus leaving much room for interpreting when and how many phases of ice advance there were **(cf. Assine et al., 2018; Le Heron, 2018)**. This is certainly the case for the Grant Group, although there are sedimentological and seismic **lines of** evidence for more than one phase of ice advance and retreat. This detrital zircon study overall suggests a model of continental ice sheet growth in the Asselian when considered in wider context, but the youngest zircons imply this could have been in the Kasimovian or Gzhelian, **which is broadly consistent with estimated timings of peak glaciation elsewhere in Gondwana (e.g. Isbell et al., 2012; Montanez & Poulsen, 2013)**. Pending future improved absolute age constraints on Carboniferous palynozones, this could explain, at least in part, the large time gap between the Reeves Formation and the Grant Group (Fig. 3). However, this would be contrary to evidence for regional climatic warming in the late Pennsylvanian (Fielding et al., 2008; Davydov et al., 2013). A third regional glaciation model scenario with significant continental ice sheet growth in both the mid-Carboniferous and Early Permian incorporating an intervening late Pennsylvanian interglacial period is also plausible, but beyond the scope of this study.

Key to improving our understanding will be further evaluation of the glacial affinity of the thick Carboniferous subsurface successions preserved in the onshore and marine basins of Western Australia due to the paucity of equivalent outcrop exposures. There are, however, relatively few Carboniferous well penetrations, so seismic **reflection data** will be important for mapping sequence and stratigraphic architecture to identify possible glacial related phenomena, such as the Permian glacial valleys identified in the Canning Basin (Al-Hinaai & Redfern, 2015), and in the Bonaparte Basin (Gorter et al., 2008). **Petrographic and other techniques investigating rock microstructure, such as CT scanning, could also be useful in identifying glacial textures considering the paucity of outcrops (e.g. Woronko, 2016).** Further radiometric age dating is also critical to improve the resolution of the LPIA stratigraphic record and regional glaciation models for Australia, which is currently largely based upon long-ranging, imprecise palynological zonations in the west (Apak & Backhouse, 1998, 1999; Mory, 2010) and SHRIMP U–Pb ages in the east (e.g., Roberts et al., 1995, fig. 13; 2006, fig. 10). Without robust absolute ages, it has long been recognized that provincial flora and fauna such as these are difficult to correlate with global equivalent successions (Mory et al., 2008). Furthermore, correlation and age control for eastern Australia successions, which is mostly provided by SHRIMP U–Pb zircon dates from interbedded volcanic intervals (e.g., Roberts et al., 1995), is also contentious given errors typically about ±3 Ma and the distance between sections. Haig et al. (2017) suggest Permian correlations in eastern Australia require CA-IDTIMS dating to be resolved, a point that seemingly applies equally well to Upper Carboniferous in that region, as well as sections elsewhere in Australia.

CONCLUSIONS

Detrital zircons from the Grant Group in the northern Canning Basin were principally sourced from basement terranes in central Australia, notably the Arunta Inlier and Musgrave Province, with a significant component likely recycled from stratigraphic units eroded beneath the Base Grant Unconformity. There are also components that can be correlated with basement terranes to the south and to the north of the Canning Basin, but they are not considered as principal source areas on this detrital zircon dataset. Conversely, there is clear outcrop evidence for ice sheets over the Pilbara–Yilgarn cratons, and subsurface and other regional evidences for ice advance into the Canning Basin on both its southern and northern margins, which imply basement terranes in these areas could have been sediment source areas for the Grant Group. This discrepancy between provenance analysis and field and subsurface observations highlights the importance of evaluating regional glaciation models with an integrated dataset.

This study shows the effectiveness of combining Hf isotopes with U–Pb dating to facilitate correlation with basement source areas with similar ages, which is essential in a study area with highly complex basement geology such as Western Australia, where individual detrital zircon crystallization ages are correlative with multiple candidate source areas. Equally important in such areas is a comprehensive geochronological database of basement areas for high confidence correlation with detrital zircons, with some residual correlation uncertainties in this provenance study due to the paucity of Hf or Nd isotope data in some basement terranes.

The youngest Grant Group detrital zircons constrain contemporaneous ice sheet development in western and central Australian uplands to a maximum late Pennsylvanian (Kasimovian) age, whereas palynology constrains a minimum Sakmarian age. The latest Pennsylvanian to early Sakmarian palynological age of the Grant Group provides a minimum duration for the presence of these ice sheets over some of these uplands, with remaining uncertainty on their earlier presence (Fig. 12B). A model is proposed where the main phase of continental ice sheet growth was in the Asselian, consistent with the LPIA evolution in eastern Australia (Fielding et al., 2008), as well as global climate proxies that indicate significant global cooling during this time (e.g. Gradstein et al., 2012; Korte et al., 2006; Montañez et al., 2007). The presence of ice sheets or glaciers older than Kasimovian in western Australia remains possible, particularly in upland areas flanking the Perth Basin (Eyles et al., 2006; Fig. 12A), but there is no direct evidence for Carboniferous glaciation in the Canning Basin, nor for significant glaciations younger than the Sakmarian. The caveat to this is the fragmentary nature of the glacial stratigraphic record whereby continental glacial deposits and associated erosional phenomena have very low preservation potential (<5% according to Eyles, 1993) due to multiple phases of ice advance and retreat, with the youngest glacial phases of any ice age clearly having greater chance of preservation.

ACKNOWLEDGEMENTS

This study was jointly funded by a Natural Environmental Research Council (UK) Studentship NER/S/A/2004/13012 and Shell International Exploration and Production (Netherlands). Thanks are due to the staff of the Western Australian Carlisle core facility (Department of Industry Regulation and Safety, Perth) for their assistance during sampling, C. Davies, H. Lock, D. Plant and V. Pashley for their help with mineral separation, CL imaging, and data acquisition, and K. Ludwig for providing a copy of Isoplot. AJM publishes with the permission of the Director, Geoscience and Resource Strategy Division, Department of Mines, Industry Regulation and Safety, Western Australia. D. Le Heron and an anonymous reviewer are thanked for their suggestions that improved this manuscript.

REFERENCES

Aitken, A.R. & Betts, P.G. (2009). Constraints on the Proterozoic supercontinent cycle from the structural evolution of the south-central Musgrave Province, central Australia. *Precambrian Research, 168*, 284–300.

Al-Hinaai, J. (2013). *Constraining the structural evolution of the Canning Basin, NW Australia, and controls on Permo-Carboniferous ice sheets development.* Ph.D. thesis, University of Manchester, UK.

Al-Hinaai, J. & Redfern J. (2015). Tectonic and climatic controls on the deposition of the Permo-Carboniferous Grant Group and Reeves Formation in the Fitzroy Trough, Canning Basin, Western Australia. *Marine and Petroleum Geology, 59,* 217–231.

Apak, S.N. & Backhouse, J. (1998). Re-interpretation of the Permo-Carboniferous succession, Canning Basin, Western Australia. In P.G. Purcell and R.R. Purcell (Eds.), *The sedimentary basins of Western Australia 2: proceedings of the Petroleum Exploration Society of Australia* (pp. 683–694). Perth, Australia.

Apak, S.N. & Backhouse, J. (1999). *Stratigraphy and petroleum exploration objectives of the Permo-Carboniferous succession on the Barbwire Terrace and adjacent areas, northeast Canning Basin, Western Australia.* Geological Society of Western Australia, Report 68, Perth, Australia.

Archbold, N.W. (1995). Studies on Western Australian brachiopods 12, additions to the late Asselian-Tastubian faunas. *Proceedings of the Royal Society of Victoria, 107,* 95–112.

Archbold, N.W. (1999). Permian Gondwanan correlations: the significance of the Western

Australian marine Permian. *Journal of African Earth Sciences, 29,* 63–75.

Archbold, N.W. & Shi, G.R. (1995). Permian brachiopods of Western Australia: Gondwanan-Asian relationships and Permian climate. *Journal of Southeast Asian Earth Sciences, 11,* 207–215.

Assine, M.L., de Santa Ana, H., Veroslavsky, G., & Vesely, F.F. (2018). Exhumed sub-glacial landscape in Uruguay: Erosional landforms, depositional environments, and paleo-ice flow in the context of the late Paleozoic Gondwanan glaciation. Sedimentary *Geology, 369,* 1-12.

Backhouse, J. (1992). *Palynology of four samples from Newcrest Mining Limited, Borehole HAC 9201, Western Canning Basin.* Geological Survey of Western Australia Paleontological Report, Perth, Australia.

Bagas, L. (2004). Proterozoic evolution and tectonic setting of the northwest Paterson Orogen, Western Australia. *Precambrian Research, 128,* 475–496.

Belousova, E.A., Griffin, W.L. & O'Reilly, S.Y. (2006). Zircon crystal morphology, trace element signatures and Hf isotope composition as a tool for petrogenetic modelling: examples from eastern Australian granitoids. *Journal of Petrology, 47,* 329–353.

Betts, P.G., Giles, D., Lister, G.S. & Frick, L.R. (2002). Evolution of the Australian lithosphere. *Australian Journal of Earth Sciences, 49,* 661-695.

Betts, P.G., Giles, D., Mark, G., Lister, G. S., Goleby, B. R., & Aillères, L. (2006). Synthesis of the Proterozoic evolution of the Mt Isa Inlier. *Australian Journal of Earth Sciences, 53,* 187–211.

Birgenheier, L.P., Fielding, C.R., Frank, T.D. & Rygel, M.C. (2007). *Nested cyclicity in the*

Carboniferous glacial record of New South Wales, Australia. AAPG Annual Conference Abstracts, Long Beach, California.

Black, L.P., Kamo, S.L., Williams, I.S., Mundil, R., Davis, D.W., Korsch, R.J., & Foudoulis, C. (2003). The application of SHRIMP to Phanerozoic geochronology; a critical appraisal of four zircon standards. *Chemical Geology, 200,* 171–188.

Blatchford, T. (1927). *The geology of portions of the Kimberley Division, with special reference to the Fitzroy Basin and the possibilities of the occurrence of mineral oil.* Geological Survey of Western Australia, Bulletin 93, Perth, Australia.

Bodorokos, S., Oliver, N.H.S. & Cawood, P.A. (1999). Thermal evolution of the central Halls Creek Orogen, northern Australia. *Australian Journal of Earth Sciences, 46,* 453–465.

Bodorkos, S., Crowley, J., Holmes, E., Laurie, J., Mantle, D., McKellar, J., Mory, A.J., Nicoll, R., Phillips, L., Smith, T., Stephenson, M. & Wood, G. (2016). New dates for Permian palynostratigraphic biozones in the Sydney, Gunnedah, Bowen, Galilee and Canning basins, Australia. *Permophiles, 63,* 19–21.

Bruguier, O., Bosch, D., Pidgeon, R.T., Byrne, D.I. & Harris, L.B. (1999). U-Pb chronology of the Northampton Complex, Western Australia - evidence for Grenvillian sedimentation, metamorphism and deformation and geodynamic implications. *Contributions to Mineralogy and Petrology, 136,* 258–272.

Buatois, L.A., Netto, R.G., Mangano, M.G. & Balistieri, P.R.M.N. (2006). Extreme freshwater release during the late Paleozoic Gondwanan deglaciation and its impact on coastal ecosystems. *Geology, 34,* 1021–1024.

Buick, I.S., Miller, J.A., Williams, I.S. & Cartwright, I. (2001). Ordovician high-grade metamorphism of a newly recognised late Neoproterozoic terrane in the northern Harts Range, central Australia. *Journal of Metamorphic Geology, 19,* 373–394.

Buick, I.S., Hand, M., Williams, I.S., Maybe, J., Miller, J.A. & Nicole, R.S. (2005). Detrital zircon provenance constraints on the evolution of the Harts Range Metamorphic Complex (central Australia): links to the Centralian Superbasin. *Journal of the Geological Society of London, 162,* 777–787.

Buick, I.S., Storkey, A. & Williams, I.S. (2008). Timing relationships between pegmatite emplacement, metamorphism and deformation during the intra-plate Alice Springs Orogeny, central Australia. *Journal of Metamorphic Geology, 26,* 915–936.

Camacho, A. & Fanning, C.M. (1995). Some isotopic constraints on the evolution of the granulite and Late amphibolite facies terranes in the eastern Musgrave Block, central Australia. *Precambrian Research, 71,* 155–181.

Cawood, P.A. & Nemchin, A.A. (2000). Provenance record of a rift basin: U-Pb ages of detrital zircons from the Perth Basin, Western Australia. *Sedimentary Geology, 134,* 209–234.

Cawood, P.A. & Tyler, I.M. (2004). Assembling and reactivating the Proterozoic Capricorn Orogen: lithotectonic elements, orogenies and significance. *Precambrian Research, 128,* 201–218.

Claoué-Long, J., Edgoose, C. & Worden, K. (2008). A correlation of Aileron Province stratigraphy in central Australia. *Precambrian Research, 166,* 230–245.

Collins, A.S. (2003). Structure and age of the northern Leeuwin Complex, Western Australia: constraints from field mapping and U-Pb isotopic analysis. *Australian Journal of*

Earth Sciences, 50, 585–599.

Collins, W.J., Williams, I.S., Shaw, S.E. & McLaughlin, N.A. (1995). The age of the Ormiston Pound Granite: implications for Mesoproterozoic evolution of the Arunta Inlier, central Australia. *Precambrian Research, 1995,* 91–105.

Corfu, F., Hanchar, J.M., Hoskin, P.W.O. & Kinny, P. (2003). Atlas of zircon textures. *Reviews in Mineralogy and Geochemistry, 53,* 469–500.

Crowe, R.W.A. & Towner, R.R. (1976). *Definitions of some new and revised rock units in the Canning Basin.* Geological Society of Western Australia, Record 1976/24, Perth, Australia.

Crowell, J.C. & Frakes, L.A. (1975). The Late Paleozoic Glaciation. In Campbell, K.S.W. (Ed.), *Gondwanan Geology* (pp. 313–331). Australian National University Press, Canberra, Australia.

Davydov, V.I., Haig, D.W. & McCartain, E. (2013). A latest Carboniferous warming spike recorded by a fusulinid-rich bioherm in Timor Leste: implications for East Gondwana deglaciation. *Paleogeography, Paleoclimatology, Paleoecology, 376,* 22–38.

de Vries, S.T., Pryler, L.L. & Fry, N. (2008). Evolution of Neoarchaean and Proterozoic basins of Australia. *Precambrian Research, 166,* 39–53.

Dillinger, A., George, A.D., & Parra-Avila, L.A. (2018). Early Permian sediment provenance and paleogeographic reconstructions in southeastern Gondwana using detrital zircon geochronology (Northern Perth Basin, Western Australia). ***Gondwana Research, 59,*** **57-75.**

Downes, P.J., Griffin, B.J. & Griffin, W.L. (2007). Mineral chemistry and zircon geochronology of xenocrysts and altered mantle and crustal xenoliths from the Aries micaceous kimberlite: Constraints on the composition and age of the central Kimberley Craton, Western Australia. *Lithos, 93,* 175–198.

Evans, D.J.A. & Benn, D.I. (2004). *A practical guide to the study of glacial sediments.* Arnold, London, UK.

Evins, P.M., Smithies, R.H., Howard, H.M., Kirkland, C.L., Wingate, M.T.D. & Bodorokos, S. (2010). Devil in the detail; The 1150–1000Ma magmatic and structural evolution of the Ngaanyatjarra Rift, west Musgrave Province, Central Australia. *Precambrian Research, 183,* 572–288.

Eyles, C.H. & Eyles, N. (2000). Subaqueous mass flow origin for Early Permian diamictites and associated facies of the Grant Group, Barbwire Terrace, Canning Basin, Western Australia. *Sedimentology, 47,* 343–356.

Eyles, N. (1993). Earth's glacial record and its tectonic setting. *Earth-Science Reviews, 35,* 1–248.

Eyles, N. & de Broekert, P. (2001). Glacial tunnel valleys in the Eastern Goldfields of Western Australia cut below the Late Paleozoic Pilbara ice sheet. *Paleogeography, Paleoclimatology, Paleoecology, 171,* 29–40.

Eyles, N., Mory, A.J. & Backhouse, J. (2002). Carboniferous-Permian palynostratigraphy of west Australian marine rift basins: resolving tectonic and eustatic controls during Gondwanan glaciations. *Paleogeography, Paleoclimatology, Paleoecology, 184,* 305–319.

Eyles, N., Mory, A.J. & Eyles, C.H. (2006). 50-million-year-long record of glacial to postglacial marine environments preserved in a Carboniferous-Early Permian graben, northern Perth Basin, Western Australia. *Journal of Sedimentary Research, 76,* 618–632.

Fedo, C.M., Sircombe, K.N. & Rainbird, R.H. (2003). Detrital zircon analysis of the sedimentary record. *Reviews in Mineralogy and Geochemistry, 53,* 277–303.

Fielding, C.R., Frank, T.D. & Isbell, J.L. (Eds.), 2008. *Resolving the Late Paleozoic Ice Age in Time and Space.* The Geological Society of America, Special Paper 441, USA.

Fielding, C.R., Frank, T.D., Birgenheier, L.P., Rygel, M.C., Jones, A.T. & Roberts, J. (2008). Stratigraphic imprint of the Late Paleozoic Ice Age in eastern Australia: a record of alternating glacial and nonglacial climate regime. *Journal of the Geological Society, London, 165,* 129–140.

Fitzsimons, I.C.W. (2003). Proterozoic basement provinces of southern and southwestern Australia, and their correlation with Antarctica. In Yoshida, M., Windley, B.F., & Dasgupta, S. (Eds.), *Proterozoic East Gondwana: supercontinent assembly and breakup* (pp. 93–130). Geological Society of London Special Publications, 26, UK.

Flowerdew, M.J., Millar, I.L., Curtis, M.L., Vaughan, A.P.M., Horstwood, M.S.A., Whitehouse, M.J. & Fanning, C.M. (2007). Combined U-Pb geochronology and Hf isotope geochemistry of detrital zircons from early Paleozoic sedimentary rocks, Ellsworth-Whitmore Mountains block, Antarctica. *Geological Society of America Bulletin, 119,* 275–288.

Foster, C.B. & Waterhouse, J.B. (1988). The *Granulatisporites confluens* Oppel-zone and Early Permian marine faunas from the Grant Formation on the Barbwire Terrace, Canning Basin, Western Australia. *Australian Journal of Earth Sciences, 35,* 135-157.

Raymond, O.L., Liu, S., Gallagher, R., Zhang, W. & Highet, L.M. (2012). 1:1 million scale Surface Geology map of Australia, Geoscience Australia.

Giles, D., Betts, P.G. & Lister, G.S. (2004). 1.8-1.5 Ga links between the North and South Australian Cratons and the Early-Middle Proterozoic configuration of Australia. *Tectonophysics, 380,* 27–41.

Glen, R.A. (2005). The Tasmanides of eastern Australia. In Vaughan, A.P.M., Leat, P.T. & Pankhurst, R.J. (Eds.), *Terrane processes at the margins of Gondwana* (pp. 23−96). Geological Society London Special Publications, 246, UK.

Gorter, J.D., Jones, P.J., Nicoll, R.S. & Golding, C.J. (2005). A reappraisal of the Carboniferous stratigraphy and petroleum potential of the southeastern Bonaparte Basin (Petrel Sub-basin) northwestern Australia. *APPEA Journal and Conference Proceedings, 45,* 275–295.

Gorter, J.D., Pynter, S.E., Bayford, S.W. & Caudullo, A. (2008). Glacially influenced petroleum plays in the Kulshill Group (late Carboniferous - early Permian) of the southeastern Bonaparte Basin, Western Australia. *APPEA Journal and Conference Proceedings, 48,* 69−113.

Gradstein, F.M., Ogg, J.G., Schmitz, M. & Ogg, G. (2012). *The Geologic Time Scale 2012.* Cambridge University Press, Cambridge, UK.

Graham, S., Lambert, D.D., Shee, S.R., Smith, C.B. & Reeves, S. (1999). Re-Os isotopic evidence for Archean lithospheric mantle beneath the Kimberley block, Western Australia. *Geology, 27,* 431–434.

Griffin, T.J., Page, R.W., Sheppard, S. & Tyler, I.M. (2000). Tectonic implications of Paleoproterozoic post-collisional, high-K felsic igneous rocks from the Kimberley region of northwestern Australia. *Precambrian Research, 101,* 1–23.

Griffin, W.L., Belousova, E.A., Shee, S.R., Pearson, N.J. & O'Reilly, S.Y. (2004). Archean crustal evolution in the northern Yilgarn Craton: U-Pb and Hf-isotope evidence from detrital zircons. *Precambrian Research, 131,* 231–282.

Griffin, W.L., Belousova, E.A., Walters, S.G. & O'Reilly, S.Y. (2006). Archean and Proterozoic crustal evolution in the Eastern Succession of the Mt Isa district, Australia: U-Pb and Hf-isotope studies of detrital zircons. *Australian Journal of Earth Sciences, 53,* 125–149.

Griffis, N.P., Mundil, R., Montanez, I.P., Isbell, I., Fedorchuk, N., Vesely, F., Iannuzzi, R. & Yin, Q.-Z. (2018). A new stratigraphic framework built on U-Pb single-zircon TIMS ages and implications for the timing of the penultimate icehouse (Paraná Basin, Brazil). *Geological Society of America Bulletin, 130,* 848-858.

Hambrey, M.J. & Harland, W.B. (1981). *Earth's pre-Pleistocene glacial record.* Cambridge University Press, Cambridge, UK.

Haig, D. W., McCartain, E., Mory, A. J., Borges, G., Davydov, V., Dixon, M., Ernst, A., Groflin, S., Hakansson, E., Keep, M., Dos Santos, Z., Shi, G.R., & Soares, J. (2014). Postglacial Early Permian (late Sakmarian–early Artinskian) shallow-marine carbonate deposition along a 2000 km transect from Timor to west Australia. *Paleogeography, Paleoclimatology, Paleoecology, 409,* 180–204.

Haig, D.W., Mory, A. J., McCartain, E., Backhouse, J., Håkansson, E., Ernst, A., Nicoll, R.S., Shi, G.R., Evan, J.C., Davydov, V.I., Hunter, A.W., Keep, M., Martin, S.K., Peyrot, D., Kossavaya, O. & Dos Santos, Z. (2017). Late Artinskian–Early Kungurian (Early

Permian) warming and maximum marine flooding in the East Gondwana interior rift, Timor and Western Australia, and comparisons across East Gondwana. *Paleogeography, Paleoclimatology, Paleoecology, 468,* 88–121.

Haines, P.W., Allen, H.-J., Wingate, M.T.D., Kirkland, C.L. & Hocking, R.M. (2011). Ice movement direction and detrital zircon provenance data for early Permian glacial deposits, Amadeus Basin, eastern Western Australia. In Hakansson, E. & Trotter, J.A. (Eds.), *Programme and abstracts, The XVII International Congress on the Carboniferous and Permian, Perth 3-8 July 2011* (pp. 63). Geological Survey of Western Australia, Record 2011/20, Perth, Australia.

Hand, M., Mawby, J., Kinny, P. & Foden, J. (1999). U-Pb ages from the Harts Range, central Australia: evidence for early Ordovician extension and constraints on Carboniferous metamorphism. *Journal of the Geological Society London, 156,* 715–730.

Hawkesworth, C.J. & Kemp, A.I.S. (2006). Using hafnium and oxygen isotopes in zircons to unravel the record of crustal evolution. *Chemical Geology, 226,* 144–162.

Hickman, A.H. (2004). Two contrasting granite-greenstone terrane in the Pilbara Craton, Australia:evidence for vertical and horizontal tectonic regimes prior to 2900 Ma. *Precambrian Research, 131,* 153–172.

Hoatson, D.M., Sun, S. & Claoue-Long, J.C. (2005). Proterozoic mafic-ultramafic intrusions in the Arunta Region, central Australia part 1: geological setting and mineral potential. *Precambrian Research, 142,* 93–133.

Hollis J.A., Carson C.J. & Glass L.M. (2009). SHRIMP U–Pb zircon geochronological evidence for Neoarchean basement in western Arnhem Land, northern Australia. *Precambrian Research, 174,* 364–380.

Hollis, J.A., Glass, L.M., Carson, C.J., Kemp, A.I.S., Yaxley, G., Armstrong, R. & Scherstén, A. (2010). U-Pb-Hf-O character of Neoarchean basement to the Pine Creek Orogen, North Australian craton. In Tyler, I. & Knox-Robinson, C.M. (Eds.), *Fifth International Archean Symposium Abstracts* (pp. 65–67). Geological Survey of Western Australia, Perth, Australia.

Hollis J.A., Kirkland, C.L., Spaggiari, C.V., Tyler, I.M., Haines, P.W., Wingate, M.T.D., Belousova, E.A., & Murphy, R.C. (2013). *Zircon U–Pb–Hf isotope evidence for links between the Warumpi and Aileron Provinces, west Arunta region.* Geological Survey of Western Australia, Record 2013/9, Perth, Australia.

Isbell, J.L., Lenaker, P.A., Askin, R.A., Miller, M.F. & Babcock, L.E. (2003). Reevaluation of the timing and extent of late Paleozoic glaciation in Gondwana: role of the Transantarctic Mountains. *Geology, 31,* 977–980.

Isbell, J.L., Henry, L.C., Gulbranson, E.L., Limarino, C.O., Fraiser, M.L., Koch, Z.J., Ciccioli, P.L., & Dineen, A.A. (2012). Glacial paradoxes during the late Paleozoic ice age: Evaluating the equilibrium line altitude as a control on glaciation. *Gondwana Research*, 22, 1-19.

Ito, H. (2010). Dating Single Zircon by Fission-Track and U-Pb Methods: a Case Study on a Granite at the Cooper Basin HFR Site, Australia. In *Proceedings of the World Geothermal Congress 2010* (pp. 1–5), Bali, Indonesia.

Ivanic, T.J., Van Kranendonk, M.J., Kirkland, C.L., Wyche, S., Wingate, M.T.D. & Belousova, E. (2013). *Juvenile crust formation and recycling in the northern Murchison Domain, Yilgarn Craton: evidence from Hf isotopes and granite geochemistry.* Geological Survey of Western Australia, Report 120, Perth, Australia.

Joly, A., Dentith, M.C., Porwal, A., Spaggiari, C.V., Tyler, I.M. & McCuaig, T.C. (2013). *An integrated geological and geophysical study of the west Arunta Orogen and its mineral prospectivity.* Geological Survey of Western Australia, Report 113, Perth, Australia.

Jones, A.T. & Fielding, C.R. (2004). Sedimentological record of the late Paleozoic glaciation in Queensland, Australia. *Geology, 32,* 153–156.

Jones, A.T., Frank, T.D. & Fielding, C.R. (2006). Cold climate in the eastern Australian mid to late Permian may reflect cold upwelling waters. *Paleogeography, Paleoclimatology, Paleoecology, 237,* 370–377.

Kemp, A.I.S., Hawkesworth, C.J., Foster, G.L., Paterson, B.A., Woodhead, J.D., Hergt, J.M., Gray, C.M., & Whitehouse, M.J. (2007). Magmatic and crustal differentiation history of granitic rocks from Hf-O isotopes in zircon. *Science, 315,* 980–983.

Kemp, E.M., Balme, B.E., Helby, R.J., Kyle, R.A., Playford, G., & Price, P.L. (1977). Carboniferous and Permian palynostratigraphy in Australia and Antarctica: a review. *Bureau of Mineral Resources Journal of Australian Geology and Geophysics, 2,* 177–208.

Kennard, J.M., Jackson, M.J., Romine, K.K., Shaw, R.D. & Southgate, P.N. (1994). Depositional sequences and associated petroleum systems of the Canning Basin, W.A. In Purcell, P.G. & Purcell, R.R. (Eds.), *The sedimentary basins of Western Australia, Proceedings of the Western Australian Basins Symposium* (pp. 657–676). Petroleum Exploration Society of Australia, Perth, Australia.

Kinny, P. D., & Maas, R. (2003). Lu-Hf and Sm-Nd isotope systems in zircon. *Reviews in Mineralogy and Geochemistry, 53,* 327–341.

Kirkland, C.L., Smithies, R.H., Woodhouse, E., Howard, H.M., Wingate, M.T.D., Belousova, E.A., Cliff, J.B., Murphy, R.C. & Spaggiari, C.V. (2012). *A multi-isotopic approach to the crustal evolution of the west Musgrave Province, central Australia.* Geological Survey of Western Australia, Report 115, Perth, Australia.

Kirkland, C.L., Johnson, S.P., Smithies, R.H., Hollis, J.A., Wingate, M.T.D., Tyler, I.M., Hickman, A.H., Cliff, J.B., Belousovan E.A., Murphyn R.C. & Tessalina, S. (2013). *The crustal evolution of the Rudall Province from an isotopic perspective.* Geological Survey of Western Australia, Report 122, Perth, Australia.

Kohn, B.P., Gleadow, A.J.W., Brown, R.W., Gallagher, O'Sullivan, P.B. & Foster, D.A. (2002). Shaping the Australian crust over the last 300 million years: insights from fission track thermotectonic imaging and denudational studies of key terranes. *Australian Journal of Earth Sciences, 49,* 697–717.

Korte, C., Jasper, T., Kozur, H.W. & Veizer, J. (2006). $^{87}Sr/^{86}Sr$ record of Permian seawater. *Paleogeography, Paleoclimatology, Paleoecology, 240,* 89–107.

Le Heron, D.P. (2018). An exhumed Paleozoic glacial landscape in Chad. *Geology, 46,* 91-94.

Ludwig, K.R. (2003). *User's manual for Isoplot 3.00: a geochronological toolkit for Microsoft Excel.* Berkeley Geochronological Centre, Special Publication 4, USA.

Maboko, M.A.H., McDougall, I., Zeitler, P.K. & Williams, I.S. (1992). Geochronological evidence for ~530-550 Ma juxtaposition of two Proterozoic metamorphic terranes in the Musgraves Ranges, central Australia. *Australian Journal of Earth Sciences, 39,* 457–471.

Maidment, D.W., Hands, M. & Williams, I.S. (2005). Tectonic cycles in the Strangeways Metamorphic Complex, Arunta Inlier, central Australia: geochronological evidence for exhumation and basin formation between two high-grade metamorphic events. *Australian Journal of Earth Sciences, 52,* 205–215.

Martin, J.R., Redfern, J., Mory, A.J. & Williams, B.P.J. (2007). Facies architecture and reservoir prediction in ancient glaciogenic sediments: a case study using integrated outcrop and subsurface studies of the Grant Group (Canning Basin, West Australia), AAPG Annual Conference, Long Beach, California.

Martin, J.R., 2008. *Sedimentological and provenance constraints on the Late Paleozoic Gondwanan Ice Age in the Canning Basin (Western Australia) and Oman.* Ph.D. thesis, The University of Manchester, UK.

Mawby, J., Hand, M. & Foden, J. (1999). Sm-Nd evidence for high-grade Ordovician metamorphism in the Arunta Block, central Australia. *Journal of Metamorphic Geology 17,* 653–658.

Metcalfe, I. (1996). Gondwanaland dispersion, Asian accretion and evolution of Eastern Tethys. *Australian Journal of Earth Sciences, 43,* 605–623.

Metcalfe, I. (2013). Gondwana dispersion and Asian accretion: Tectonic and paleogeographic evolution of eastern Tethys. *Journal of Asian Earth Sciences, 66,* 1–33.

Montañez, I.P. Tabor, N.J., Niemeier, D., DiMichele, W.A., Frank, T.D., Fielding, C.R., Isbell, J.L., Birgenheier, L.P. & Rygel, M.C. (2007). CO_2-forced climate and vegetation instability during the late Paleozoic deglaciation. *Science, 315,* 87–91.

Montañez, I.P. & Poulsen, C.J. (2013). The late Paleozoic ice age: an evolving paradigm.

***Annual Review of Earth and Planetary Sciences, 41,* 629-656.**

Mory, A.J. (2010). *A review of mid-Carboniferous to Triassic stratigraphy, Canning Basin, Western Australia.* Geological Survey of Western Australia, Report 107, Perth, Australia.

Mory, A.J., Martin, J.R. and Redfern, J. (2008). A review of Permo-Carboniferous glacial deposits in Western Australia. In Fielding, C.R., Frank, T.D. & Isbell, J.L. (Eds.), *Resolving the Late Paleozoic Ice Age in Time and Space* (pp. 29–40). The Geological Society of America, Special Paper 441, USA.

Mory, A.J., Crowley, J.L., Backhouse, J., Nicole, R.S., Bryan, S.E., Lopez Martinez, M. & Mantle, D.J. (2017). Apparent conflicting Roadian-Wordian (middle Permian) CA-IDTIMS and palynology ages from the Canning Basin, Western Australia. *Australian Journal of Earth Sciences, 64,* 889–901.

Mulder, T. & Alexander, J. (2001). The physical character of subaqueous sedimentary density flows and their deposits. *Sedimentology, 48,* 269–299.

Nelson, D.R., Myers, J.S. & Nutman, A.P. (1995). Chronology and evolution of the Middle Proterozoic Albany-Fraser Orogen, Western Australia. *Australian Journal of Earth Sciences, 42,* 481–495.

Neumann, N.L. & Fraser, G.L. (2007). *Geochronological synthesis and Time-Space plots for Proterozoic Australia.* Geoscience Australia, Record 2007/06, Australia.

O'Brien, P.E. & Christie-Blick, N. (1992). Glacially grooved surfaces in the Grant Group, Grant Ranges, Canning Basin and the extent of late Paleozoic Pilbara ice sheets. *BMR Journal of Australian Geology and Geophysics, 13,* 87–92.

O'Brien, P.E., Lindsay, J.F., Knauer, K., & Sexton, M.J. (1998). Sequence stratigraphy of a sandstone-rich Permian glacial succession, Fitzroy Trough, Canning Basin, Western Australia. *Australian Journal of Earth Sciences, 45,* 533–545.

Occhipinti, S.A. & Reddy, S.M. (2009). Neoproterozoic reworking of the Paleoproterozoic Capricorn Orogen of Western Australia and implications for the amalgamation of Rodinia. In Murphy, J. B., Keppie, J. D. & Hynes, A. J. (Eds.), *Ancient Orogens and Modern Analogues* (pp. 445–456). Geological Society of London, Special Publication 327, UK.

Offler, R. & Shaw, S. (2006). Hornblende gabbro block in serpentinite Melange, Peel-Manning Fault System, New South Wales, Australia: Lu-Hf and U-Pb isotopic evidence for mantle-derived, Late Ordovician igneous activity. *Journal of Geology, 114,* 211–230.

Osterloff, P.A., Penney, R.A., Aitken, J.F., Clark, N.D. & Al-Husseini, M.I. (2004). Depositional sequences of the Al Khlata Formation, subsurface Interior Oman. In Al-Husseini, M.I. (Ed.), *Carboniferous, Permian and early Triassic stratigraphy* (pp. 61–81). GeoArabia, Special Publication 3, Gulf PetroLink, Bahrain.

Pedersen, S.A.S. (2012). Glaciodynamic sequence stratigraphy. In Huuse, M., Redfern, J., Le Heron, D.P., Dixon, R.J., Moscariello, A. & Craig, J. (Eds.), *Glaciogenic reservoirs and hydrocarbon systems* (29–51). Geological Society of London, Special Publication 368, UK.

Playford, P. (2002). Paleokarst, pseudokarst, and sequence stratigraphy in Devonian reef sequences of the Canning Basin, Western Australia. In Keep, M. & Moss, S.J. (Eds.), *The sedimentary basin of Western Australia 3: Proceedings of the Petroleum Explora-*

tion Society of Australia Symposium (pp. 763–794), Perth, Western Australia.

Playford, P.E., Hocking, R.M. & Cockbain, A.E. (2009). *Devonian reef complexes of the Canning Basin, Western Australia.* Geological Survey of Western Australia Bulletin 145, Perth, Australia.

Playford G. & Mory, A.J. (2017). Composition and occurrence of the *Grandispora maculosa* zonal assemblage (Mississippian) in the subsurface of the Carnarvon Basin and the Coolcalalaya Sub-basin of Western Australia, and its Gondwanan distribution. *Revista Italiana di Paleontologiia e Stratigrafia, 123,* 275–318.

Redfern, J. (1990). *The sedimentology and stratigraphy of the Permo-Carboniferous Grant Group, Barbwire Terrace, Canning Basin, Western Australia.* Ph.D. thesis, University of Bristol, UK.

Redfern, J. & Millward, E. (1994). A review of the sedimentology and stratigraphy of the Permo-Carboniferous Grant Group, Canning Basin, Western Australia. In Purcell, P.G. & Purcell, R.R. (Eds.), *The sedimentary basins of Western Australia, Proceedings of the Petroleum Exploration Society of Australia* (pp. 753–756), Perth, Australia.

Redfern, J. & Williams, B.P.J. (2002). Canning Basin Grant Group glaciogenic sediments: part of the Gondwanan Permo-Carboniferous hydrocarbon province. In Keep, M. & Moss, S.J. (Eds.), *The sedimentary basins of Western Australia 3, Proceedings of the West Australian basins symposium* (pp. 851–871), Perth, Australia.

Roberts, J., Claoue-Long, J.C., Jones, P. & Foster, C.B. (1995). SHRIMP zircon age control of Gondwanan sequences in Late Carboniferous and Early Permian Australia. In Dunnay, R.A. & Hailwood, A.E. (Eds.), *Non-biostratigraphical methods of dating and correlation* (pp. 145–174). Geological Society London, Special Publication 89, UK.

Roberts, J., Claoue-Long, J.C. & Foster, C.B. (1996). SHRIMP dating of the Permian System of eastern Australia. *Australian Journal of Earth Sciences, 43,* 401–421.

Rubatto, D., Williams, I.S. & Buick, I.S. (2001). Zircon and monazite response to prograde metamorphism in the Reynolds Range, central Australia. *Contributions to Mineralogy and Petrology, 140,* 458–468.

Schmidt, P.W., Williams, G.E. and Camacho, A., 2006. Assembly of proterozoic Australia: Implications of a revised pole for the similar to 1070 Ma Alcurra Dyke Swarm, central Australia. Geophysical Journal International, 167: 626–634.

Scrimgeour, I.R. & Close, D.F. (1999). Regional high-pressure metamorphism during intra-cratonic deformation: the Petermann Orogeny, central Australia. *Journal of Metamorphic Geology, 17,* 557–572.

Sener, A.K., Young, C., Groves, D.I., Krapez, B. & Fletcher, I.R. (2005). Major orogenic gold episode associated with Cordilleran-style tectonics related to the assembly of Paleoproterozoic Australia? *Geology, 33,* 225–-228.

Sheppard, S., Griffin, T.J., Tyler, I.M. & Page, R.W. (2001). High- and low-K granites and adakites at a Paleoproterozoic plate boundary in northwestern Australia. *Journal of the Geological Society, London, 158,* 547–560.

Sircombe, K.N. & Freeman, M.J. (1999). Provenance of detrital zircons on the Western Australia coastline - implications for the geologic history of the Perth basin and denudation of the Yilgarn craton. *Geology, 27,* 879–882.

Sun, S., Warren, R.G. & Shaw, R.D. (1995). Nd isotope study from the Arunta Inlier, central Australia: constraints on geological models and limitations of the method. *Precambri-*

an Research, 71, 301–314.

Taboada, C.S., Mory, A.J., Shi, G.-R., Haig, D.W. & Pinilla, M.K. (2015). An Early Permian brachiopod–gastropod fauna from the Calytrix Formation, Barbwire Terrace, Canning Basin, Western Australia. *Alcheringa: an Australasian Journal of Paleontology, 39,* 207–223.

Tyler, I.M., Page, R.W. & Griffin, T.J. (1999). Depositional age and provenance of the Marboo Formation from SHRIMP U–Pb zircon geochronology: Implications for the early Paleoproterozoic tectonic evolution of the Kimberley region, Western Australia. *Precambrian Research, 95,* 225–243.

Van Kronendonk, M.J., Smithies, R.H., Hickman, A.H. & Champion, D.C. (2007). Review: secular tectonic evolution of Archean continental crust: interplay between horizontal and vertical processes in the formation of the Pilbara Craton, Australia. *Terra Nova, 19,* 1–38.

Veevers, J.J. (2004). Gondwanaland from 650-500 Ma assembly through 320 Ma merger in Pangea to 185-100 Ma breakup: supercontinental tectonics via stratigraphy and radiometric dating. *Earth-Science Reviews, 68,* 1–132.

Veevers, J.J. (2009). Mid-Carboniferous Centralian uplift linked by U-Pb zircon chronology to the onset of Australian glaciation and glacio-eustasy. *Australian Journal of Earth Sciences, 56,* 711–717.

Veevers, J.J., Saeed, A., Belousova, E.A. & Griffin, W.L. (2005). U-Pb ages and source composition by Hf-isotope and trace element analysis of detrital zircons in Permian sandstone and modern sand from southwestern Australia and a review of the paleogeographical and denudational history of the Yilgarn Craton. *Earth-Science Reviews, 68,* 245–279.

Veevers, J.J. & Tewari, R.C. (1995). Permian-Carboniferous and Permian-Triassic magmatism in the rift zone bordering the Tethyan margin of southern Pangea. *Geology, 23,* 467–470.

Wade, B.P., Hand, M. & Barovich, K.M. (2005). Nd isotopic and geochemical constraints on provenance of sedimentary rocks in the eastern Officer Basin, Australia: implications for the duration of the intracratonic Petermann Orogeny. *Journal of the Geological Society London, 162,* 513–530.

Wade, B.P., Barovich, K.M., Hand, M., Scrimgeour, I.R. & Close, D.F. (2006). Evidence for early Mesoproterozoic arc magmatism in the Musgrave Block, central Australia: Implications for Proterozoic crustal growth and tectonic reconstructions of Australia. *Journal of Geology, 114,* 43–63.

Waterhouse, J.B. & Shi, G.R. (2013). Climatic implications from the sequential changes in diversity and biogeographic affinities for brachiopods and bivalves in the Permian of eastern Australia and New Zealand. *Gondwana Research, 24,* 139–147.

Weber, U.B., Kohn, B.P., Gleadow, A.J.W. & Nelson, D.R. (2005). Low temperature Phanerozoic history of the Northern Yilgarn Craton, Western Australia. *Tectonophysics, 400,* 127–151.

White, R.W., Clarke, G.L. & Nelson, D.R. (1999). SHRIMP U-Pb zircon dating of Grenville-age events in the western part of the Musgrave Block, central Australia. *Journal of Metamorphic Geology, 17,* 465–481.

Wilde, S.A. (1999). Evolution of the western margin of Australia during the Rodinian and Gondwanan Supercontinent cycles. *Gondwana Research, 2,* 481–499.

Williams, B.P.J., Wild, E.K. & Suttill, R.J. (1987). Late Paleozoic cold-climate aeolianites, southern Cooper Basin, South Australia. In Frostick, L. & Reid, I. (Eds.), *Desert sediments: ancient and modern* (pp. 233–249), Geological Society of London, Special Publication 35, UK.

Williams, I.R. (2007). *Geology of the Yilgalong 1:100,000 scale geological map: explanatory notes.* Geological Survey of Western Australia, Perth, Australia.

Worden K.E., Carson C.J., Scrimgeour I.R., Lally J., & Doyle N. (2008). A revised Paleoproterozoic chronostratigraphy for the Pine Creek Orogen, northern Australia: Evidence from SHRIMP U-Pb zircon geochronology. *Precambrian Research, 166,* 122–144.

Woronko, B. (2016). Frost weathering versus glacial grinding in the micromorphology of quartz sand grains: processes and geological implications. *Sedimentary geology, 335,* 103-119.

Zhao, J-X. & McCulloch, M.T. (1993). Sm-Nd mineral isochron ages of Late Proterozoic dyke swarms in Australia: evidence for two distinct events of mafic magmatism and crustal extension. *Chemical Geology, 109,* 341–354.

Zhao, J-X. & McCulloch, M.T. (1995). Geochemical and Nd isotopic systematics of granites from the Arunta Inlier, central Australia: implications for Proterozoic crustal evolution. *Precambrian Research, 71,* 265–299.

Zhao, J-X., McCulloch, M.T. & Bennett, V.C. (1992). Sm-Nd and U-Pb zircon isotopic constraints on the provenance of sediments from the Amadeus Basin, central Australia:

evidence for REE fractionation. *Geochimica et Cosmochimca Acta, 56,* 921–940.

APPENDIX A: ZIRCON DATING METHODOLOGY

Samples were crushed, sieved, and separated using gravitational and centrifugal heavy liquid techniques. Zircons were further separated from the heavy mineral fraction using Frantz magnetic techniques, hand picked randomly under a binocular microscope, mounted on an epoxy block and polished to expose an equatorial section. Every grain was imaged using cathodoluminescence (CL) to identify compositional zonation and the ablation target area. U–Pb ages were determined using an Elemental Axiom double focussing MC-ICPMS coupled to a New Wave Research Microprobe UP193SS nm, Nd:YAG laser ablation system, at the Natural Environment Research Council Isotope Geosciences Laboratory (NIGL), UK. Analytical procedure for U–Pb dating using the Axiom is fully outlined in Horstwood et al. (2003). A minimum of 60 U–Pb ages was determined for each sample (Table 2); analysis of 60 grains provides a 95% probability of finding a population comprising 5% of the total (Dodson et al., 1988). Spot size and laser repetition rate were maintained at 50 μm and 5 Hz generating c. 2.6–3.4 $J.cm^{-2}$ per pulse, with ablated material transferred from the sample cell to the Axiom plasma source by argon. Elemental fractionation was minimized by adopting standard protocol such as ablating pits with a low aspect ratio and calculating Pb/U ratios with reference to standard zircon 91500, which was analysed after every fifth detrital zircon analysis. Ages were calculated using the Isoplot add-in (Ludwig, 2003) for Microsoft Excel using the decay constants recommended by Steiger and Jäger (1977). Ages quoted in this paper are $^{206}Pb^*/238U$ for < 1000 Ma and $^{207}Pb^*/^{206}Pb^*$ for > 1000 Ma, with 2σ error (Figs. 8 and 9). The ^{204}Pb signal for each analysis was used to assess the amount of common Pb (Horstwood et al., 2003), with correction applied as necessary.

Hf isotope analyses were performed (Table 5) after U–Pb geochronology using a Nu Plasma HR (Nu Instruments) MC-ICP-MS coupled to a UP193SS (New Wave Research) laser ablation system. Ablations were targeted adjacent to the U–Pb ablation spots where possible using CL images. Similar zones within the same grains were targeted for Hf analyses placement immediately adjacent to the pre-existing U–Pb ablation pit was not possible (e.g. Fig. 5). The analytical methodology was modified after Woodhead et al. (2004) to allow for the use of the U–Pb collector block on the Nu Plasma HR at NIGL. This collector block is limited to 7 central Faraday detectors for use with isotope systems other than U–Pb, necessitating the sacrifice of the ^{180}Hf and ^{172}Yb peaks. Only the ^{178}Hf/^{177}Hf stable isotope ratio is therefore used to monitor the accuracy of the Hf mass bias correction, whilst a modified ^{176}Yb/^{173}Yb ratio is determined prior to analysis through Yb-doping of the JMC475 Hf isotope reference material. This characterizes the difference between Hf and Yb instrumental mass bias and allows correction of the ^{176}Yb isobaric interference through measurement of the ^{173}Yb peak, without the need to measure both the ^{172}Yb and ^{173}Yb peaks simultaneously. Peak jumping experiments to allow simultaneous Yb mass bias correction of the Yb isobaric interference correction show no difference within uncertainty to those data determined using the doping approach. Monitoring of the ^{180}Hf/^{177}Hf ratio through a dynamic acquisition also demonstrates accurate stable isotope values.

Mass spectrometer performance was checked each session by running reference material JMC475 with and without Yb doping. Session averages for corrected ^{176}Hf/^{177}Hf and ^{178}Hf/^{177}Hf were 0.282148–63 +/- 40–110ppm and 1.467210–38 +/- 10–32ppm 2SD respectively. Laser spot size and repetition rate were maintained at 50μm and 5Hz respectively, using a fluence of 6–8J.cm^{-2} per pulse. Sample data were normalized relative to reference material 91500 assuming ^{176}Hf/^{177}Hf = 0.282306 (Woodhead et al., 2004). ^{178}Hf/^{177}Hf for 91500 gave session averages of 1.46724–27 with average reproducibility of c. 35ppm 2SD.

Interferences on ^{176}Hf were corrected by measuring ^{173}Yb and ^{175}Lu and using ^{176}Yb/^{173}Yb = 0.79462 and ^{176}Lu/^{175}Lu = 0.02653. Lu–Hf sample data were normalized using reference material 91500 relative to an expected $^{176}Lu/^{177}Hf$ of 0.000311 (Woodhead et al., 2004).

All uncertainties were propagated using quadratic addition to reflect the reproducibility of replicate measurements of the Mudtank reference material with the εHf and T_{DM} uncertainties incorporating components to reflect the uncertainty on the determined $^{176}Hf/^{177}Hf$, $^{176}Yb/^{177}Hf$ and $^{176}Lu/^{177}Hf$ ratios as well as the uncertainty on the U-Pb age. The ^{176}Lu decay constant and chondrite and depleted mantle values of Blitchert-Toft and Albarede (1997) were used to calculate εHf and T_{DM} model ages.

<u>References:</u>

Blitchert-Toft, J.& Albarede, F. (1997). The Lu-Hf isotope geochemistry of chondrites and the evolution of the mantle-crust system. *Earth and Planetary Science Letters, 148,* 243–258.

Dodson, M.H., Compston, W., Williams, I.S. & Wilson, J.F. (1988). A search for ancient detrital zircons in Zimbabwean sediments. *Journal of the Geological Society London, 145,* 977–983.

Horstwood, M.S.A., Foster, G.L., Parrish, R.R., Noble, S.R. & Nowell, G.M. (2003). Common-Pb corrected in situ U-Pb accessory mineral geochronology by LA-MC-ICPMS. *Journal of Analytical Atomic Spectrometry, 18,* 837–846.

Steiger, R.H. & Jager, E. (1977). Subcommission on geochronology: convention on the use of decay constants in geo- and cosmochronology. *Earth and Planetary Science Letters, 36,* 359–362.

Woodhead, J.D., Hergt, J., Shelley, M., Eggins, S. & Kemp, R. (2004). Zircon Hf-isotope analysis with an excimer laser, depth profiling, ablation of complex geometries, and concomitant age estimation. *Chemical Geology, 209,* 121–135.

FIGURE CAPTIONS

Fig. 1. [A] Map of the Canning Basin showing its sub-basins, detrital zircon sample locations, and place names mentioned in the text. [B] Map of Australia showing basement terranes discussed in the text and location of detrital zircon samples (CAP: Capparis-1, CYC: Cycas-1, DRO: Drosera-1). Geological map modified from Raymond et al. (2012). YIL: Yilgarn Craton, CAO: Capricorn Orogen. PIL: Pilbara Craton, RUD: Rudall Complex, PAO: Paterson Orogen, MUS: Musgrave Block, ARU: Arunta Inlier, GRT: Granites Tanami, HC-KL: Hall's Creek- King Leopold Orogen, KIM: Kimberley Basin, PCO: Pine Creek Orogen, TCI: Tennant Creek Inlier, MII: Mt Isa Inlier, NEO: New England Orogen, LFB: Lachlan Fold Belt, GAW: Gawler Craton.

Fig. 2. Photographs of Grant Group exposed in the Fitzroy River valley and Pilbara region and cores from Barbwire Terrace (BWT). [A] Glacially striated basement **pavements** exposed in the Oakover River area (UTM 298790E 7627510N) indicating ice flow towards ~ NNW (n=76) into Canning Basin from Pilbara Craton. Overlying tillites dated as Early Permian (Backhouse, 1992). [B] Homogenous muddy siltstone at base of upper Grant facies associations at Grant Range, with out-sized exotic clast, deposited by rainout of debris from floating ice or glacial gravity flow within glaciomarine environment. [C] Massive, matrix-supported diamictite of lower facies association from BWT (Eremophila-3, 251.3 m), with faceted Devonian carbonate clasts and rounded, exotic granitic clasts, deposited from cohesive debris flows (*sensu* Mulder and Alexander, 2001). Similar diamictites were associated with CAP detrital zircon sample (Fig. 6). [D] Massive and thinly bedded turbidite sandstones of lower facies association of BWT (Melaleuca-1, 306.7 m). Similar sandstones were sampled for detrital zircons from Drosera-1 (DRO; Fig. 6). [E] Thin interbeds of sandstone and muddy silt-

stone of upper facies associations at Grant Range. Internal bedforms and sole structures in sandstone beds indicate deposition from turbidity currents, during regressive phase following maximum flooding in the basin. [F] Sub-vertical *Skolithos* burrows up to 0.5 m long within planar cross-bedded nearshore/beach sandstones of upper facies association in St. George Ranges. Note overlying, intensely bioturbated *Macaronichnus segregatis* bed. Such trace fossils in upper facies associations of the Grant Group form part of a low diversity assemblage reflecting the abundance of freshwater input into the Canning Basin upon deglaciation (cf. Buatois et al., 2006). [G] Large scale channel-belt complexes of lower facies associations exposed at Grant Range. Their vertical association with glaciomarine deposits suggests deposition within extensive proglacial outwash channel-belt complexes, demonstrating the large flux of meltwater and sand-grade sediment from retreating ice margins into the Fitzroy Trough. CYC detrital zircons were sampled from a similar channel sandstone. [H] Typical view of upper Grant Group exposures in Fitzroy Valley (in St. George Ranges), showing scree-covered mud- and siltstones recording maximum flooding, overlain by regressive channel sandstone complexes deposited in response to increased sediment supply during deglaciation.

Fig. 3. Canning Basin LPIA-related stratigraphy with relative position of detrital zircon samples. Two youngest Grant Group detrital zircon ages with maximum age error bars (2 sigma) shown. Stages following Gradstein et al. (2012), palynological zones modified from Apak and Backhouse (1998, 1999), Archbold (1999), Mory (2010), Taboada et al. (2015), Bodorokos et al. (2016) and Mory et al. (2017) with dashed lines recognising the current uncertainty in age range of Pennsylvanian to Sakmarian zones, Grant Group macrofaunal age from Archbold (1995) and Taboada et al. (2015), and eastern Australia glacial phases after Fielding et al. (2008; blue boxes) and Waterhouse & Shi (2013; grey boxes).

Fig. 4. Rose diagram of all Grant Group paleocurrents measured from Fitzroy Valley outcrops, demonstrating strongly offshore trend (towards NW). Measurements made from various structures including cross-bedding, ripple lamination, and intraformational striae.

Fig. 5. CL images illustrating internal textures of different zircon age groups discussed in text. Ablation target area circled for U–Pb (unlabeled) and Hf (labeled).

Fig. 6. Sedimentary logs of petroleum well cores sampled for this detrital zircon study (see Fig. 1 for location). Lithofacies code modified from Evans and Benn (2004).

Fig. 7. U–Pb Concordia diagrams for, [A] all detrital zircons, [B] detrital zircons with U–Pb ages < 2000 Ma, and [C] detrital zircons with U–Pb ages < 600 Ma. Plotted with Isoplot (Ludwig, 2003).

Fig. 8. Age probability distribution plot of U–Pb ages for all analyses and for U–Pb ages with < 10% discordance filter applied. Ages < 1000 Ma based on $^{206}Pb^{*}/^{238}U$ ratios and ages > 1000 Ma based on $^{207}Pb^{*}/^{206}Pb^{*}$ ratios. Applying a 10% discordance cut off biases the data to older $^{207}Pb^{*}/^{206}Pb^{*}$ ages relative to younger $^{206}Pb^{*}/^{238}U$ ages, despite many young ages intercepting concordia (Fig. 6C). Plotted using Isoplot (Ludwig, 2003).

Fig. 9. Epsilon Hf (εHf) versus crystallization age plot, and U–Pb age probability distribution plots for detrital zircon samples DRO, CAP and CYC. Ages < 1000 Ma based on $^{206}Pb^{*}/^{238}U$ ratios and ages > 1000 Ma based on $^{207}Pb^{*}/^{206}Pb^{*}$ ratios. A 10% shift for ages of 300 and 1500 Ma equates with a shift of c. 0.5 and 3 εHf values, respectively. Hf evolution curves

marked for chondrites unfractionated reservoir (CHUR) and depleted mantle (DM). Probability distributions plotted using Isoplot (Ludwig, 2003).

Fig. 10. Weighted average $^{206}Pb^{*}/^{238}U$ age for two youngest Grant Group detrital zircons from sample CAP (cap44b and cap103a; Tables 3 and 4). Plotted using Isoplot (Ludwig, 2003).

Fig. 11. Epsilon Hf (εHf) versus crystallization age plot for western and central Australian basement terranes, plotted against Canning Basin detrital zircon dataset (location map in Fig. 1 and basement references discussed in text). Note the similarity between Canning Basin Mesoproterozoic detrital zircons and Arunta and Musgrave terranes, and similarly for Neoproterozoic–Cambrian detrital zircons with those from the Yilgarn terrane.

Fig. 12. Schematic maps summarising erosional and depositional evidence for the LPIA regional glaciation model in western and central Australia. A) Mid-Carboniferous (c. Bashkirian) evidence for glaciation is limited to only sedimentological data for the glaciomarine Nangetty Formation in the Perth Basin. There is currently no direct evidence for the Reeves Formation in the Canning Basin having a glacial association. B) Evidence for extensive glaciation in the Early Permian (c. Asselian) is preserved in the stratigraphic record of all western and central Australian Phanerozoic basins (e.g. Mory et al., 2008) with information on ice-sheet dynamics provided by erosional phenomena and products, including: Grant Group detrital zircons (this study), sub-glacial striated **pavements** and valleys (this study; O'Brien et al., 1998; Eyles & de Broekert, 2001; Gorter et.al., 2008; Mory, 2010; Haines et al., 2011; Al-Hinaai, 2014; Al-Hinaai & Redfern, 2015), and intra-formational striae and Grant Group paleocurrents (this study; O'Brien & Christie-Blick, 1992).

Table 1. Heavy mineral count for detrital zircon samples with cored petroleum well/sample name (DRO: Drosera-1, CAP: Capparis-1, CYC: Cycas-1), depth of sample (m), number, N, of grains counted, and heavy mineral percentage of total (An: anatase, Ap: apatite, Bi: biotite, Cd: chloritoid, Ct: chlorite, Ep: epidote, Ga: garnet, Mo: monazite, Ru: rutile, Sp: sphene, To: tourmaline, Zr: zircon).

Table 2. All Grant Group detrital zircon U-Pb laser ablation MC-ICP-MS analyses.

Table 3. U-Pb laser ablation MC-ICP-MS analyses of two youngest detrital zircons from sample CAP.

Table 4. Hf-isotope laser ablation MC-ICP-MS analyses of two youngest detrital zircons from sample CAP.

Table 5. All Grant Group detrital zircon Hf-isotope laser ablation MC-ICP-MS analyses.

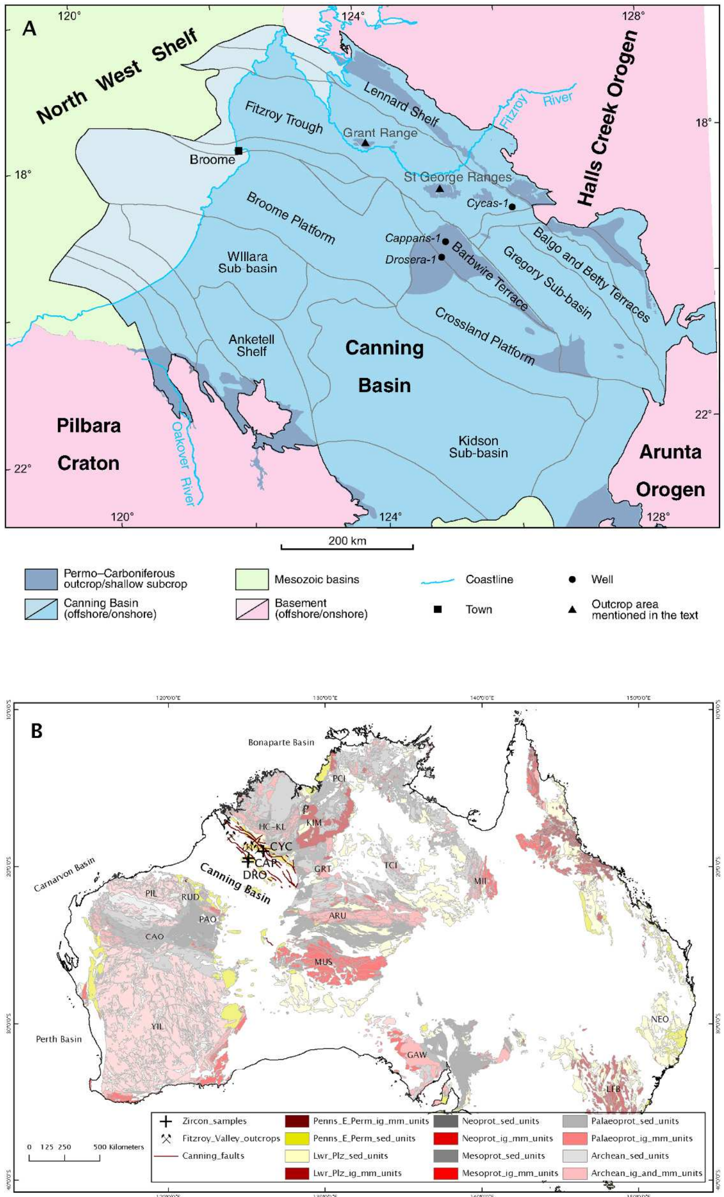

Fig. 1. [A] Map of the Canning Basin showing its sub-basins, detrital zircon sample locations, and place names mentioned in the text. [B] Map of Australia showing basement terranes discussed in the text and location of detrital zircon samples (CAP: Capparis-1, CYC: Cycas-1, DRO: Drosera-1). Geological map modified from Raymond et al. (2012). YIL: Yilgarn Craton, CAO: Capricorn Orogen. PIL: Pilbara Craton, RUD: Rudall Complex, PAO: Paterson Orogen, MUS: Musgrave Block, ARU: Arunta Inlier, GRT: Granites Tanami, HC-KL: Hall's Creek- King Leopold Orogen, KIM: Kimberley Basin, PCO: Pine Creek Orogen, TCI: Tennant Creek Inlier, MII: Mt Isa Inlier, NEO: New England Orogen, LFB: Lachlan Fold Belt, GAW: Gawler Craton.

151x251mm (300 x 300 DPI)

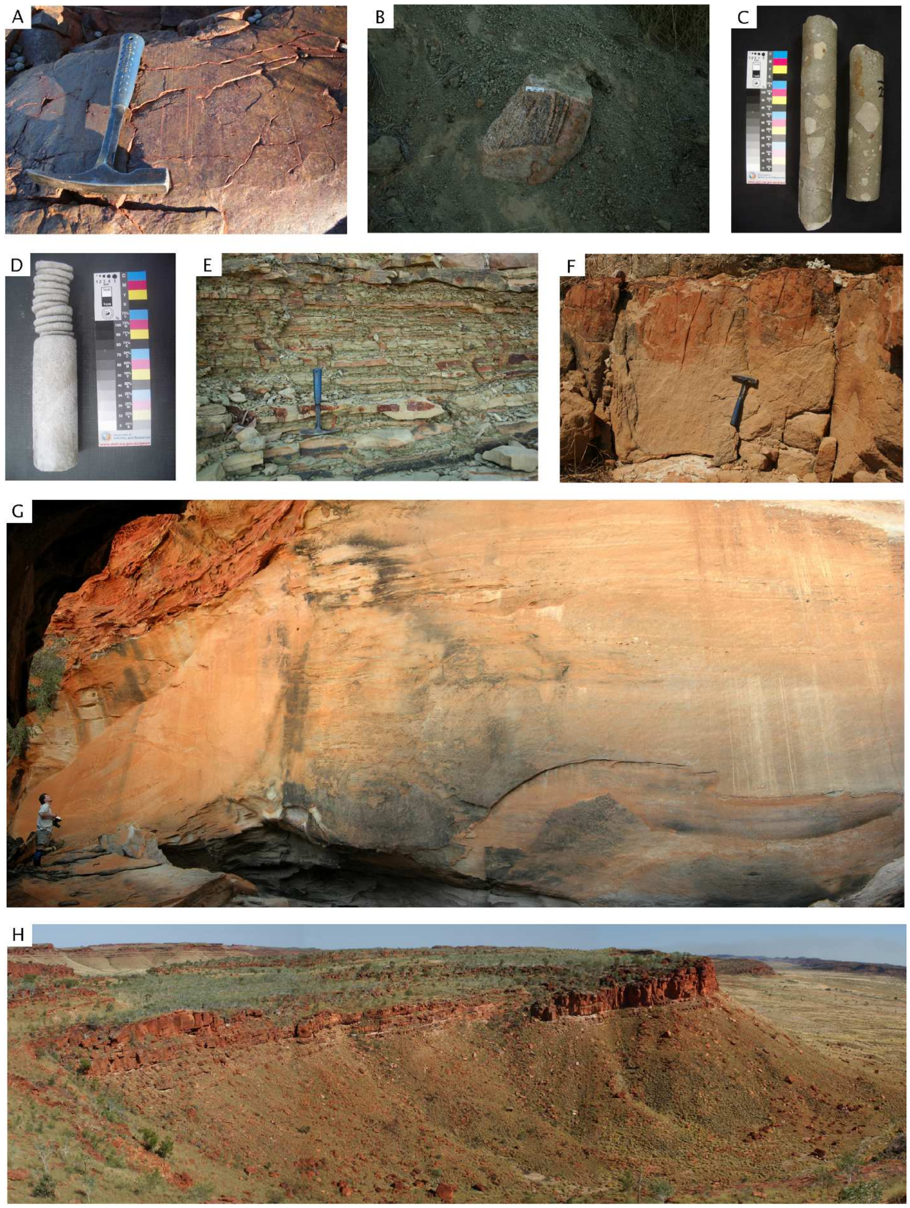

Fig. 2. Photographs of Grant Group exposed in the Fitzroy River valley and Pilbara region and cores from Barbwire Terrace (BWT). [A] Glacially striated basement pavements exposed in the Oakover River area (UTM 298790E 7627510N) indicating ice flow towards ~ NNW (n=76) into Canning Basin from Pilbara Craton. Overlying tillites dated as Early Permian (Backhouse, 1992). [B] Homogenous muddy siltstone at base of upper Grant facies associations at Grant Range, with out-sized exotic clast, deposited by rainout of debris from floating ice or glacial gravity flow within glaciomarine environment. [C] Massive, matrix-supported diamictite of lower facies association from BWT (Eremophila-3, 251.3 m), with faceted Devonian carbonate clasts and rounded, exotic granitic clasts, deposited from cohesive debris flows (*sensu* Mulder and Alexander, 2001). Similar diamictites were associated with CAP detrital zircon sample (Fig. 6). [D] Massive and thinly bedded turbidite sandstones of lower facies association of BWT (Melaleuca-1, 306.7 m). Similar sandstones were sampled for detrital zircons from Drosera-1 (DRO; Fig. 6). [E] Thin interbeds of sandstone and muddy siltstone of upper facies associations at Grant Range. Internal bedforms and sole structures in sandstone beds indicate deposition from turbidity currents, during regressive phase following maximum

flooding in the basin. [F] Sub-vertical *Skolithos* burrows up to 0.5 m long within planar cross-bedded nearshore/beach sandstones of upper facies association in St. George Ranges. Note overlying, intensely bioturbated *Macaronichnus segregatis bed*. Such trace fossils in upper facies associations of the Grant Group form part of a low diversity assemblage reflecting the abundance of freshwater input into the Canning Basin upon deglaciation (cf. Buatois et al., 2006). [G] Large scale channel-belt complexes of lower facies associations exposed at Grant Range. Their vertical association with glaciomarine deposits suggests deposition within extensive proglacial outwash channel-belt complexes, demonstrating the large flux of meltwater and sand-grade sediment from retreating ice margins into the Fitzroy Trough. CYC detrital zircons were sampled from a similar channel sandstone. [H] Typical view of upper Grant Group exposures in Fitzroy Valley (in St. George Ranges), showing scree-covered mud- and siltstones recording maximum flooding, overlain by regressive channel sandstone complexes deposited in response to increased sediment supply during deglaciation.

179x237mm (300 x 300 DPI)

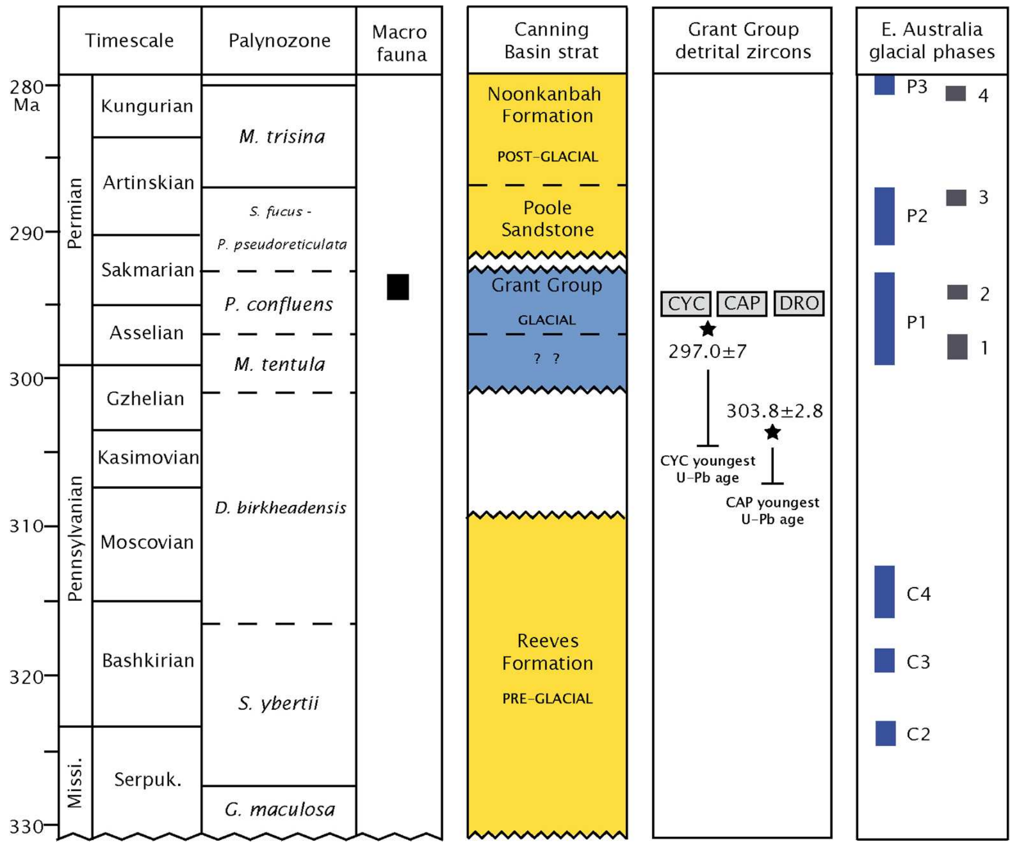

Fig. 3. Canning Basin LPIA-related stratigraphy with relative position of detrital zircon samples. Two youngest Grant Group detrital zircon ages with maximum age error bars (2 sigma) shown. Stages following Gradstein et al. (2012), palynological zones modified from Apak and Backhouse (1998, 1999), Archbold (1999), Mory (2010), Taboada et al. (2015), Bodorokos et al. (2016) and Mory et al. (2017) with dashed lines recognising the current uncertainty in age range of Pennsylvanian to Sakmarian zones, Grant Group macrofaunal age from Archbold (1995) and Taboada et al. (2015), and eastern Australia glacial phases after Fielding et al. (2008; blue boxes) and Waterhouse & Shi (2013; grey boxes).

151x126mm (300 x 300 DPI)

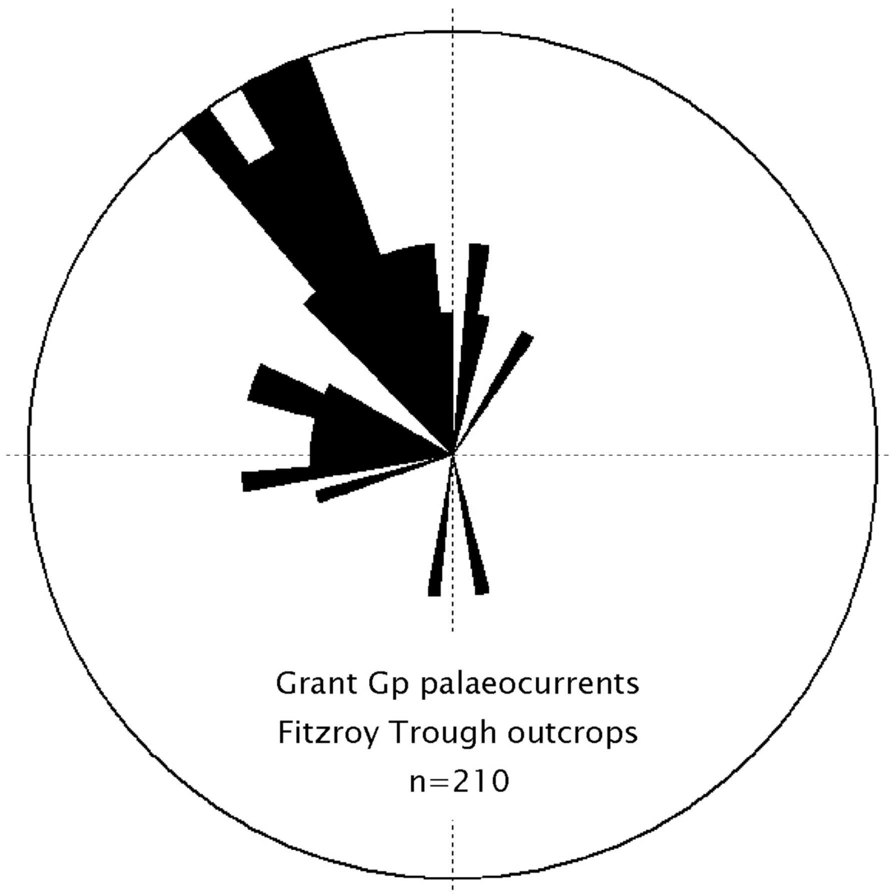

Fig. 4. Rose diagram of all Grant Group paleocurrents measured from Fitzroy Valley outcrops, demonstrating strongly offshore trend (towards NW). Measurements made from various structures including cross-bedding, ripple lamination, and intraformational striae.

113x112mm (300 x 300 DPI)

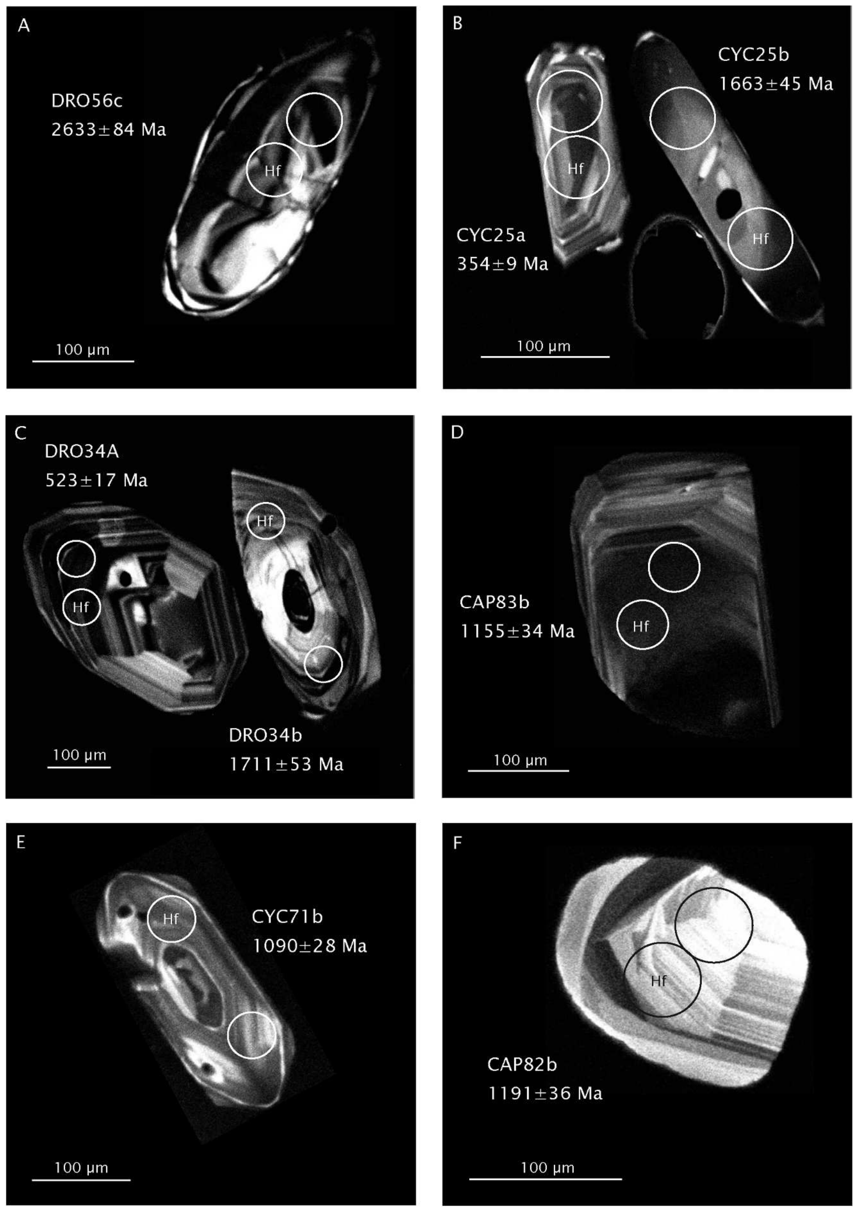

Fig. 5. CL images illustrating internal textures of different zircon age groups discussed in text. Ablation target area circled for U-Pb (unlabeled) and Hf (labeled).

162x230mm (300 x 300 DPI)

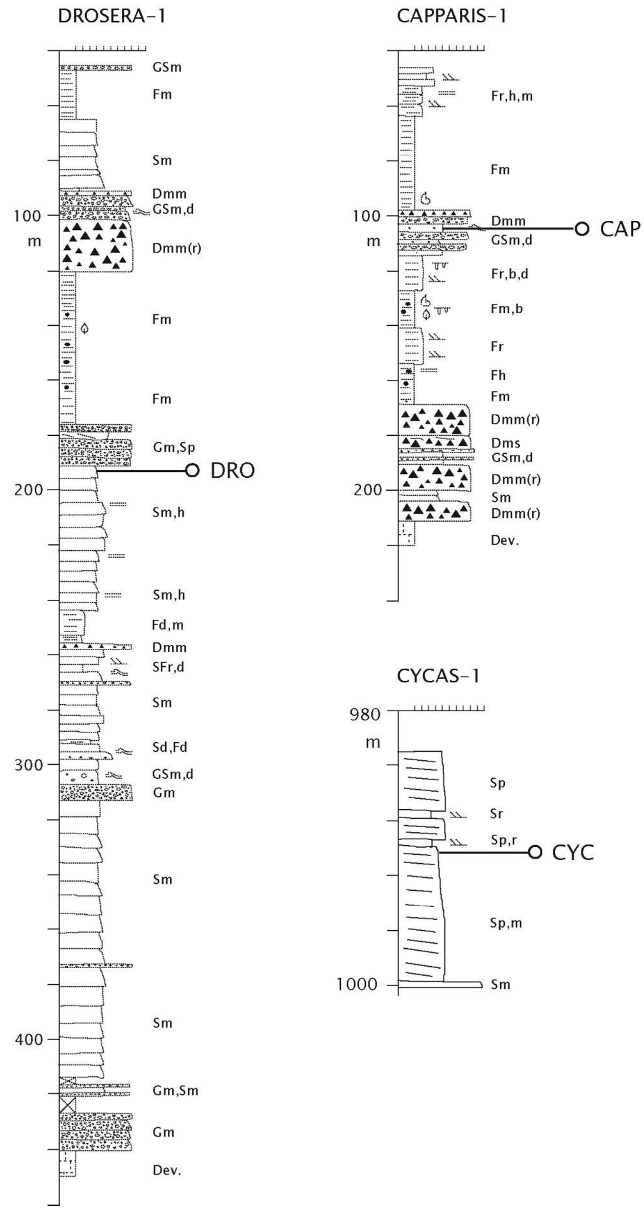

Fig. 6. Sedimentary logs of petroleum well cores sampled for this detrital zircon study (see Fig. 1 for location). Lithofacies code modified from Evans and Benn (2004).

104x198mm (300 x 300 DPI)

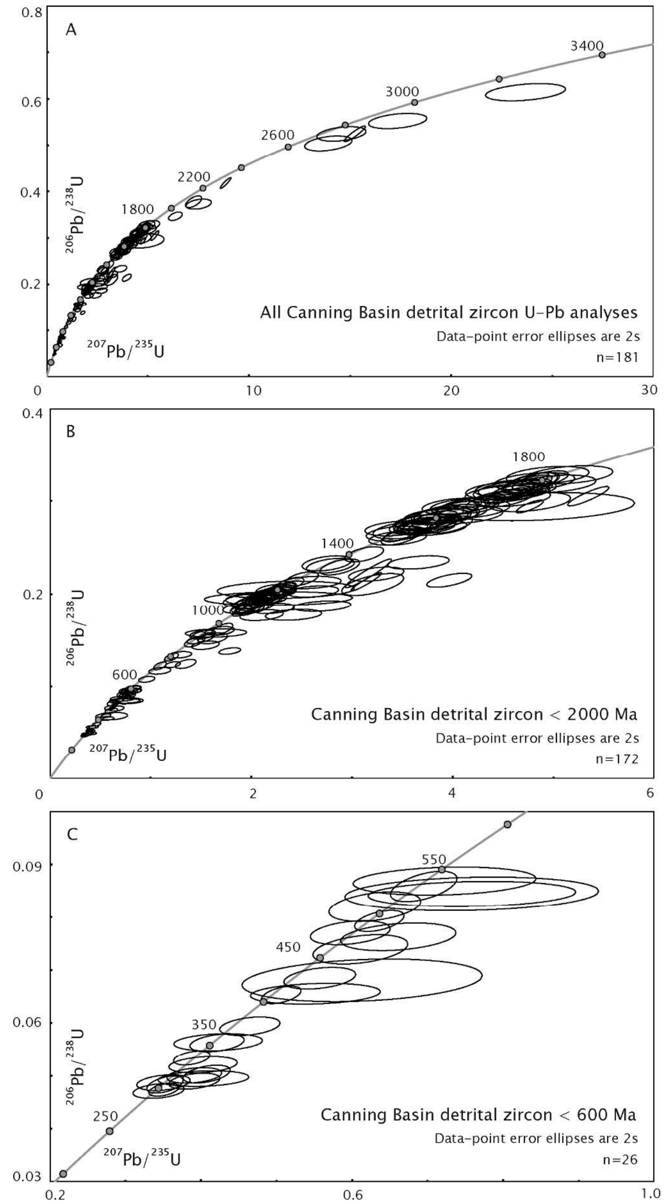

Fig. 7. U-Pb Concordia diagrams for, [A] all detrital zircons, [B] detrital zircons with U-Pb ages < 2000 Ma, and [C] detrital zircons with U-Pb ages < 600 Ma. Plotted with Isoplot (Ludwig, 2003).

137x254mm (300 x 300 DPI)

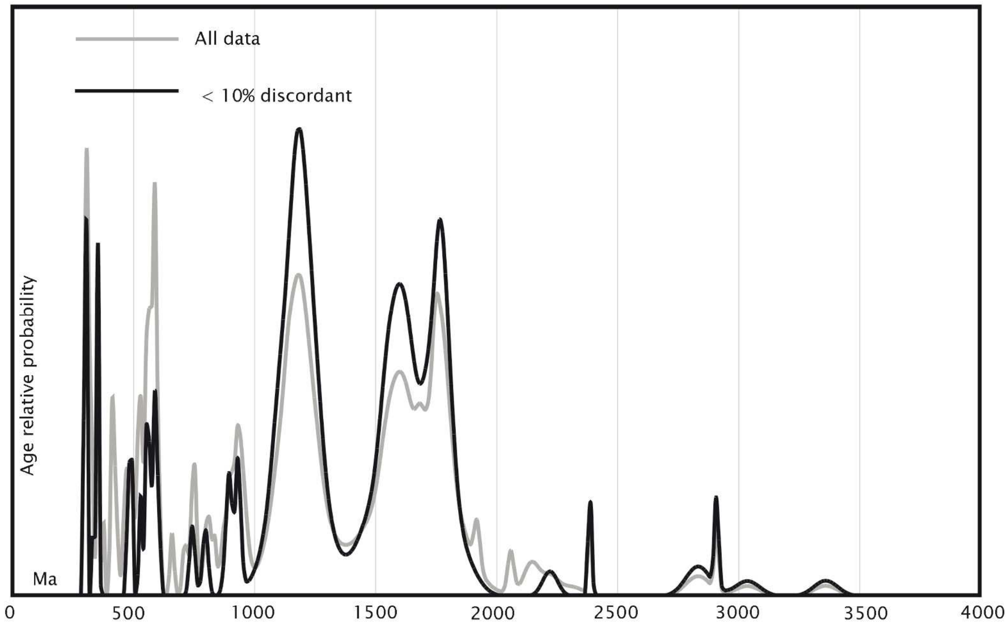

Fig. 8. Age probability distribution plot of U-Pb ages for all analyses and for U-Pb ages with < 10% discordance filter applied. Ages < 1000 Ma based on $^{206}Pb^{*}/^{238}U$ ratios and ages > 1000 Ma based on $^{207}Pb^{*}/^{206}Pb^{*}$ ratios. Applying a 10% discordance cut off biases the data to older $^{207}Pb^{*}/^{206}Pb^{*}$ ages relative to younger $^{206}Pb^{*}/^{238}U$ ages, despite many young ages intercepting concordia (Fig. 6C). Plotted using Isoplot (Ludwig, 2003).

197x123mm (300 x 300 DPI)

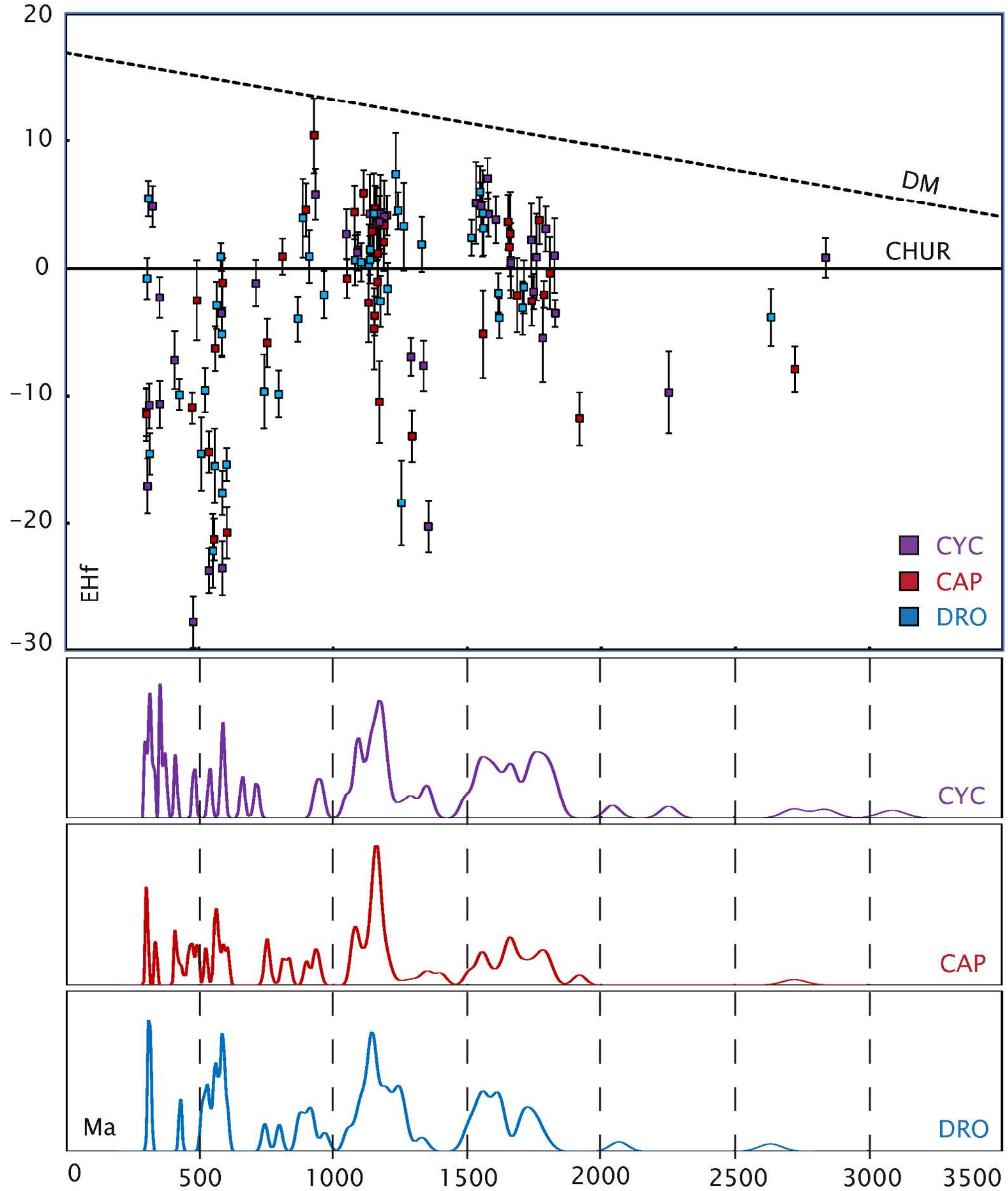

Fig. 9. Epsilon Hf (εHf) versus crystallization age plot, and U-Pb age probability distribution plots for detrital zircon samples DRO, CAP and CYC. Ages < 1000 Ma based on $^{206}Pb^{*}/^{238}U^{*}$ ratios and ages > 1000 Ma based on $^{207}Pb^{*}/^{206}Pb^{*}$ ratios. A 10% shift for ages of 300 and 1500 Ma equates with a shift of c. 0.5 and 3 εHf values, respectively. Hf evolution curves marked for chondrites unfractionated reservoir (CHUR) and depleted mantle (DM). Probability distributions plotted using Isoplot (Ludwig, 2003).

176x212mm (300 x 300 DPI)

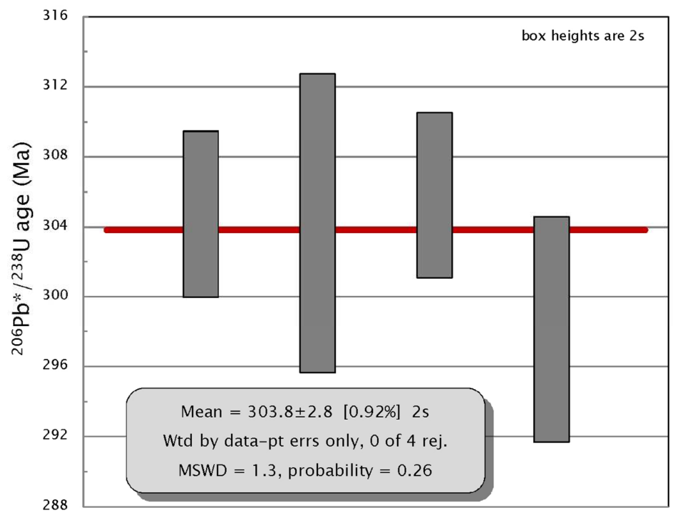

Fig. 10. Weighted average $^{206}Pb^{*}/^{238}U^{*}$ age for two youngest Grant Group detrital zircons from sample CAP (cap44b and cap103a; Tables 3 and 4). Plotted using Isoplot (Ludwig, 2003).

166x108mm (300 x 300 DPI)

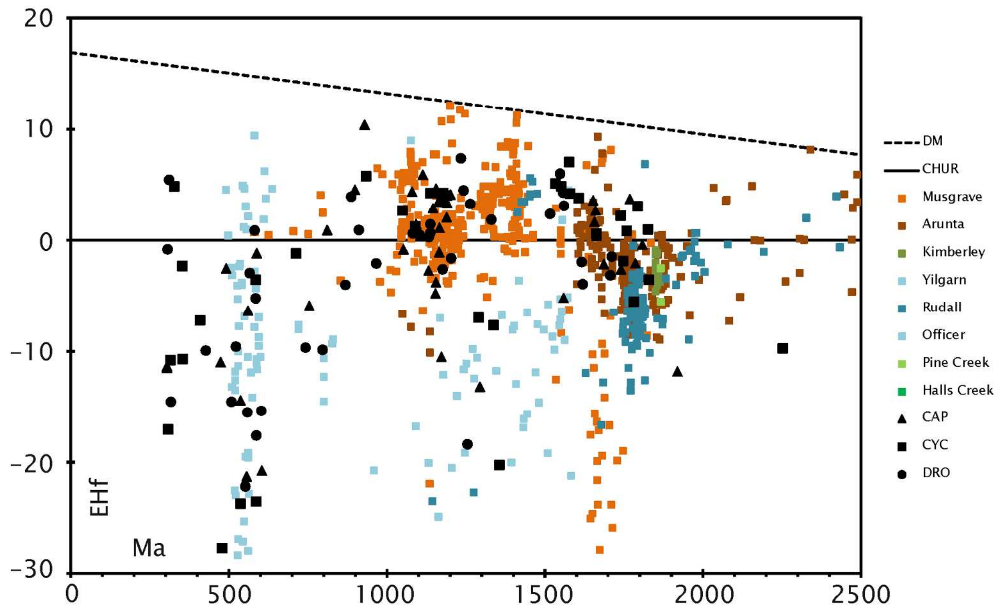

Fig. 11. Epsilon Hf (εHf) versus crystallization age plot for western and central Australian basement terranes, plotted against Canning Basin detrital zircon dataset (location map in Fig. 1 and basement references discussed in text). Note the similarity between Canning Basin Mesoproterozoic detrital zircons and Arunta and Musgrave terranes, and similarly for Neoproterozoic - Cambrian detrital zircons with those from the Yilgarn terrane.

173x105mm (300 x 300 DPI)

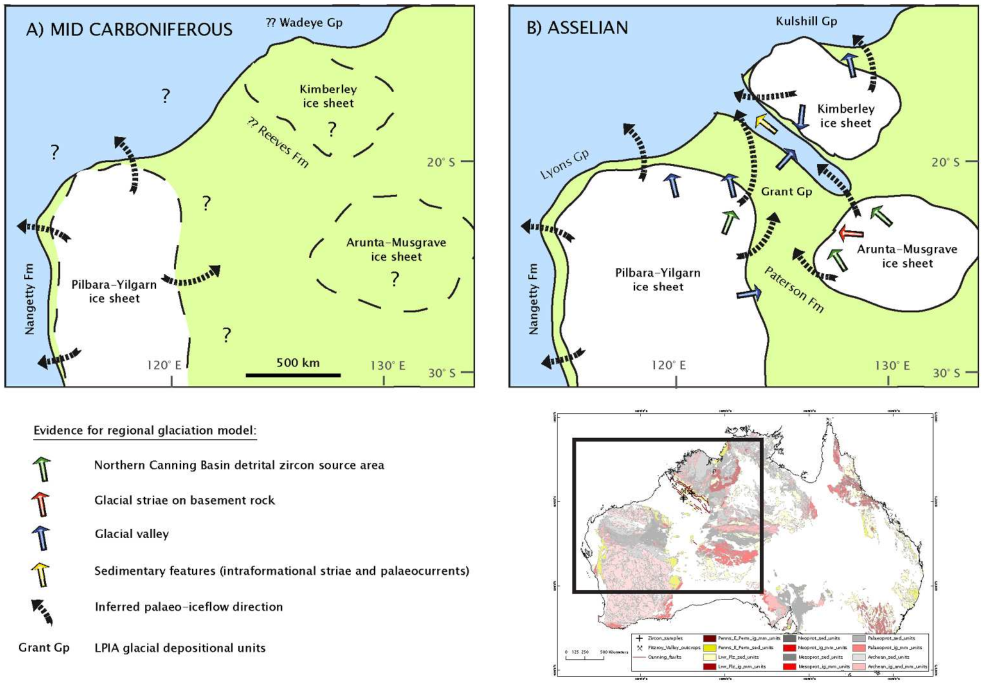

Fig. 12. Schematic maps summarising erosional and depositional evidence for the LPIA regional glaciation model in western and central Australia. A) Mid-Carboniferous (c. Bashkirian) evidence for glaciation is limited to only sedimentological data for the glaciomarine Nangetty Formation in the Perth Basin. There is currently no direct evidence for the Reeves Formation in the Canning Basin having a glacial association. B) Evidence for extensive glaciation in the Early Permian (c. Asselian) is preserved in the stratigraphic record of all western and central Australian Phanerozoic basins (e.g. Mory et al., 2008) with information on ice-sheet dynamics provided by erosional phenomena and products, including: Grant Group detrital zircons (this study), sub-glacial striated pavements and valleys (this study; O'Brien et al., 1998; Eyles & de Broekert, 2001; Gorter et.al., 2008; Mory, 2010; Haines et al., 2011; Al-Hinaai, 2014; Al-Hinaai & Redfern, 2015), and intra-formational striae and Grant Group paleocurrents (this study; O'Brien & Christie-Blick, 1992).

179x123mm (300 x 300 DPI)

Sample	Depth	N	%An	%Ap	%Bi	%Cd
DRO	990.6	500	1	5	0	0
CAP	106.9	500	0	4	1	0
CYC	990.6	500	4	4	0	< 1

%Ct	%Ep	%Ga	%Mo	%Ru	%Sp	%To
0	< 1	65	0	2	< 1	11
< 1	0	68	< 1	2	0	12
0	2	25	< 1	8	3	7

%Zr
15
13
47

Table 2 - All LA U-Pb MC-ICP-MS data

	Signals (mV)						Ratios							Ages (Ma)							
Sample	^{204}Pb	^{206}Pb*	^{207}Pb*	^{238}U	f206 %	Uppm**	^{207}Pb*/^{206}Pb*	1σ%	^{206}Pb*/^{238}U	1σ%	^{207}Pb*/^{235}U	1σ%	Rho	^{207}Pb/^{206}Pb	2σ abs	^{206}Pb*/^{238}U	2σ abs	^{207}Pb*/^{235}U	2σ abs	% disc***	Cm-Pb corr'd?
cap gr1-1	0.001	32.5	3.54	73	0.1	206	0.1087	1.3	0.3195	1.0	4.790	1.7	0.62	1778	48	1787	43	1783	152	-0.5	N
cap gr2-1	0.003	6.1	0.37	82	0.9	234	0.0527	2.3	0.0534	1.0	0.388	2.5	0.41	317	105	335	7	333	20	-5.7	N
cap 4a-1	0.001	24.3	1.86	98	0.1	279	0.0761	1.4	0.1801	1.0	1.889	1.7	0.60	1097	54	1067	24	1077	63	2.7	N
cap4b-1	0.012	5.8	0.83	24	3.4	69	0.0760	7.5	0.1575	1.1	1.650	7.5	0.15	1094	299	943	23	990	226	13.8	Y
cap4c-1	0.000	25.9	2.81	63	0.0	179	0.1071	1.3	0.3047	1.1	4.499	1.7	0.62	1750	49	1714	41	1731	145	2.1	N
cap5-1	0.000	29.8	2.53	112	0.0	318	0.0794	1.4	0.1994	1.0	2.184	1.7	0.61	1183	53	1172	27	1176	73	0.9	N
cap6-1	0.001	12.8	0.94	64	0.1	180	0.0690	1.5	0.1551	1.0	1.475	1.8	0.57	898	60	929	20	920	52	-3.4	N
cap7a-1	0.000	9.5	1.20	23	0.0	65	0.1102	1.6	0.3237	1.1	4.918	1.9	0.57	1802	57	1808	45	1805	175	-0.3	N
cap7b-1	0.010	28.5	3.27	75	0.6	213	0.1049	1.4	0.2990	1.2	4.326	1.8	0.63	1713	53	1686	45	1698	150	1.6	Y
cap8c-1	-0.003	8.9	0.65	107	-0.6	303	0.0562	1.8	0.0653	1.0	0.506	2.1	0.49	461	82	408	9	416	22	11.5	N
cap9-1	-0.001	7.9	0.63	77	-0.1	218	0.0582	1.8	0.0793	1.0	0.636	2.1	0.49	538	80	492	10	500	27	8.5	N
cap11c-1	0.000	3.6	0.43	14	-0.2	40	0.0789	2.5	0.1959	1.1	2.130	2.7	0.39	1169	98	1153	27	1159	110	1.3	N
cap12-1	-0.001	2.1	0.18	9	-0.8	26	0.0770	3.4	0.1920	1.0	2.038	3.6	0.29	1121	137	1132	26	1128	138	-1.0	N
cap-15	-0.001	1.0	0.09	9	-1.9	27	0.0652	7.3	0.0844	1.2	0.759	7.4	0.16	780	307	523	13	573	108	33.0	N
cap16a-1	0.000	11.7	1.37	35	0.1	99	0.0954	1.4	0.2632	1.1	3.464	1.8	0.60	1537	55	1506	37	1519	120	2.0	N
cap16b-1	0.007	73.3	8.65	203	0.2	575	0.1175	0.7	0.2941	1.0	4.765	1.2	0.82	1919	24	1662	36	1779	106	13.4	Y
cap23-1	0.001	8.0	0.70	32	0.1	91	0.0816	1.7	0.1983	1.0	2.233	2.0	0.51	1237	69	1166	26	1191	88	5.7	N
cap24-1	0.004	12.1	0.93	51	0.6	144	0.0793	1.4	0.1950	1.0	2.132	1.7	0.59	1180	55	1148	26	1159	73	2.7	N
cap28-1	0.004	26.1	2.07	96	0.3	314	0.0794	1.9	0.1977	1.0	2.164	2.2	0.47	1182	76	1163	26	1170	92	1.7	N
cap30a-1	0.019	29.5	6.10	67	1.0	219	0.1192	8.0	0.2938	2.1	4.829	8.3	0.25	1945	286	1660	79	1790	596	14.6	Y
cap35-1	0.003	12.7	1.27	36	0.4	119	0.1000	1.9	0.2736	1.3	3.771	2.3	0.56	1623	72	1559	46	1587	165	3.9	N
cap37a-1	-0.003	2.7	0.27	10	-1.8	34	0.0809	3.3	0.1945	1.1	2.169	3.4	0.31	1218	128	1146	27	1171	141	6.0	N
cap37b-1	0.001	4.6	0.37	28	0.3	92	0.0788	2.7	0.1242	1.6	1.349	3.1	0.52	1166	106	755	26	867	82	35.3	N
cap37c-1	0.018	16.1	1.67	42	1.8	139	0.0982	2.2	0.2850	1.5	3.859	2.7	0.55	1591	83	1616	54	1605	189	-1.6	Y
cap38-1	-0.003	35.5	3.49	103	-0.2	337	0.0962	1.9	0.2718	1.0	3.606	2.2	0.47	1552	71	1550	36	1551	147	0.1	N
cap40a-1	0.002	6.4	0.47	55	0.5	181	0.0589	2.5	0.0901	1.1	0.731	2.7	0.39	563	109	556	12	557	39	1.2	N
cap40b-1	0.023	59.3	6.13	220	0.6	719	0.1032	0.9	0.2224	2.8	3.163	3.0	0.95	1682	34	1294	80	1448	175	23.0	Y
cap40c-1	0.015	16.1	1.02	173	1.6	567	0.0600	3.9	0.0739	1.5	0.611	4.2	0.36	603	169	460	14	484	51	23.7	Y
cap41-1	-0.001	56.6	5.77	154	0.0	505	0.1006	1.9	0.2922	1.0	4.054	2.2	0.47	1635	71	1653	38	1645	163	-1.1	N
cap44a-1	-0.001	11.3	0.91	49	-0.2	162	0.0768	2.0	0.1836	1.1	1.944	2.2	0.47	1115	79	1087	25	1096	85	2.5	N
cap44b-1	-0.001	10.4	0.57	177	-0.2	578	0.0538	2.1	0.0473	1.1	0.351	2.3	0.45	363	94	298	6	306	17	17.8	N
cap44e-1	-0.004	27.3	3.04	71	-0.2	231	0.1084	1.9	0.3100	1.0	4.634	2.2	0.47	1773	70	1741	40	1755	185	1.8	N
cap44f-1	0.001	4.6	0.37	19	0.3	61	0.0803	2.3	0.1982	1.0	2.195	2.5	0.42	1205	89	1165	27	1179	105	3.3	N
cap44h-1	0.000	57.4	7.69	134	0.0	438	0.1332	1.9	0.3467	1.1	6.367	2.2	0.49	2140	66	1919	47	2028	248	10.3	N
cap46b-1	0.281	6.7	0.38	77	42.7	251	0.0654	10.3	0.0681	2.4	0.613	10.6	0.23	786	433	425	21	486	124	46.0	Y
cap48c-1	-0.002	8.3	0.69	34	-0.5	112	0.0786	2.1	0.1964	1.0	2.127	2.3	0.44	1161	84	1156	26	1158	97	0.4	N
cap49_1	0.002	15.8	1.18	133	0.2	436	0.0602	2.0	0.0955	1.0	0.792	2.2	0.46	609	85	588	13	592	35	3.5	N
cap59a-1	0.005	57.8	12.29	91	0.1	297	0.2103	0.5	0.5253	1.3	15.233	1.4	0.93	2908	17	2722	88	2830	363	6.4	Y
cap59b-1	0.004	24.8	2.80	64	0.3	211	0.1088	1.9	0.3157	1.0	4.736	2.2	0.48	1780	70	1768	42	1774	191	0.6	N
cap60b-1	0.003	4.7	0.40	28	1.1	92	0.0938	2.2	0.1381	1.0	1.786	2.5	0.42	1505	85	834	18	1040	86	44.6	N
cap60c-1	0.001	5.7	0.42	26	0.4	86	0.0757	2.2	0.1823	1.1	1.902	2.4	0.43	1086	88	1080	25	1082	90	0.6	N
cap61a-1	-0.004	7.1	0.58	47	-1.1	153	0.0718	2.3	0.1234	1.0	1.221	2.5	0.42	979	92	750	17	810	60	23.4	N
cap61c-1	0.006	20.7	2.23	63	0.5	206	0.1050	1.8	0.2745	1.4	3.975	2.3	0.60	1715	67	1564	48	1629	169	8.8	Y
cap64c-1	-0.002	5.5	0.50	29	-0.7	96	0.0704	2.3	0.1496	1.0	1.452	2.5	0.41	940	94	899	20	911	71	4.4	N
cap65a-1	0.003	8.0	0.78	69	0.6	226	0.0588	2.2	0.0908	1.0	0.736	2.5	0.42	559	97	561	12	560	36	-0.2	N
cap67d-1	0.002	5.5	0.33	46	0.7	151	0.0627	2.5	0.0982	1.1	0.850	2.7	0.38	699	108	604	13	624	46	13.6	N
cap68b-1	0.003	9.0	0.62	81	0.6	266	0.0625	2.4	0.0926	1.1	0.799	2.6	0.44	692	101	571	14	596	42	17.5	N
cap69a-1	-0.001	5.9	0.55	25	-0.3	83	0.0764	2.2	0.1886	1.0	1.985	2.5	0.42	1104	90	1114	25	1110	95	-0.8	N
cap70b-1	0.005	3.1	0.25	19	3.0	61	0.0699	3.5	0.1340	1.1	1.292	3.7	0.29	926	144	811	18	842	92	12.4	N
cap72-1	0.003	4.3	0.48	14	1.0	39	0.0790	2.9	0.1847	1.4	2.012	3.3	0.43	1172	116	1093	33	1120	125	6.8	N
cap73c-1	0.007	2.9	0.38	8	3.6	24	0.0830	11.7	0.2047	1.8	2.343	11.9	0.15	1270	458	1201	48	1226	449	5.4	Y
cap75b-1	0.004	13.2	1.55	25	0.5	71	0.1083	1.9	0.3193	1.4	4.769	2.3	0.60	1771	68	1786	57	1779	203	-0.8	N
cap84a-1	0.001	25.4	2.76	55	0.1	156	0.1005	1.8	0.2931	1.4	4.061	2.3	0.60	1633	68	1657	52	1646	173	-1.4	N
cap81a-1	0.010	19.5	1.77	61	0.8	173	0.0819	2.2	0.2026	1.4	2.288	2.6	0.54	1243	87	1189	37	1209	116	4.3	Y
cap83a-1	0.006	11.9	1.07	32	0.8	91	0.0856	3.3	0.2331	1.4	2.750	3.6	0.39	1329	130	1351	42	1342	185	-1.6	Y
cap83a-2	0.001	13.7	1.33	37	0.1	105	0.0932	2.1	0.2427	1.4	3.120	2.5	0.54	1492	81	1401	43	1438	149	6.1	N
cap83b-1	-0.004	12.9	1.13	43	-0.5	123	0.0788	1.9	0.1963	1.3	2.132	2.3	0.58	1167	74	1155	34	1159	95	1.0	N

cap82b-1	0.004	7.4	0.91	23	0.9	66	0.0820	2.4	0.2028	1.4	2.293	2.8	0.50	1245	95	1191	36	1210	123	4.4	N
cap104-1	0.000	2.2	0.20	18	0.0	52	0.0629	4.5	0.0763	1.4	0.661	4.7	0.30	704	191	474	14	515	61	32.7	N
cap103a-1	0.002	6.9	0.36	96	0.4	271	0.0529	2.4	0.0483	1.4	0.352	2.8	0.49	324	110	304	8	307	20	6.2	N
dro2b-1	-0.001	9.5	0.80	26	-0.2	73	0.0819	2.0	0.2109	1.4	2.382	2.4	0.57	1244	76	1234	37	1237	109	0.8	N
dro2c-1	0.000	6.7	0.55	44	0.1	124	0.0587	2.2	0.0859	1.4	0.695	2.6	0.53	556	96	531	15	536	36	4.4	N
dro2d-1	0.001	2.5	0.15	16	0.5	45	0.0630	3.1	0.0905	1.4	0.786	3.4	0.40	708	133	559	16	589	53	21.1	N
dro3a-1	-0.002	2.9	0.20	20	-1.6	57	0.0557	3.7	0.0820	1.4	0.630	3.9	0.36	442	164	508	15	496	49	-15.0	N
dro3b-1	0.000	15.3	1.00	73	0.0	208	0.0649	1.9	0.1221	1.4	1.093	2.4	0.60	772	80	743	22	750	51	3.8	N
dro7a-1	0.003	20.5	1.94	45	0.2	129	0.0965	1.8	0.2616	1.4	3.482	2.3	0.60	1558	68	1498	45	1523	148	3.9	N
dro7b-1	0.002	10.7	0.86	31	0.3	87	0.0816	1.9	0.2058	1.4	2.316	2.3	0.58	1237	74	1206	36	1217	103	2.4	N
dro8-1	0.003	3.4	0.23	11	1.5	30	0.0792	2.2	0.1921	1.4	2.097	2.6	0.53	1177	88	1133	34	1148	106	3.8	N
dro10a-1	-0.002	6.8	0.56	21	-0.5	58	0.0789	2.0	0.1957	1.4	2.129	2.4	0.57	1170	78	1152	35	1158	99	1.6	N
dro10b-1	0.002	5.2	0.34	21	0.7	60	0.0702	2.2	0.1475	1.4	1.428	2.6	0.53	935	92	887	26	901	74	5.1	N
dro10c-1	0.000	6.1	0.61	13	-0.1	37	0.0989	2.0	0.2801	1.4	3.820	2.4	0.56	1604	75	1592	49	1597	173	0.8	N
dro11b-1	-0.002	8.6	0.88	19	-0.4	53	0.0972	1.9	0.2733	1.4	3.665	2.4	0.58	1572	72	1558	48	1564	163	0.9	N
dro12a-1	0.003	12.2	0.71	83	0.5	235	0.0607	1.9	0.0893	1.4	0.748	2.4	0.57	628	83	552	16	567	35	12.1	N
dro12b-1	0.002	27.8	2.72	62	0.1	175	0.0982	1.8	0.2726	1.4	3.690	2.3	0.60	1589	67	1554	48	1569	156	2.2	N
dro14b-1	0.003	24.6	3.27	70	0.2	197	0.1338	1.8	0.2149	1.4	3.966	2.3	0.62	2149	63	1255	39	1627	170	41.6	N
dro17a-1	-0.002	25.0	2.76	48	-0.1	135	0.1087	1.8	0.3199	1.4	4.794	2.3	0.61	1778	66	1789	56	1784	199	-0.6	N
dro17b-1	0.034	19.0	1.58	54	2.9	152	0.0839	2.3	0.2165	1.4	2.503	2.7	0.53	1289	89	1263	39	1273	128	2.0	Y
dro17c-1	0.006	20.8	1.68	62	0.5	177	0.0810	2.2	0.2051	1.4	2.291	2.6	0.53	1221	87	1203	37	1209	115	1.5	Y
dro16a-1	0.008	59.9	7.66	121	0.2	343	0.1271	0.7	0.3051	1.4	5.345	1.6	0.89	2058	25	1716	54	1876	157	16.6	Y
dro16c-1	0.009	21.8	1.68	84	0.7	239	0.0768	1.9	0.1617	1.6	1.713	2.5	0.63	1117	76	966	32	1014	82	13.5	Y
dro19a-1	-0.003	24.6	2.01	78	-0.2	222	0.0793	1.8	0.1942	1.4	2.123	2.3	0.60	1179	72	1144	34	1156	94	3.0	N
dro21b-1	0.003	4.4	0.22	55	1.2	156	0.0588	2.8	0.0503	1.4	0.408	3.1	0.44	559	122	316	9	347	25	43.4	N
dro22-1	0.000	11.6	0.94	36	0.0	102	0.0800	1.9	0.2002	1.4	2.209	2.3	0.59	1198	73	1176	35	1184	99	1.8	N
dro24c-1	-0.002	21.5	1.62	88	-0.2	250	0.0737	1.8	0.1530	1.4	1.554	2.3	0.60	1032	74	918	27	952	70	11.1	N
dro24b-1	0.002	9.4	0.87	25	0.4	72	0.0911	2.3	0.2292	1.5	2.879	2.8	0.54	1449	89	1330	45	1377	151	8.2	N
dro31a-1	-0.002	5.1	0.33	34	-0.9	97	0.0575	3.1	0.0917	1.4	0.727	3.3	0.41	511	134	566	16	555	48	-10.8	N
dro32a-1	0.000	22.4	1.78	77	0.0	218	0.0787	1.8	0.1827	1.4	1.982	2.3	0.60	1164	72	1082	32	1109	88	7.0	N
dro32b-1	0.000	33.2	3.62	67	0.0	190	0.1082	1.8	0.3120	1.4	4.657	2.3	0.60	1770	66	1751	54	1759	194	1.1	N
dro33b-1	0.001	66.8	9.36	112	0.0	317	0.1394	1.8	0.3779	1.4	7.266	2.2	0.60	2220	62	2066	65	2145	287	6.9	N
dro34a-1	0.061	7.1	0.46	53	13.1	150	0.0652	8.9	0.0844	1.5	0.759	9.0	0.17	779	375	523	17	573	131	33.0	Y
dro34b-1	-0.001	26.9	2.96	57	0.0	161	0.1090	1.8	0.3040	1.4	4.570	2.3	0.60	1783	66	1711	53	1744	190	4.0	N
dro36-1	-0.002	17.0	1.17	83	-0.2	235	0.0666	1.9	0.1315	1.3	1.208	2.3	0.58	825	78	797	23	804	55	3.4	N
dro35b-1	-0.001	1.7	0.14	6	-0.7	16	0.0717	3.7	0.1930	1.4	1.907	4.0	0.36	977	151	1137	35	1084	143	-16.4	N
dro37b-1	-0.001	7.4	0.59	32	-0.2	91	0.0776	3.4	0.1443	1.3	1.545	3.6	0.35	1138	135	869	24	948	108	23.6	N
dro37c-1	0.005	13.3	1.00	44	0.6	126	0.0799	3.2	0.1930	1.2	2.126	3.4	0.35	1195	126	1138	30	1157	138	4.8	N
dro65b-1	0.002	33.8	3.33	81	0.1	229	0.0985	3.2	0.2739	1.2	3.720	3.4	0.35	1596	119	1560	42	1576	229	2.2	N
dro66b-1	0.000	6.7	0.53	23	0.1	64	0.0793	3.3	0.1870	1.3	2.045	3.5	0.35	1180	131	1105	30	1131	138	6.3	N
dro66c-1	-0.004	4.2	0.28	54	-1.6	154	0.0522	3.9	0.0487	1.2	0.350	4.1	0.30	295	180	306	8	305	29	-3.8	N
dro64c-1	0.005	24.2	2.62	53	0.3	150	0.1098	3.2	0.3031	1.2	4.588	3.4	0.36	1796	116	1707	48	1747	276	5.0	N
dro64e-1	0.007	20.6	1.20	145	0.6	412	0.0570	3.2	0.0953	1.2	0.750	3.4	0.35	493	142	587	15	568	51	-19.1	Y
dro63f-1	0.005	2.9	0.24	11	2.7	31	0.0990	4.5	0.1772	1.4	2.419	4.7	0.29	1606	169	1051	31	1248	209	34.5	N
dro63e-1	0.000	4.0	0.41	10	0.0	28	0.1013	3.5	0.2714	1.3	3.790	3.8	0.34	1648	132	1548	44	1591	255	6.1	N
dro63b-1	0.000	1.8	0.14	6	-0.2	18	0.0733	4.5	0.1952	1.2	1.973	4.7	0.26	1022	183	1150	31	1106	172	-12.5	N
dro61b-1	-0.001	2.3	0.15	16	-0.8	46	0.0616	4.7	0.0949	1.2	0.807	4.9	0.25	661	203	585	15	601	77	11.5	N
dro61a-1	0.000	2.2	0.14	30	0.1	86	0.0592	6.0	0.0494	1.2	0.403	6.1	0.20	574	259	311	8	344	49	45.8	N
dro60b-1	-0.001	5.6	0.55	14	-0.3	41	0.0940	3.3	0.2651	1.2	3.437	3.5	0.35	1509	124	1516	42	1513	220	-0.5	N
dro60e-1	0.000	21.1	1.71	71	0.0	203	0.0810	3.2	0.2022	1.2	2.259	3.4	0.35	1221	125	1187	31	1199	145	2.8	N
dro60d-1	0.005	48.0	5.28	163	0.2	462	0.1105	3.2	0.2104	2.3	3.206	3.9	0.58	1808	116	1231	62	1459	228	31.9	N
dro60c-1	0.005	12.3	1.27	28	0.6	79	0.1077	3.2	0.3126	1.2	4.641	3.4	0.35	1761	117	1753	48	1757	279	0.4	N
dro59b-1	0.004	31.9	3.17	79	0.2	225	0.1000	3.2	0.2856	1.2	3.939	3.4	0.35	1625	118	1620	44	1622	241	0.3	N
dro58d-1	-0.003	27.2	2.81	68	-0.2	192	0.1010	3.2	0.2875	1.2	4.004	3.4	0.36	1643	118	1629	45	1635	245	0.8	N
dro58c-1	0.001	14.6	1.44	38	0.1	107	0.0989	3.2	0.2828	1.2	3.858	3.4	0.36	1604	119	1605	44	1605	238	-0.1	N
dro58a-1	0.000	7.9	0.47	59	0.0	168	0.0588	3.4	0.0944	1.2	0.765	3.6	0.34	559	146	581	15	577	54	-4.0	N
dro57-1	-0.003	2.3	0.24	7	-1.9	21	0.0883	4.7	0.2125	1.3	2.587	4.8	0.26	1388	179	1242	34	1297	226	10.5	N
dro56c-1	0.001	22.7	4.54	33	0.1	93	0.2002	3.2	0.5045	1.3	13.926	3.4	0.38	2828	104	2633	84	2745	682	6.9	N
dro56a-1	0.033	2.4	0.20	9	18.4	25	0.0843	13.2	0.1952	1.5	2.270	13.2	0.12	1300	511	1150	39	1203	478	11.6	Y
dro55a-1	0.000	57.2	6.07	148	0.0	420	0.1057	3.2	0.2850	1.3	4.152	3.4	0.38	1726	117	1616	47	1665	254	6.3	N
dro55b-1	0.000	5.8	0.36	43	-0.1	122	0.0609	3.5	0.0979	1.2	0.823	3.7	0.32	637	150	602	15	610	60	5.4	N
dro54-1	0.003	12.5	0.70	133	0.4	377	0.0590	3.3	0.0685	1.2	0.557	3.5	0.35	568	142	427	11	450	39	24.9	N
dro51a-1	0.004	3.7	0.33	15	1.8	42	0.1049	4.1	0.1868	1.3	2.702	4.3	0.29	1712	153	1104	31	1329	214	35.5	N

dro52d-1	-0.001	5.3	0.42	26	-0.2	74	0.0773	3.3	0.1518	1.6	1.619	3.6	0.43	1129	131	911	31	977	113	19.3	N
cyc1a-1	0.003	28.9	6.59	32	0.2	89	0.2277	3.2	0.5528	1.2	17.351	3.4	0.36	3036	102	2837	85	2954	791	6.6	N
cyc3-1	0.002	22.0	2.08	48	0.2	137	0.0948	3.2	0.2684	1.4	3.508	3.5	0.40	1524	120	1533	48	1529	222	-0.6	N
cyc5-1	0.003	29.9	3.01	59	0.1	168	0.1015	3.2	0.2942	1.2	4.118	3.4	0.35	1652	118	1662	45	1658	250	-0.6	N
cyc7a-1	-0.001	52.4	5.66	101	0.0	285	0.1073	3.2	0.3098	1.2	4.583	3.4	0.35	1754	116	1740	47	1746	275	0.8	N
cyc9-1	0.000	29.6	3.26	55	0.0	155	0.1095	3.2	0.3274	1.2	4.942	3.4	0.35	1791	116	1826	50	1809	294	-1.9	N
cyc10b-1	0.002	30.3	2.40	98	0.1	277	0.0792	3.2	0.1929	1.2	2.107	3.4	0.35	1177	126	1137	30	1151	136	3.4	N
cyc11b-1	0.001	24.2	2.58	48	0.0	136	0.1061	3.2	0.3074	1.2	4.496	3.4	0.35	1733	117	1728	47	1730	271	0.3	N
cyc14b-1	0.012	145.2	22.53	208	0.1	589	0.1535	0.4	0.4182	1.1	8.849	1.2	0.93	2385	15	2252	61	2323	199	5.6	Y
cyc15a-1	-0.001	15.3	1.23	46	-0.1	131	0.0796	3.2	0.2002	1.2	2.199	3.4	0.35	1188	126	1177	31	1181	142	1.0	N
cyc30a-	0.002	51.6	10.42	60	0.0	171	0.2014	3.2	0.5250	1.2	14.576	3.4	0.36	2837	104	2720	82	2788	699	4.1	N
cyc17-1	-0.002	6.6	0.56	20	-0.6	57	0.0795	3.4	0.1990	1.2	2.183	3.6	0.33	1186	133	1170	31	1176	147	1.3	N
cyc20a-1	-0.004	17.6	1.95	35	-0.3	100	0.1065	3.2	0.3136	1.2	4.606	3.4	0.35	1741	117	1758	49	1750	278	-1.0	N
cyc21-1	0.005	3.7	0.29	12	2.1	33	0.0935	3.8	0.2028	1.2	2.614	3.9	0.31	1498	142	1190	32	1305	191	20.5	N
cyc33c-1	-0.004	23.6	2.63	45	-0.3	127	0.1087	3.2	0.3209	1.2	4.811	3.4	0.35	1778	116	1794	50	1787	288	-0.9	N
cyc34-1	-0.002	87.9	9.38	183	0.0	519	0.1045	3.3	0.2913	1.4	4.200	3.6	0.39	1706	123	1648	52	1674	269	3.4	N
cyc34b-1	0.000	10.5	0.66	70	-0.1	198	0.0614	3.3	0.0949	1.2	0.803	3.5	0.34	653	141	585	15	599	55	10.5	N
cyc57b-1	0.000	40.2	4.61	79	0.0	224	0.1141	3.2	0.3182	1.2	5.005	3.4	0.36	1865	115	1781	49	1820	297	4.5	N
cyc58b-1	-0.001	8.6	0.50	70	-0.2	198	0.0563	3.4	0.0770	1.2	0.598	3.6	0.33	463	151	478	12	476	43	-3.3	N
cyc91b-1	-0.002	4.2	0.45	9	-1.0	27	0.0986	3.4	0.2721	1.2	3.697	3.6	0.34	1597	127	1551	43	1571	241	2.9	N
cyc91c-1	-0.002	38.6	10.87	38	-0.1	107	0.2794	3.2	0.6146	1.2	23.674	3.4	0.36	3359	99	3088	97	3255	975	8.1	N
cyc93-1	-0.005	12.0	0.72	127	-0.8	361	0.0543	3.3	0.0563	1.2	0.421	3.5	0.35	383	146	353	9	357	29	7.9	N
cyc90b-1	0.000	4.3	0.34	15	0.0	41	0.0764	3.5	0.1890	1.2	1.992	3.7	0.33	1107	140	1116	30	1113	140	-0.8	N
cyc85-1	-0.001	15.2	1.74	42	-0.1	119	0.1134	3.2	0.2340	1.2	3.658	3.4	0.36	1854	115	1355	38	1562	227	26.9	N
cyc84a-1	0.005	9.9	0.50	135	0.9	382	0.0580	3.3	0.0490	1.2	0.391	3.5	0.35	529	144	308	8	335	28	41.8	N
cyc84c-1	0.003	52.9	4.20	176	0.1	498	0.0797	3.2	0.1990	1.2	2.187	3.4	0.35	1190	125	1170	31	1177	141	1.7	N
cyc82a-1	-0.002	12.9	1.31	30	-0.2	85	0.0982	3.2	0.2830	1.2	3.834	3.4	0.36	1591	119	1607	44	1600	237	-1.0	N
cyc50-1	-0.003	10.8	0.67	122	-0.5	346	0.0567	3.3	0.0594	1.2	0.465	3.5	0.34	481	146	372	9	388	33	22.5	N
cyc49c-1	0.000	2.6	0.23	10	0.2	30	0.0863	4.0	0.1767	1.4	2.103	4.2	0.32	1344	153	1049	31	1150	165	22.0	N
cyc49b-1	0.001	1.4	0.06	11	1.6	31	0.0603	6.7	0.0869	1.2	0.723	6.8	0.18	615	291	537	14	552	96	12.7	N
cyc49a-1	0.002	58.2	8.55	109	0.0	309	0.1463	3.2	0.3728	1.2	7.521	3.4	0.35	2304	109	2042	57	2176	418	11.3	N
cyc48a-1	-0.001	24.0	2.81	55	-0.1	157	0.1156	3.2	0.2988	1.4	4.765	3.5	0.40	1890	114	1686	54	1779	290	10.8	N
cyc47-1	0.002	5.6	0.42	19	0.7	55	0.0790	3.4	0.1996	1.2	2.173	3.6	0.33	1172	134	1173	31	1173	147	-0.1	N
cyc45a-1	0.004	27.4	2.58	75	0.2	213	0.0963	3.2	0.2601	1.2	3.454	3.4	0.35	1554	119	1490	40	1517	214	4.1	N
cyc45b-1	0.013	13.6	0.91	84	1.6	239	0.0678	3.9	0.1168	1.3	1.091	4.1	0.31	861	162	712	19	749	87	17.3	Y
cyc46c-1	0.002	21.5	2.13	55	0.2	155	0.1000	3.2	0.2840	1.2	3.916	3.4	0.36	1624	118	1612	45	1617	240	0.8	N
cyc44a-1	-0.004	19.3	1.76	60	-0.3	169	0.0876	3.2	0.2305	1.4	2.786	3.5	0.40	1374	123	1337	42	1352	180	2.7	N
cyc41-1	0.004	5.9	0.28	90	1.3	255	0.0567	3.6	0.0500	1.2	0.391	3.8	0.31	480	159	315	8	335	30	34.5	N
cyc40-1	0.000	4.0	0.36	17	-0.1	47	0.0873	3.6	0.1842	1.3	2.217	3.9	0.33	1367	141	1090	30	1186	160	20.2	N
cyc25a-1	0.015	10.6	0.59	137	2.5	388	0.0544	5.5	0.0564	1.2	0.423	5.7	0.21	386	249	354	9	358	47	8.4	Y
cyc25b-1	-0.002	19.3	1.96	49	-0.1	139	0.0993	3.2	0.2943	1.2	4.031	3.4	0.35	1611	119	1663	45	1640	246	-3.2	N
cyc38c-1	0.000	7.9	0.60	37	0.0	106	0.0767	3.3	0.1597	1.2	1.688	3.5	0.34	1112	131	955	25	1004	113	14.1	N
cyc38b-1	0.003	3.3	0.15	49	1.4	138	0.0561	4.4	0.0521	1.2	0.403	4.6	0.26	458	196	327	8	344	37	28.5	N
cyc38a-1	0.004	19.5	1.48	74	0.3	210	0.0776	3.2	0.1949	1.2	2.086	3.4	0.35	1138	129	1148	30	1144	136	-0.9	N
cyc39-1	-0.001	4.5	0.30	36	-0.5	101	0.0633	3.7	0.0953	1.2	0.832	3.9	0.31	718	157	587	15	615	64	18.2	N
cyc37b-1	-0.002	15.7	1.56	43	-0.2	122	0.0976	3.2	0.2776	1.2	3.736	3.4	0.35	1579	120	1579	43	1579	231	0.0	N
cyc37c	-0.001	14.3	1.13	60	-0.1	169	0.0774	3.2	0.1841	1.2	1.965	3.4	0.35	1131	128	1089	28	1103	128	3.7	N
cyc60c-1	0.003	13.8	0.95	69	0.3	197	0.0706	3.2	0.1559	1.3	1.518	3.5	0.37	946	132	934	25	938	102	1.3	N
cyc59a-1	0.011	42.6	4.63	100	0.4	282	0.1079	1.0	0.3207	1.2	4.770	1.6	0.76	1764	37	1793	49	1780	140	-1.7	Y
cyc97a-1	0.001	7.7	0.80	19	0.2	55	0.1050	3.2	0.3114	1.2	4.508	3.4	0.35	1714	119	1748	48	1732	274	-2.0	N
cyc67-1	0.000	3.8	0.35	11	0.0	31	0.0922	3.5	0.2704	1.2	3.440	3.7	0.32	1472	133	1543	41	1514	230	-4.8	N
cyc71b-1	-0.002	18.0	1.36	74	-0.2	211	0.0738	3.2	0.1842	1.2	1.876	3.4	0.35	1037	129	1090	28	1072	123	-5.1	N
cyc72-1	0.032	9.1	0.89	18	5.4	52	0.0987	3.4	0.2770	1.3	3.770	3.6	0.35	1600	125	1576	45	1586	243	1.5	Y
cyc77a-1	0.030	92.9	9.97	247	0.5	700	0.1068	0.6	0.2133	1.9	3.141	2.0	0.95	1746	23	1246	51	1443	119	28.6	Y
cyc78a-1	-0.001	26.8	1.77	141	-0.1	399	0.0648	3.2	0.1077	1.2	0.962	3.4	0.35	767	134	659	17	684	64	14.1	N
cyc78b-1	-0.003	3.4	0.22	41	-1.6	116	0.0530	3.8	0.0471	1.2	0.344	4.0	0.30	327	174	297	7	300	28	9.4	N
cyc79-1	0.000	8.8	0.70	24	-0.1	69	0.0792	3.3	0.2047	1.2	2.237	3.5	0.35	1178	129	1201	32	1193	147	-1.9	N
cy109e-1	-0.001	61.3	7.07	102	0.0	288	0.1141	3.2	0.3280	1.2	5.160	3.4	0.36	1866	115	1829	51	1846	305	2.0	N
cyc110-1	0.002	24.6	1.94	73	0.1	208	0.0791	3.2	0.1937	1.2	2.112	3.4	0.36	1175	126	1141	30	1153	137	2.8	N
cyc118a-1	0.004	111.3	11.84	292	0.1	827	0.1061	3.2	0.2216	1.4	3.240	3.5	0.40	1733	116	1290	40	1467	206	25.6	N
cyc118b-1	0.001	1.6	0.08	14	1.3	40	0.0610	6.3	0.0656	1.2	0.552	6.4	0.19	640	269	409	10	446	69	36.1	N

* = radiogenic
** uncertainty on U concentration c.25%

*** discordance is percentage difference between $^{207}Pb/^{206}Pb$ and $^{206}Pb/^{238}U$ ages

Cm-Pb corr'd? = common lead corrected data Yes or No

Table 3 - Multiple analyses of two youngest grains from sample CAP.

	Signals (mV)					Ratios							Ages (Ma)							
Sample	^{204}Pb	^{206}Pb*	^{207}Pb*	^{238}U	Uppm**	^{207}Pb*/^{206}Pb*	1σ%	^{206}Pb*/^{238}U	1σ%	^{207}Pb*/^{235}U	1σ%	Rho	^{207}Pb/^{206}Pb	2σ abs	^{206}Pb*/^{238}U	2σ abs	^{207}Pb*/^{235}U	2σ abs	% disc***	Cm-Pb corr'd?
cap44b-1	-0.001	10.4	0.57	177	578	0.0538	2.0	0.0473	1.1	0.351	2.3	0.45	363	94	298	6	306	17	17.8	N
cap44b-2	0.005	7.4	0.34	164.7	412	0.0562	1.7	0.0484	0.8	0.375	1.9	0.41	462	75	305	5	324	14	34.0	N
cap103a-1	0.002	6.9	0.36	96	271	0.0529	2.0	0.0483	1.4	0.352	2.8	0.49	324	110	304	8	307	20	6.2	N
cap103a-2	0.006	10.7	0.46	244	610	0.0544	1.6	0.0486	0.7	0.365	1.7	0.43	389	70	306	5	316	13	21.3	N

* = radiogenic
** uncertainty on U concentration c.25%
*** discordance is percentage difference between 207Pb/206Pb and 206Pb/238U ages
Cm-Pb corr'd? = common lead corrected data Yes or No

Table 4 - Hf analyses from two 305Ma grains from sample CAP

Sample	Total Hf (V)	^{178}Hf/^{177}Hf	1σ%	^{176}Hf/^{177}Hf	1σ%	^{176}Yb/^{177}Hf	1σ%	^{176}Lu/^{177}Hf	1σ%	Age	1s	EHf	2s	TDM	2s
cap44b	3.68	1.46727	0.0055	0.282264	0.0157	0.281	8.2	0.00129	7.7	305	3	-11.3	1.7	1352	63
cap103a	3.48	1.46731	0.0051	0.282257	0.0151	0.179	5.3	0.000861	4.8	305	4	-11.5	1.6	1346	59

Table 5 - All Hf analyses

Sample	Total Hf (V)	$^{178}Hf/^{177}Hf$	1σ%	$^{176}Hf/^{177}Hf$	1σ%	$^{176}Yb/^{177}Hf$	1σ%	$^{176}Lu/^{177}Hf$	1σ%	Age	1s	EHf	2s	TDM	2s
dro2b	1.02	1.46718	0.0074	0.282196	0.0274	0.113	61.0	0.00081	6.4	1234	18	7.4	3.2	1425	105
dro2d	0.86	1.46715	0.0071	0.281974	0.0273	0.019	60.9	0.00014	6.3	559	8	-15.5	2.9	1691	101
dro3a	1.12	1.46737	0.0068	0.282036	0.0267	0.049	61.1	0.00036	7.2	508	7	-14.5	2.8	1619	100
dro3b	1.24	1.46721	0.0066	0.282029	0.0263	0.112	61.1	0.00080	7.3	743	11	-9.7	2.9	1647	101
dro8	1.11	1.46719	0.0071	0.282058	0.0270	0.095	61.0	0.00067	6.7	1133	17	0.3	3.1	1603	103
dro10a	1.11	1.46728	0.0071	0.282167	0.0276	0.151	60.9	0.00110	6.3	1152	17	4.3	3.2	1476	107
dro10b	0.99	1.4673	0.0074	0.282319	0.0276	0.082	60.9	0.00069	6.7	887	13	3.9	3.1	1257	105
dro11b	0.95	1.4673	0.0070	0.281897	0.0279	0.091	60.9	0.00072	6.2	1558	24	4.3	3.4	1818	106
dro12a	1.17	1.46723	0.0072	0.281791	0.0270	0.016	60.9	0.00016	6.1	552	8	-22.2	2.9	1930	99
dro14b	1.14	1.46726	0.0075	0.281450	0.0284	0.083	61.0	0.00060	7.3	1255	20	-18.4	3.3	2398	107
dro17b	1.08	1.46722	0.0069	0.282077	0.0287	0.216	61.1	0.00145	7.9	1263	21	3.3	3.4	1611	115
dro17c	2.27	1.46728	0.0051	0.281994	0.0149	0.100	7.4	0.00062	5.3	1203	18	-1.6	2.0	1739	61
dro16c	3.17	1.46734	0.0058	0.282099	0.0149	0.105	8.2	0.00072	5.2	966	16	-2.1	1.9	1551	57
dro21b	2.24	1.46727	0.0050	0.282162	0.0151	0.129	7.1	0.00086	4.6	316	4	-14.5	1.6	1473	58
dro22	2.60	1.46726	0.0050	0.281943	0.0158	0.064	7.0	0.00044	4.6	1176	18	-2.6	2.0	1745	60
dro24b	3.29	1.46721	0.0050	0.281979	0.0160	0.129	7.3	0.00085	5.4	1330	22	1.9	2.2	1716	62
dro31a	2.33	1.46727	0.0052	0.282327	0.0167	0.052	7.4	0.00035	4.9	566	8	-2.9	1.9	1236	63
dro32a	1.93	1.46729	0.0052	0.282095	0.0155	0.067	7.1	0.00045	4.6	1082	16	0.6	1.9	1546	59
dro34a	2.07	1.46714	0.0052	0.282171	0.0155	0.099	7.3	0.00074	4.6	523	8	-9.6	1.8	1456	60
dro34b	2.57	1.4672	0.0050	0.281628	0.0145	0.070	7.2	0.00052	4.6	1711	26	-1.5	2.1	2161	55
dro36	2.46	1.46719	0.0051	0.281984	0.0157	0.069	7.1	0.00047	4.4	797	11	-9.9	1.8	1692	59
dro35b	2.55	1.46722	0.0056	0.282086	0.0154	0.083	7.7	0.00061	4.7	1137	17	1.5	2.0	1564	59
dro37b	2.61	1.46723	0.0053	0.282108	0.0147	0.108	10.5	0.00075	9.4	869	12	-4.0	1.8	1540	58
dro37c	2.96	1.4672	0.0056	0.282061	0.0149	0.069	7.2	0.00048	5.4	1138	15	0.7	1.9	1592	56
dro65b	2.32	1.46722	0.0053	0.281868	0.0157	0.129	7.8	0.00092	6.2	1560	21	3.1	2.1	1867	61
dro66c	2.53	1.46721	0.0052	0.282557	0.0151	0.130	7.1	0.00088	4.4	306	4	-0.8	1.6	943	59
dro64c	2.59	1.46724	0.0054	0.281588	0.0151	0.091	7.0	0.00064	5.1	1707	24	-3.1	2.1	2220	58
dro64e	2.58	1.46731	0.0057	0.281900	0.0155	0.067	15.8	0.00044	10.7	587	7	-17.6	1.7	1801	60
dro63e	2.67	1.46716	0.0053	0.281950	0.0145	0.096	7.6	0.00067	5.6	1548	22	6.0	2.0	1746	56
dro61b	2.51	1.46723	0.0051	0.282250	0.0158	0.042	7.5	0.00028	4.9	585	8	-5.2	1.8	1335	59
dro61a	2.74	1.4673	0.0042	0.282735	0.0129	0.208	12.0	0.00159	8.8	311	4	5.5	1.4	716	53
dro60b	4.30	1.46722	0.0036	0.281870	0.0085	0.108	12.1	0.00073	8.5	1516	21	2.4	1.4	1854	35
dro59b	3.71	1.46725	0.0036	0.281636	0.0097	0.163	12.0	0.00108	8.6	1620	22	-3.9	1.6	2182	42
dro58a	3.98	1.4672	0.0033	0.282427	0.0088	0.088	12.5	0.00057	8.7	581	7	0.9	1.1	1109	34
dro57	3.14	1.46726	0.0038	0.282118	0.0099	0.182	12.2	0.00118	9.0	1242	17	4.5	1.5	1544	42
dro56c	2.76	1.46723	0.0034	0.280962	0.0113	0.092	13.1	0.00074	9.6	2633	42	-3.9	2.3	3040	47
dro55a	3.30	1.46715	0.0037	0.281684	0.0093	0.104	11.9	0.00077	8.3	1616	24	-1.9	1.5	2101	38
dro55b	2.27	1.46722	0.0046	0.281956	0.0108	0.094	11.9	0.00072	8.4	602	7	-15.4	1.3	1740	43

dro54	3.44	1.4671	0.0034	0.282227	0.0108	0.194	11.9	0.00141	8.4	427	5	-9.9	1.2	1406	46
dro52d	2.06	1.46725	0.0053	0.282219	0.0165	0.112	15.9	0.00074	14.1	911	15	0.9	2.1	1392	66
dro51a	2.39	1.46728	0.0045	0.282082	0.0111	0.089	12.0	0.00073	9.3	1104	15	0.5	1.5	1574	44
cap5	4.02	1.46728	0.0044	0.281720	0.0092	0.078	4.4	0.00034	3.3	1172	13	-10.5	1.2	2031	34
cap6	3.61	1.46724	0.0061	0.282486	0.0092	0.311	3.0	0.00137	2.8	929	10	10.4	1.2	1052	36
cap7a	2.92	1.46733	0.0030	0.281597	0.0104	0.127	4.6	0.00059	3.6	1808	22	-0.4	1.6	2205	40
cap7b	4.57	1.46718	0.0072	0.281636	0.0151	0.179	4.1	0.00081	3.9	1686	22	-2.1	2.1	2168	58
cap9	4.75	1.46721	0.0054	0.282389	0.0147	0.131	4.7	0.00061	4.2	492	5	-2.5	1.6	1162	56
cap11c	4.64	1.46723	0.0053	0.281900	0.0145	0.111	4.1	0.00056	3.9	1153	13	-4.7	1.8	1808	55
cap12	4.21	1.46725	0.0057	0.281970	0.0153	0.107	4.7	0.00051	4.2	1132	13	-2.7	1.8	1713	58
cap23	3.63	1.46722	0.0075	0.282054	0.0160	0.082	4.1	0.00040	3.9	1166	13	1.1	1.9	1598	60
cap28	5.29	1.46729	0.0074	0.282124	0.0153	0.098	4.1	0.00050	3.9	1163	13	3.5	1.8	1509	58
cap30a	4.92	1.4673	0.0065	0.281775	0.0161	0.108	4.4	0.00049	3.9	1660	39	2.7	2.5	1968	60
cap35	3.90	1.46722	0.0055	0.281643	0.0147	0.244	4.9	0.00116	4.5	1559	23	-5.2	2.0	2178	58
cap37a	3.90	1.46726	0.0060	0.282121	0.0159	0.124	4.2	0.00059	3.9	1146	13	2.9	1.9	1517	60
cap37b	3.21	1.46721	0.0054	0.282123	0.0139	0.082	4.1	0.00039	3.9	755	13	-5.9	1.7	1506	52
cap40a	4.29	1.46723	0.0062	0.281816	0.0148	0.083	4.2	0.00040	3.9	556	6	-21.3	1.6	1910	55
cap40b	4.97	1.46724	0.0057	0.281574	0.0140	0.154	10.6	0.00069	9.6	1294	40	-13.2	2.4	2242	56
cap41	3.38	1.46721	0.0059	0.281820	0.0142	0.175	4.6	0.00084	4.4	1653	19	3.6	1.9	1926	55
cap44b	**3.68**	**1.46727**	**0.0055**	**0.282264**	**0.0157**	**0.281**	**8.2**	**0.00129**	**7.7**	**304**	**3**	**-11.3**	**1.7**	**1352**	**63**
cap44e	3.28	1.46724	0.0055	0.281581	0.0145	0.136	5.4	0.00063	5.2	1741	20	-2.6	2.0	2230	55
cap44f	3.09	1.46724	0.0054	0.281993	0.0150	0.088	5.2	0.00042	4.8	1165	13	-1.1	1.8	1679	56
cap44h	3.98	1.46721	0.0067	0.281217	0.0153	0.205	4.7	0.00095	4.8	1919	24	-11.8	2.1	2726	60
cap48c	3.67	1.46729	0.0063	0.282163	0.0143	0.109	4.1	0.00054	3.9	1156	13	4.7	1.7	1459	54
cap49	4.09	1.46731	0.0054	0.282365	0.0151	0.105	5.4	0.00050	4.9	588	6	-1.1	1.7	1190	58
cap59a	3.45	1.46728	0.0064	0.280767	0.0153	0.053	4.8	0.00028	4.3	2722	44	-7.9	2.4	3253	56
cap59b	4.20	1.46725	0.0053	0.281744	0.0155	0.150	4.5	0.00071	4.4	1768	21	3.8	2.1	2020	59
cap60c	3.31	1.46727	0.0057	0.282214	0.0145	0.212	4.6	0.00098	4.3	1080	12	4.4	1.8	1408	57
cap62	3.12	1.46732	0.0056	0.282023	0.0162	0.113	4.2	0.00050	4.1	537	13	-14.4	1.9	1643	61
cap64c	2.45	1.46727	0.0070	0.282332	0.0144	0.199	5.6	0.00081	4.7	899	10	4.6	1.7	1244	56
cap65a	3.06	1.46732	0.0056	0.282234	0.0147	0.053	4.2	0.00025	3.9	561	6	-6.3	1.6	1355	55
cap67d	3.72	1.46732	0.0069	0.281800	0.0163	0.080	7.3	0.00037	7.2	604	7	-20.7	1.8	1929	61
cap69a	2.48	1.46723	0.0064	0.282223	0.0159	0.081	4.1	0.00040	3.9	1114	13	5.9	1.9	1375	60
cap70b	3.15	1.46725	0.0064	0.282284	0.0151	0.160	5.9	0.00077	5.8	811	9	0.9	1.7	1307	59
cap72	2.45	1.46728	0.0071	0.282116	0.0169	0.143	4.1	0.00068	3.9	1093	17	1.4	2.1	1527	64
cap73c	2.53	1.46732	0.0061	0.282104	0.0159	0.087	4.1	0.00041	3.9	1201	24	4.2	2.1	1533	60
cap75b	3.17	1.4673	0.0066	0.281559	0.0171	0.089	4.8	0.00043	4.7	1786	28	-2.1	2.4	2246	64
cap84a	2.95	1.46729	0.0057	0.281761	0.0147	0.167	4.4	0.00080	4.2	1657	26	1.7	2.1	2003	56
cap81a	3.13	1.46721	0.0064	0.282067	0.0150	0.109	4.2	0.00049	3.9	1189	18	2.1	1.9	1585	57
cap83b	3.31	1.46716	0.0064	0.281927	0.0151	0.115	4.2	0.00055	3.9	1155	17	-3.7	1.9	1772	57
cap82b	3.00	1.46718	0.0060	0.282101	0.0150	0.081	4.1	0.00040	3.9	1191	18	3.4	1.9	1536	56
cap104	3.24	1.46728	0.0057	0.282161	0.0151	0.098	6.4	0.00051	6.9	474	7	-11.0	1.7	1461	58

cap103a	**3.03**	**1.46731**	**0.0051**	**0.282257**	**0.0151**	**0.179**	**5.3**	**0.00086**	**4.8**	**304**	**4**	**-11.5**	**1.6**	**1346**	**59**
cap54a	3.48	1.46725	0.0063	0.282075	0.0144	0.102	4.5	0.00049	4.1	1052	371	-0.8	9.9	1574	54
cyc3	4.38	1.46736	0.0046	0.28194	0.0090	0.154	3.5	0.00093	3.2	1533	24	5.1	1.5	1768	35
cyc5	4.40	1.46728	0.0052	0.28172	0.0081	0.129	2.6	0.00072	1.9	1662	22	0.6	1.3	2046	31
cyc7a	4.67	1.46727	0.0052	0.28172	0.0084	0.119	3.6	0.00069	3.4	1740	24	2.2	1.4	2052	32
cyc9	4.41	1.46725	0.0066	0.28163	0.0095	0.131	3.8	0.00068	3.1	1826	25	1.0	1.6	2171	36
cyc10b	4.07	1.46718	0.0054	0.28219	0.0110	0.342	2.8	0.00195	2.5	1137	15	4.3	1.5	1471	45
cyc14b	3.94	1.46726	0.0052	0.28106	0.0100	0.164	2.5	0.00090	2.3	2252	31	-9.7	1.7	2931	38
cyc15a	3.95	1.46733	0.0059	0.28214	0.0100	0.100	2.4	0.00055	2.1	1177	15	4.3	1.4	1492	38
cyc20a	3.49	1.46725	0.0069	0.28166	0.0093	0.099	3.9	0.00055	3.6	1758	24	0.9	1.5	2116	35
cyc21	3.40	1.46724	0.0067	0.28212	0.0088	0.100	2.4	0.00055	1.9	1190	16	4.0	1.3	1513	33
cyc34b	4.20	1.46721	0.0055	0.28230	0.0081	0.108	3.4	0.00056	2.3	585	7	-3.5	1.0	1278	31
cyc57b	4.41	1.46734	0.0052	0.28149	0.0095	0.208	2.7	0.00115	2.3	1781	25	-5.5	1.5	2379	37
cyc58b	3.24	1.46722	0.0059	0.28168	0.0088	0.059	2.5	0.00030	1.9	478	6	-27.7	1.0	2079	33
cyc91b	3.71	1.46730	0.0057	0.28193	0.0086	0.182	2.6	0.00100	2.0	1551	21	4.9	1.4	1794	33
cyc93	3.71	1.46730	0.0051	0.28249	0.0095	0.298	2.7	0.00166	2.6	353	4	-2.3	1.1	1054	38
cyc85	3.02	1.46725	0.0054	0.28133	0.0098	0.110	2.4	0.00060	1.9	1355	19	-20.2	1.4	2551	36
cyc84a	2.25	1.46721	0.0069	0.28210	0.0113	0.235	2.9	0.00132	2.9	308	4	-17.1	1.2	1576	45
cyc82a	2.98	1.46725	0.0058	0.28187	0.0105	0.213	2.4	0.00121	2.3	1607	22	3.8	1.6	1883	41
cyc49c	3.64	1.46716	0.0056	0.28218	0.0095	0.101	2.8	0.00066	2.8	1049	15	2.7	1.3	1443	36
cyc49b	3.24	1.46722	0.0048	0.28176	0.0093	0.111	3.8	0.00063	2.7	537	7	-23.7	1.1	1992	35
cyc47	3.86	1.46718	0.0047	0.28212	0.0079	0.070	2.5	0.00040	1.9	1173	15	3.6	1.2	1512	30
cyc45b	3.59	1.46718	0.0040	0.28229	0.0078	0.117	2.7	0.00065	2.1	712	9	-1.2	1.0	1300	30
cyc44a	3.96	1.46725	0.0047	0.28170	0.0081	0.094	2.6	0.00049	1.9	1337	21	-7.6	1.3	2070	30
cyc41	3.11	1.46728	0.0050	0.28227	0.0108	0.287	3.8	0.00160	3.6	315	4	-10.8	1.2	1350	44
cyc25a	3.34	1.46733	0.0055	0.28225	0.0100	0.188	2.4	0.00114	2.2	354	4	-10.7	1.1	1370	39
cyc25b	3.49	1.46730	0.0043	0.28172	0.0082	0.106	4.3	0.00062	4.2	1663	23	0.4	1.4	2052	32
cyc38b	3.33	1.46721	0.0045	0.28271	0.0095	0.210	2.7	0.00123	2.3	327	4	4.9	1.0	749	37
cyc39	3.33	1.46725	0.0048	0.28173	0.0093	0.010	2.9	0.00004	2.2	587	7	-23.5	1.1	2005	34
cyc37b	3.49	1.46729	0.0048	0.28189	0.0103	0.184	2.6	0.00110	2.0	1579	22	4.2	1.5	1842	40
cyc60c	2.87	1.46728	0.0051	0.28235	0.0097	0.177	7.2	0.00104	5.4	934	13	5.8	1.3	1230	39
cyc59a	3.42	1.46727	0.0055	0.28171	0.0098	0.128	2.3	0.00074	2.0	1793	24	3.1	1.6	2066	37
cyc97a	3.41	1.46726	0.0044	0.28159	0.0091	0.101	2.8	0.00053	2.0	1748	24	-1.8	1.5	2207	34
cyc71b	2.83	1.46724	0.0056	0.28212	0.0090	0.224	2.9	0.00128	2.1	1090	14	1.2	1.2	1539	36
cyc72	3.74	1.46737	0.0063	0.28196	0.0100	0.134	2.5	0.00079	1.9	1576	22	7.1	1.5	1732	38
cyc109e	3.89	1.46726	0.0048	0.28151	0.0084	0.198	3.1	0.00106	2.4	1829	26	-3.5	1.5	2345	33
cyc118a	4.47	1.46727	0.0047	0.28179	0.0086	0.463	2.5	0.00217	2.0	1290	20	-6.9	1.3	2037	36
cyc118b	3.02	1.46726	0.0044	0.28231	0.0100	0.176	2.6	0.00096	2.5	409	5	-7.2	1.1	1276	39
cyc1a	3.64	1.46727	0.0067	0.28099	0.0103	0.255	2.6	0.00135	2.6	2837	43	0.8	2.1	3047	41

All data are normalised to JMC475 176Hf/177Hf = 0.282160 and 91500 176Lu/177Hf = 0.000311 run at the time of analysis.

Laser ablation of 91500 gave 176Hf/177Hf = 0.282296-0.282325 for the various sessions over the period of analysis.
Uncertainties for reproducibility of 91500 178Hf/177Hf, 176Hf/177Hf and 176Lu/177Hf are propagated into the sample data uncertainties.
Epsilon Hf is calculated after correction for decay of 176Lu
Epsilon Hf and Model age uncertainties are calculated by calculating through the outer error limits.